LEVEL
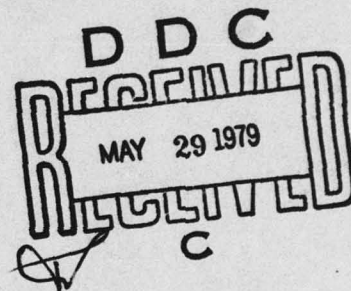
ANNUAL REPORT OF THE LAWRENCE LIVERMORE LABORATORY TO THE FAA ON THE HIGH ALTITUDE POLLUTION PROGRAM-1978

Frederick M. Luther

Principal Investigator

SEPTEMBER 1978

Annual Report

Prepared for:

HIGH ALTITUDE POLLUTION PROGRAM

U.S. DEPARTMENT OF TRANSPORTATION
Federal Aviation Administration
Office of Environment and Energy
Washington, D.C. 20591

79 05 24 010

FAA-AEE

1. Report No. 19 FAA-EE-79-04	2. Government Accession No.	3. Recipient's Catalog No.
4. Title and Subtitle ANNUAL REPORT OF THE LAWRENCE LIVERMORE LAB TO THE FAA ON THE HIGH ALTITUDE POLLUTION PROGRAM-1978		5. Report Date September 1978
		6. Performing Organization Code
7. Author(s) Frederick M. Luther, Principal Investigator		8. Performing Organization Report No. UCRL-50042-78
9. Performing Organization Name and Address Lawrence Livermore Laboratory University of California Livermore, California 94550		10. Work Unit No. (TRAIS)
		11. Contract or Grant No. DOT-FA76WAI-653
12. Sponsoring Agency Name and Address Department of Transportation Federal Aviation Administration High Altitude Pollution Program Washington, D.C. 20591		13. Type of Report and Period Covered Annual Report
		14. Sponsoring Agency Code

15. Supplementary Notes

56p.

16. Abstract

This report discusses the research done at Lawrence Livermore Laboratory in the area of numerical modeling of the atmospheric response to stratospheric perturbations. The one-dimensional transport-kinetics model was used to simulate observed stratospheric variations and for several assessment studies. The effects of a solar eclipse on stratospheric chemistry have been modeled along with the possible variations due to the 11-year solar cycle. Assessment studies included: potential changes in ozone due to SST and Space Shuttle emissions, chlorofluoromethane and N_2O releases, solar power satellite launch vehicle emissions, and massive pulse injections of NO_x into the stratosphere. Other studies include the potential effects of stratospheric perturbations on the earth's radiation budget and the resultant climatic implications, and the effect of ozone reductions on erythema dose. Changes to the one-dimensional transport-kinetics model during the past year are included in an appendix along with a listing of the chemical reactions and species used in the model.

17. Key Words Ozone perturbations, Total Ozone, NO_x Injections, Stratospheric Model, Erythema Dose, Anthropogenic Activities, Ozone, and Solar Variability.	18. Distribution Statement Available to the public through National Technical Information Service, Springfield, Virginia 22161.		
19. Security Classif. (of this report) UNCLASSIFIED	20. Security Classif. (of this page) UNCLASSIFIED	21. No. of Pages 54	22. Price

390 999

LAWRENCE LIVERMORE LABORATORY

University of California / Livermore, California 94550

UCRL-50042-78

ANNUAL REPORT OF LAWRENCE LIVERMORE LABORATORY TO THE FAA ON THE HIGH ALTITUDE POLLUTION PROGRAM — 1978

Frederick M. Luther, Principal Investigator

MS. date: September 30, 1978

PREFACE

Since July 1, 1975, Lawrence Livermore Laboratory (LLL) has been participating in the High Altitude Pollution Program sponsored by the U.S. Department of Transportation's Federal Aviation Administration. This report describes the major accomplishments and significant findings during the fiscal year ending September 30, 1978, for work performed at LLL under Reimbursable Agreement DOT-FA76WAI-653. Two major research areas are covered by this agreement: (1) numerical modeling of the atmospheric response to stratospheric perturbations, and (2) the processing, archiving, and analysis of satellite ozone data. Progress on the second research area has recently been published in a report by Lovill *et al.* (1978). Only work performed in the first area will be reported here. The successful accomplishment of the many subtasks within the numerical modeling area has required contributions and cooperation from many participants. The work reported here is the result of the collective effort of all those listed below.

Scientific Administration

Joseph B. Knox, Division Leader
Frederick M. Luther, Principal Investigator

Participants

Julius S. Chang
William H. Duewer
Joyce E. Penner
Raymond L. Tarp
Donald J. Wuebbles

CONTENTS

ANNUAL REPORT OF LAWRENCE LIVERMORE LABORATORY TO THE FAA ON THE HIGH ALTITUDE POLLUTION PROGRAM — 1978

1. INTRODUCTION

The High Altitude Pollution Program (HAPP) was initiated by the Federal Aviation Administration to ensure that aircraft engine emissions in the stratosphere will not result in unacceptable effects on the biosphere. Lawrence Livermore Laboratory (LLL) has participated in HAPP since July 1975. The primary research emphasis at LLL is on numerical modeling of the atmospheric response to stratospheric perturbations. A fundamental tool in the LLL effort has been the one-dimensional transport-kinetics model. We are also in the process of developing a two-dimensional transport-kinetics model.

Support for model development is shared between HAPP and another project at LLL involving assessment of the chemical and climatic effects of atmospheric nuclear explosions. The latter project is funded by the Division of Military Application (DMA) of the Department of Energy. Although the same numerical models are used for both studies, the applications of the models are quite different. For example, the study of the climatic effect of nuclear explosions is primarily concerned with the time-dependent response of the atmosphere to pulse injections of NO_x, whereas the HAPP study is concerned with steady-state injections of NO_x and other species.

In August 1976, LLL's participation in HAPP was extended to include a feasibility study to determine whether good quality total ozone values could be derived from infrared measurements by a multichannel filter radiometer (MFR) sensor carried aboard a series of satellites operated by the U.S. Air Force. Infrared radiance data became available in March 1977 from the first of a new series of satellites, which are a part of the Defense Meteorological Satellite Program Block 5D series. The MFR sensor aboard these satellites is unique in that it is the first cross-track scanning sensor capable of providing ozone measurements, thus increasing the amount of ozone data collected. The instrument has a higher resolution than previous instruments, and it provides global coverage day and night. Since mid-1977, this series of satellites has provided the only available global ozone data. The second satellite began transmitting MFR measurements in July 1977, and the third in the series began transmitting MFR measurements in September 1978. The fourth (and last) satellite in the series is yet to be launched. The designed lifetime of each satellite is two years. The ozone data derived from these satellite measurements are potentially useful to the scientific community for assessing changes in the ozone layer that may be due to natural or man-made causes.

The feasibility study was completed in June 1978, with the successful processing of 20 days of data taken during 1977. The quality of the data was demonstrated by comparison with corresponding ozone data obtained at selected stations in the world surface network of Dobson observatories. A description of the methodology used and a presentation of the results of the feasibility study are contained in a report by Lovill et al. (1978). The project is now undergoing a transition into the operational phase during which all of the MFR data from the satellites will be processed and made available for distribution to the scientific community.

In this annual report we describe LLL's major accomplishments and findings since October 1, 1977. Earlier HAPP work is described in our previous annual reports (Luther et al., 1976, 1977). In the present report we discuss the results in only the atmospheric modeling area; the work on satellite ozone-data processing and analysis has recently been reported separately.

A modeling effort is important to HAPP for two primary reasons. First, modeling constitutes a means of relating engine emissions and other man-made perturbations to changes in atmospheric composition. Because of the complex physical processes and feedback mechanisms involved, it is essentially impossible to assess the effects of emissions without incorporating these processes into a model and allowing them to interact. Second, modeling contributes to the interpretation and analysis of experimental results and helps determine the relative priorities for carrying out this work.

Due to the ever-increasing complexity of the system of governing physical and chemical processes, theoretical models of atmospheric trace species distributions have become essential tools both diagnostically and prognostically. Such models are based on a set of conservation equations describing the effect on individual trace species of atmospheric transport, chemical and photochemical kinetics, and various natural and anthropogenic sources.

Since the detailed modeling of atmospheric chemistry is a relatively young science and since overall information is limited, although rapidly increasing, most models have been diagnostic in their scope. The most comprehensive validation of all classes of models remains diagnostic. Within limits, the distributions and variabilities of most of the trace species have been modeled reasonably well.[*]

When the question of anthropogenic influence of the ozone layer was raised, there was a demand for the models in prognostic applications. The prognostic capability of the models for making predictions over decades or centuries has never been demonstrated and in all likelihood will never be demonstrated without a well-developed long-term atmospheric monitoring program of comparable duration. Limited prognostic validations, such as the model predictions of the effects of Polar Cap Absorption (PCA) events on polar stratospheric ozone and the current stratospheric chlorofluoromethane distributions, are reassuring but not conclusive. In particular, the study of PCA events requires reexamination because of the strong coupling of NO_x, ClO_x, and HO_x cycles in the current chemistry, which was not accounted for in the original study. In a sensitivity study with one-dimensional models, Duewer et al. (1977) demonstrated that under limited circumstances diagnostically similar one-dimensional models of the stratosphere can indeed yield very different predictions on the effect of NO_x effluents from SST's on ozone. Consequently, it is necessary to recognize the distinction between prognostic and diagnostic applications of the same model and affirm their individual limitations and uncertainties.

Diagnostically and prognostically, box models can provide only limited information. In fact, due to its simple structure, in certain applications it is highly sensitive to uncertainties in input variables. For example, analysis of atmospheric lifetime of long-lived halocarbons with box models is highly sensitive to uncertainties in the ratio of measured global abundance to the total amount released. For F-11 and F-12, an uncertainty of 5-10% in this ratio would lead to an uncertainty of 25-50% in the deduced atmospheric lifetime (Chang and Penner, 1978). Understanding this type of uncertainty is of particular importance for the box model because of its application in lifetime analysis. Similar uncertainties are in the more complex models but their applications are normally beyond such simple analysis. At present

there exist several useful techniques for the analysis of box model sensitivity and uncertainty. Therefore one would expect such an analysis prior to the interpretation of modeling results. Box models, with or without associated sensitivity analysis, can best serve to establish the relative importance of physical processes and suggest those problems that are most worthy of detailed examination with more complex models.

The structure of one-dimensional models has been analyzed in detail in the report by the National Research Council (1976b) and in the NASA report (Hudson, 1977). The vertical transport parameterization is based on globally averaged values of vertical distributions of tracers such as N_2O and CH_4. Consequently, for other predominantly upward moving tracers the one-dimensional model should be considered to be a globally averaged model. This is probably also true for the net downward moving tracers in the altitude range of the tropopause. But in the stratosphere the detailed representation of the photochemical interactions is such that only local variables such as temperature and solar flux intensity (both in space and time) can be used. This is a necessary condition that significantly complicates the interpretation of model results. The local chemical lifetime of all stratospheric chemical trace species depends on the local concentrations of ozone and the closely coupled atomic oxygens $O(^3P)$ and $O(^1D)$. These concentrations are directly proportional to the local solar flux. As a result, the self-consistently derived odd oxygen concentrations in the one-dimensional model are positively correlated with the seasonal solar flux intensity, contrary to observation of the seasonal variation of hemispherical and global ozone distributions. In the absence of detailed information on the spatial and temporal variations of all the trace species, either from measurements or more complex models, it is not possible to derive the proper averaging (weighting) factors for the nonlinear photochemical and chemical interaction processes in the one-dimensional model. Therefore, all one-dimensional models are limited to representing local stratospheric conditions, in particular that latitudinal region and season where the model-derived ozone profile closely represents the local measurements. Typically, one-dimensional models best represent the photochemistry of about 30° N latitude at about the fall equinox. That this is not completely satisfactory is quite obvious since this is also the region where there is considerable stratospheric and tropospheric exchange, hence we expect local concentrations of trace species in the altitude range of 10-30 km to be strongly affected by fluctuations in atmospheric

---

[*]The most notable exceptions may be the high ClO measurements of Anderson (1978).

transport processes. Consequently, because of this mix of partially local and global representations, both the diagnostic and prognostic application of the one-dimensional model must be applied and analyzed with great care with regard to the intrinsic compatibility of the model and its intended use, case by case.

The results of a model calculation can be evaluated by comparison with suitably obtained atmospheric measurements. Several basic types of information have proven to be useful: height and latitudinal distributions of individual species and groups of species, partitioning of related species, and local diurnal and seasonal variations of individual species. These comparisons when available constitute a necessary test mostly for the diagnostic and at times prognostic adequacy of the model. Interpretation of the results from such tests are not always

simple. Many of the comparisons must be accepted with degrees of qualification. It is the overall reasonableness of the models and their predictions that provide a high level of confidence in their basic correctness. Of course, this is often a matter of judgment.

The measured atmospheric trace species concentrations, which constitute the data base for comparison with model results, have shown a significant level of local variability. This atmospheric variability has caused such comparisons between measurement data and modeling results to be influenced by judgment and at times provided a ready excuse for inconclusiveness. As data base and theoretical models continue to improve, a more precise formulation of atmospheric variability and its influence on data interpretation must be developed and applied.

2. MODEL SIMULATION OF OBSERVED STRATOSPHERIC VARIATIONS

2.1 The Natural Stratosphere

A fundamental tool in the LLL effort has been the one-dimensional transport-kinetics model (Chang and Wuebbles, 1977; Luther *et al.*, 1977). This model, which includes as complete a set of the important chemical and photochemical reactions as is feasible, is designed for time-dependent perturbation and sensitivity studies. The model i ncludes 30 chemical species and 97 chemical and photochemical reactions. The chemical rate coefficients currently used in the model are listed in Table A-1 (Appendix A). Stratospheric water vapor concentrations are now computed at altitudes above 12 km in our standard model, although a fixed concentration profile may be specified as a user option.

Species concentrations are computed at 44 levels in the atmosphere, extending from the ground to an altitude of 55 km. The model uses an accurate numerical method for solving stiff systems of differential equations. Vertical transport is parameterized using a one-dimensional diffusion formulation that describes hemispheric-average net vertical transport by an altitude-dependent diffusion coefficient. The Chang (1976) diffusion coefficient profile was used for all of the calculations presented in this annual report. The model can include temperature coupling between changes in composition and reaction rate coefficients, but this feature is not used in

the standard model. The standard model includes a totally self-consistent diurnal averaging procedure for nonlinear chemical reaction terms (Luther *et al.*, 1977). Unless otherwise stated, the standard model was used for the calculations presented in the following sections. Changes made to the model during the past year are described in Appendix A. In this section we describe the natural stratosphere as computed by the model. The sensitivity of the model to various stratospheric perturbations is described in Sec. 3.1.

The ambient stratospheric species concentrations that are presented here correspond to a simulation of present-day conditions. The historical release of CFM's is included assuming constant production since 1975. Since the chlorine budget of the stratosphere is continuously increasing, this time-dependent calculation not only provides a current stratosphere for diagnostic purposes, but it also provides a test for the model in predicting the accumulation of CFM's in the troposphere and their vertical distribution in the stratosphere. In this calculation it is assumed that presently observed tropospheric concentrations of CCl_4 and CH_3Cl are the sources for background chlorine. The species CH_3CCl_3 is not used because of difficulties with data precision and accuracy and the apparent conflict with measured HO concentrations in the lower troposphere (see the discussion on CH_3CCl_3). With or without CH_3CCl_3 as a source of present stratospheric chlorine, the

analysis of the following sections is the same with certain exceptions as noted.

The computed stratospheric distributions of minor trace species corresponding to January 1978 are shown in Figs. 1 through 6. These are all diurnally (24-hr) averaged quantities. The relevant noontime and nighttime values are discussed in individual sections. The performance of stratospheric models in predicting the vertical distribution of known trace species that are believed to be important to ozone chemistry are discussed in the following sections.
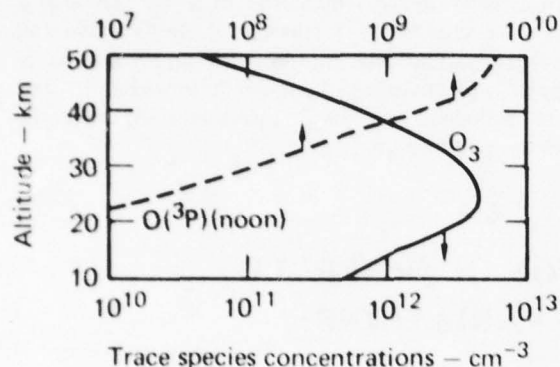

FIG. 1. Species concentration profiles for O_3 and $O(^3P)$ computed for January 1978.

Trace Species With Long Stratospheric Chemical Lifetimes

The trace species N_2O, CF_2Cl_2, $CFCl_3$, CCl_4, CH_3CCl_3, CH_4, CH_3Cl, and H_2O all have stratospheric chemical lifetimes of at least a year. Consequently, their stratospheric abundance is totally determined by fluxes from the troposphere (strictly speaking this is not true for H_2O as will be explained). In fact, these species are the sources for all the minor trace species in the stratosphere that are known to be essential in ozone chemistry.

N_2O:

The basic input variable for modeling N_2O is its observed tropospheric mixing ratio. Models can either use this number directly or convert it to a source flux derived from the measured mixing ratio and an assumed atmospheric lifetime. As a result, agreement with observations in the troposphere is expected (320 ppbv vs 325 $\pm$ 10 ppbv). In the stratosphere, the N_2O local chemical lifetime increases from 6 months at 35 km to thousands of years near the tropopause. In fact, one may state that the variability of its vertical concentration profile in the stratosphere is strictly due to atmospheric transport processes. One-dimensional, and even two-dimensional models, can at best provide a global
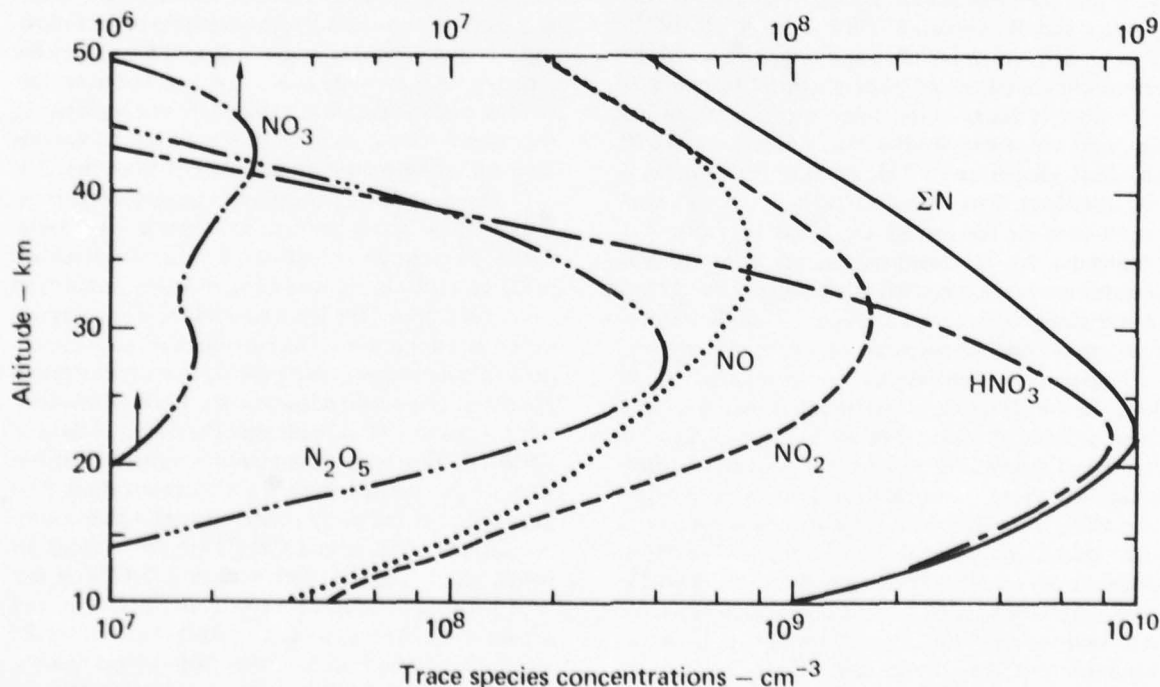
FIG. 2. Concentration profile for species containing nitrogen computed for January 1978.

4
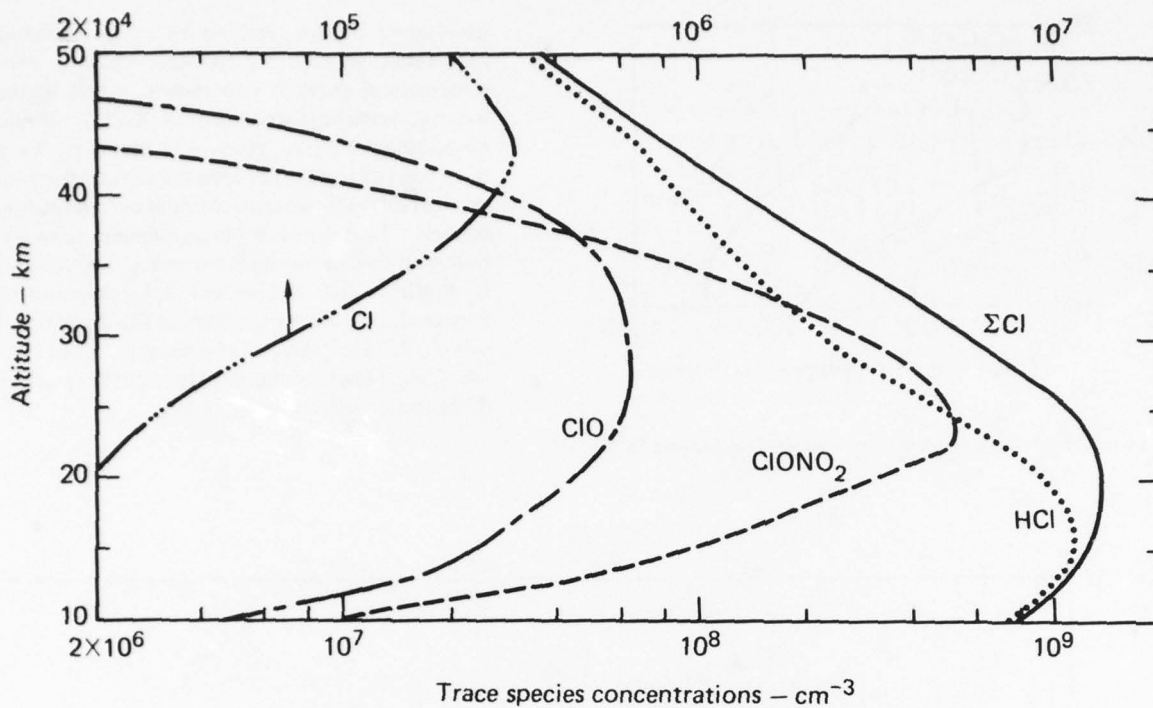
FIG. 3. Concentration profiles for species containing chlorine as computed for January 1978.
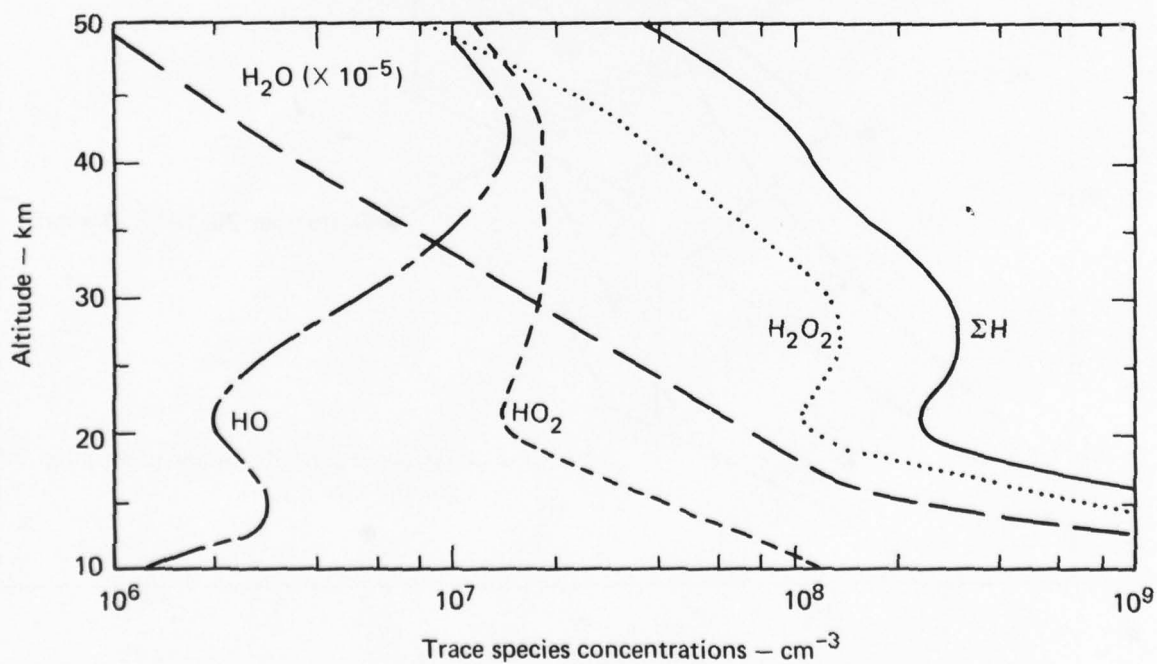
FIG. 4. Concentration profile for species containing hydrogen computed for January 1978.
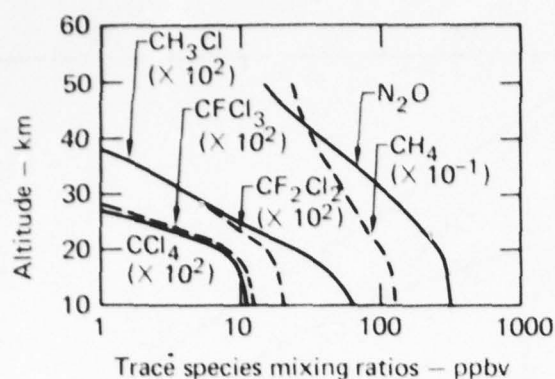
FIG. 5. Trace species mixing ratios computed for January 1978.

qualitative picture but no exact quantitative agreement locally. As is well known, one-dimensional models can indeed simulate the average vertical distribution of N_2O. It should be emphasized that both N_2O and CH_4 have been used as tracers for deriving the effective net vertical diffusion coefficient in one-dimensional models. Therefore, such agreement between data and model results is a necessary condition. It confirms that the model is functioning as expected, i.e., the more complex full model does not change the expected chemical cycles of N_2O and CH_4, hence no reevaluation of the effective diffusion coefficient is necessary.
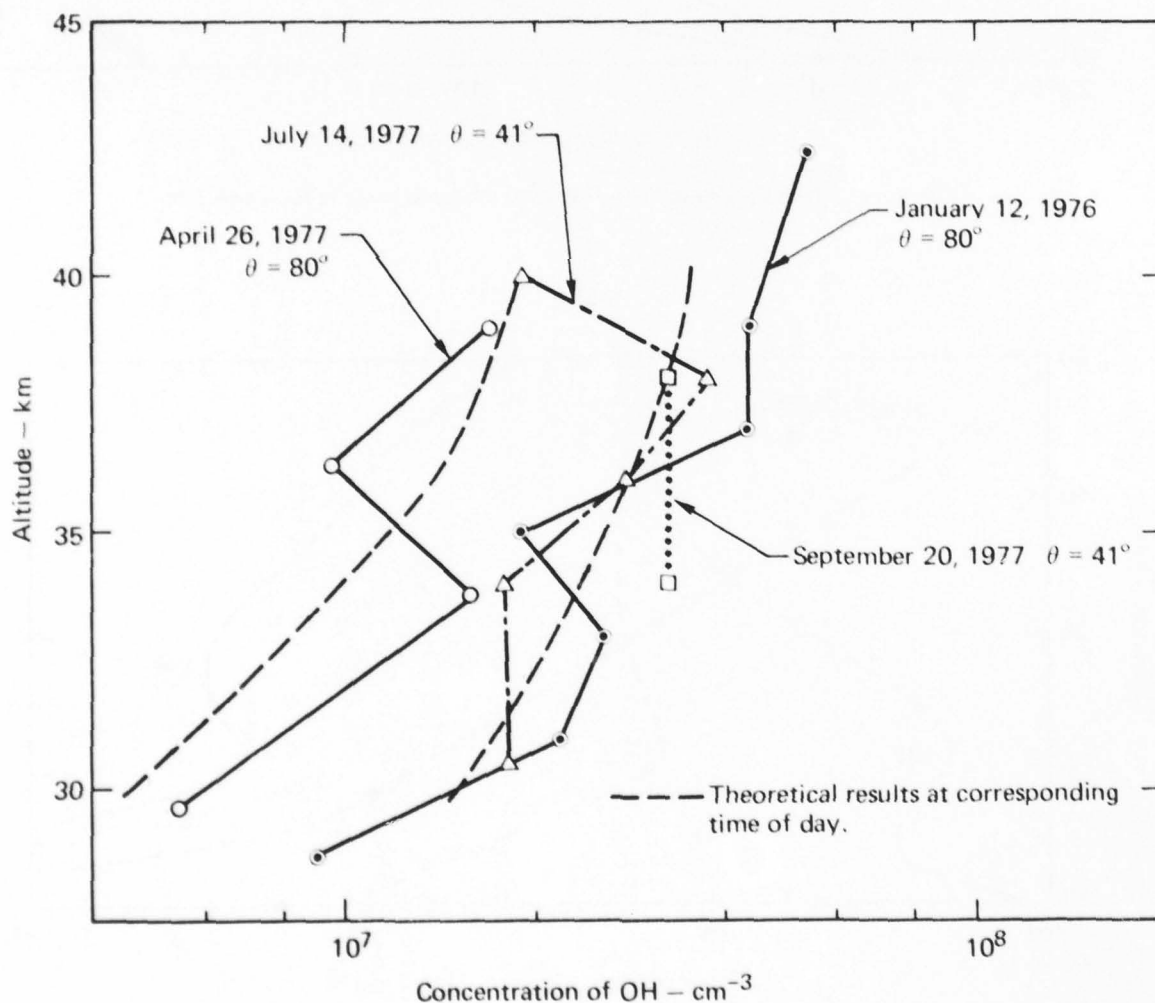
FIG. 6. Theoretical and measured concentrations of OH.

CH₄:

Methane behaves much the same as N_2O in the atmosphere, except that it has a comparatively short lifetime in the troposphere. The model used 1.31 ppmv based on earlier data, which is 20% less than current data (1.65 ± 0.1 ppmv). This leads to similar underestimates throughout the stratosphere. It also leads to lesser HO_x from CH_4, which would have a small effect on the effectiveness of added chlorine on ozone. Since the local chemical lifetime of CH_4 increases from 6 months at 40 km to more than 10 years at the tropopause, its stratospheric variability is also controlled by transport processes. In particular the qualitative latitudinal similarity in the vertical profiles of N_2O and CH_4 from 5°S and 40°N confirms this view.

CCl₄ and CH₃Cl:

The model used approximately the measured concentrations as input parameters. The tropospheric concentration of CCl_4 is 112 ppbv, which is at least 10% lower than the currently available averages but certainly within the limits of data uncertainty. The CCl_4 is not destroyed in the troposphere but begins to photodissociate quickly in the stratosphere. Its local chemical lifetime is of the order of 6 months at about 24 km. Therefore, in addition to the instrumentation difficulties associated with grab sampling, there should be a high level of transport variability which makes stratospheric measurement of CCl_4 and its data interpretation a rather difficult task. The CH_3Cl measurement data have shown such fluctuations that it is difficult to assess the adequacy of model results. Nevertheless, with an input of 746 pptv at the surface (which is approximately in the middle of the range for Rasmussen's data in 1977), the model estimates 580 pptv at the tropopause, which seems to be consistent with the 550 pptv reported by Cronn *et al.* (1977). The estimated local chemical lifetime is approximately 1 year up to 26 km. This again makes transport variability an important factor in the interpretation of CH_3Cl data.

CF₂Cl₂ and CFCl₃:

The total abundance and vertical distributions of F-11 and F-12 serve as true tests of the ability of simple one-dimensional models to represent the average net vertical transport of trace species. Together with CH_3CCl_3 the release rates of these man-made chemicals are well documented. Since the model uses the time-dependent release rate in computing its atmospheric distribution, a comparison of both the model-derived tropospheric and stratospheric budgets with measurement data would be a stringent test of the adequacy of the model. Global averages of F-11 and F-12 in the troposphere are not easily obtainable. If the observed northern-hemispheric averages in January 1977 are used to estimate the global average in January 1978, then the model is at most 10% lower in the tropospheric burdens of F-11 and F-12. About 5-8% of this is attributable to the accuracy of the source function approximation used in the model. This then provides a partial (but important) confirmation that the transport approximations based primarily on N_2O and CH_4 indeed have a more general validity and applicability. Similar to other trace species with long local chemical lifetimes, both F-11 and F-12 are sensitive to variations in local transport processes (at altitudes up to 30 km for $CFCl_3$ and up to 40 km for CF_2Cl_2). This is again consistent with observation. In general the model-predicted stratospheric vertical profiles of CF_2Cl_2 and $CFCl_3$ are both slightly on the high side of the data averages (taking the model tropopause to be at 12 km). The model seems to show slightly more destruction in the lower stratosphere (5-10 km above tropopause) for $CFCl_3$ than the data suggest. On the other hand, this could be due to weaker net upward transport in the model. Fortunately, in the regions of maximum destruction of $CFCl_3$ and CF_2Cl_2 (20-30 km and 25-35 km, respectively), the model-predicted profiles are in reasonable agreement with available data.

CH₃CCl₃:

At this time there is considerable uncertainty in the interpretation of data and the modeling of atmospheric concentrations of CH_3CCl_3. A simple box model analysis based on measurement data would yield a CH_3CCl_3 atmospheric lifetime of 5-12 years, which in turn would imply an average tropospheric HO concentration of less than 10^6 molecules/cm^3. However, most coupled stratospheric-tropospheric models have more HO than this estimate, which then leads to a much lower CH_3CCl_3 concentration in the atmosphere if the well-known release rates are used (Neely and Plonka, 1978). Furthermore, there is no generally accepted set of HO measurements in the troposphere. Although CH_3CCl_3 is estimated to be a major source of stratospheric chlorine and could provide another direct test on the adequacy of models at this time, it is not constructive to include it in the one-dimensional model in the

same manner as the other sources of stratospheric chlorine. The model used for these calculations did not include this source, which could contribute from 0.2 to 0.3 ppbv of chlorine. This omission is of no practical consequence to the present study.

H_2O:

Methane is the principal source of stratospheric water. At the tropopause H_2O is maintained both by a downward flux from the stratosphere and an upward flux from the troposphere. At this altitude the tropospheric-stratospheric exchange process serves to maintain H_2O at the saturation level. This fixed boundary condition helps maintain the H_2O concentration in the rest of the stratosphere. With such control it is not surprising to see one-dimensional models generate reasonable H_2O vertical profiles, starting with 3 ppmv at the tropopause and slowly increasing to 5 ppmv at 50 km. This is well within the uncertainty of the data. Again, since stratospheric water vapor has only weak chemical sources and sinks, its variability is mostly due to transport fluctuations.

.

Table 1 summarizes the sources of chlorine in the model and compares them with estimates from tropospheric data. As was already pointed out, the model underestimates the total budget by not including the uncertain contribution of methyl chloroform. With a total ClO_x mixing ratio of 2 ppbv in the troposphere, the ClO_x mixing ratio is reduced to 1.7 ppbv at 40 km due to the natural time delay in upward transport and the photochemical destruction of the source molecules at lower altitudes. In comparison, the total NO_x mixing ratio at 40 km at 15.9 ppbv, and the total HO_x mixing ratio at 40 km is 3.2 ppbv.

Table 1. Sources of stratospheric chlorine.

Species	Estimate from tropospheric data, ppbv	L.L.L. model, ppbv
CH_3Cl	0.47–0.77	0.75
CH_3CCl_3	0.12–0.27	0.00
CF_2Cl_2	0.48	0.42
$CFCl_3$	0.42	0.38
CCl_4	0.49	0.45
Total	1.98–2.43	2.00

Trace Species with Intermediate Stratospheric Chemical Lifetimes

Trace species such as HNO_3 and HCl have stratospheric chemical lifetimes of about a week. Similarly, the trace species families O_x ($O(^1D)$ + $O(^3P)$ + O_3) and NO_y (N + NO + NO_2 + NO_3 + HNO_3 + $2N_2O_5$) also have net stratospheric chemical lifetimes of about a week. The chlorine family ClO_x (Cl + ClO + HCl) has a somewhat shorter stratospheric chemical lifetime on the order of 1/2 to 1 day. This is due to the strength of the coupling reaction ClO + NO_2 + $M \rightarrow ClONO_2$ + M, since none of the above (usual) families includes $ClONO_2$. If we consider the broader family ClO_y (ClO_x + $ClONO_2$), then it becomes a pure tracer with no chemical loss, except possibly through the yet-to-be completely quantified reactions involving $HOCl$. In other words, if simultaneous measurements are made of all the members of the ClO_y family, then all variability in the data must be due to physical processes other than photochemistry. On the other hand, if only ClO_x family members are measured simultaneously (i.e., without $ClONO_2$), then the variations due to chemical reactions involving $ClONO_2$ must be considered.

Together with HO_x (H + HO + H_2 + $2H_2O_2$), the O_x, NO_y and ClO_y families include almost all the trace species that are of major interest in stratospheric chemistry. Their short net stratospheric chemical lifetimes signify the dominance of chemistry in their life cycles and their primary stratospheric origin. The O_x, HNO_3 and HCl downward fluxes from the stratosphere represent almost all the transport loss of the trace species in their respective families, and the transport time scales are all of the order of a year or more. Because of these similarities and relations, it is appropriate to discuss these families here and leave the partitioning within individual families to the next sections.

O_x:

For the most part, the stratospheric O_x species are in the form of O_3. The $O(^3P)$ begins to contribute more than a few percent only at altitudes above approximately 45 km. A comparison of model-derived O_3 distribution with atmospheric data actually represents an evaluation of the whole O_x family in the stratosphere. The model-derived vertical profile of O_3 (Fig. 1) compares well with the average profile obtained by Watanabe and Tohmatsu (1976) at 30° N. Below 25 km the O_3 concentrations are less than the midlatitude profile of Krueger and Minzner (1976). This is an expected result since the midlatitude profile included contributions from high-latitude ozone distributions that are the result of meridional transport. Within the one-

dimensional model framework, this translates to a lower average vertical diffusion coefficient in the range of 15-20 km.

NO_y:

The principal source of odd nitrogen in the stratosphere is N_2O through the reaction with $O(^1D)$. There is also a small amount produced from cosmic ray bombardment. Since most of the production is below 35 km with a small net loss from the $N + NO$ reaction above 45 km, total NO_y is fairly uniformly distributed between 30-45 km with a mixing ratio of 19 ppb at 40 km. The corresponding NO_y mixing ratio of 10.4 ppbv at 25 km compares well with observations, whereas at 35 km the NO_y mixing ratio from the model (15.4 ppbv) is at the high end of the stratospheric data range.

Throughout the stratosphere, the local chemical lifetimes of NO_y are of the order of several days. Consequently, all (except a set of exactly simultaneous) measurements of NO, NO_2, and HNO_3 could be subject to unknown influences due to chemical and transport processes. The HNO_3 concentrations computed by the model are on the high side of the data range, but this is quite typical of all one-dimensional models. The HNO_3 mixing ratio peaks at about 23-28 km and is consistent with all the available data. The HNO_3 has a local chemical lifetime of 10-20 days throughout the altitudes where HNO_3 is most abundant and can vary significantly over a few days, as was found by Murcray et al. (1978). Qualitatively, the increase toward the pole in column HNO_3 is consistent with the present photochemical theory, but two-dimensional models have not provided sufficiently detailed quantitative analysis yet.

ClO_y:

Since the total stratospheric chlorine in the model can only be removed as HCl through downward transport across the tropopause, its stratospheric mixing ratio is approximately the same as that of the source species. If we reject the three high values of ClO vertical profiles by Anderson (1978), then the total ClO_y mixing ratio at 20 km is approximately 0.5-1.0 ppbv, and at 35 km it is 1.6-2.3 ppbv. The LLL model gives 0.75 ppbv at 20 km and 1.65 ppbv at 35 km, which are quite comparable to the experimental values. The high ClO profiles by themselves would indicate a ClO_y mixing ratio of 1.8-9.0 ppbv of chlorine at about 40 km. Together with the estimated 1.0-1.5 ppbv of HCl, this would require a source of 3-10 ppbv of tropospheric chlorine. This is simply not accounted for by

current understanding of the sources and sinks of chlorine in the atmosphere. Although Waters et al. (1978) provided some data suggesting disagreement with one of the three high-profile measurements, a more definitive explanation on the source of error either on the photochemical theory or the measurements by Anderson is still required. In the lower stratosphere, HCl is the predominant form of ClO_y. The model gives 0.28 ppbv at 15 km and 0.55 ppbv at 20 km, which can be compared to the measured values of 0.2 ppbv and 0.3-0.7 ppbv at 15 and 20 km, respectively. If these values are used to estimate the downward flux of odd chlorine, then theory and experiment are within a factor of 2.5. This again provides another independent estimate on the uncertainty due to transport. The dip of the HCl vertical profile at 30 km as reported by Lazrus et al. (1977) and Williams et al. (1976) is not explainable within the context of one-dimensional models. But a preliminary two-dimensional calculation by Pyle (1978) suggests that HCl has local maxima and minima in the vertical direction extending from near the equator to the polar region. If one were to fly a balloon around $32°N$, it would quite likely sample through this minimum region and obtain a dip in the vertical profile. This result coupled with the ClO result (see next section) further demonstrates the limitations of a one-dimensional model and at the same time expresses a strong vote of confidence for the potential benefit of two-dimensional models.

Trace Species with Short Stratospheric Chemical Lifetimes

The trace species NO, NO_2, NO_3, N_2O_5, $O(^3P)$, Cl, ClO, $ClONO_2$, HO, HO_2, and H_2O_2 all have much shorter chemical lifetimes than the previously discussed species. As a result, their individual local concentrations are quite variable, usually on the time scale of hours to seconds. They all vary diurnally (except for H_2O_2), seasonally, and probably even on the time scale of changing albedos due to the presence of aerosols and clouds at lower altitudes. As is expected, it is not possible (and usually impossible) to always obtain local conditions such as solar flux, temperature, and local concentrations of other trace species when doing a particular measurement. Hence, it is rarely possible to quantitatively interpret the available data on these trace species with theoretical models. However, if individual collections of data are used as a group, then the total local variability in the data is often a good guiding criterion for

testing the theory. Furthermore, variability in the shape of individual vertical profiles is also a useful indicator of the domain of physical results.

NO, NO$_2$, NO$_3$ and N$_2$O$_5$:

Since 1972 there have been a considerable number of NO measurements in the stratosphere. By now its stratospheric variability is well established and any attempt to model a particular set of data has long been deemed as relatively unimportant, except for the diurnal variations of the NO, species. As was pointed out in our previous work (Luther et al., 1976), successful modeling of the NO, diurnal variations confirmed locally some of the chemical mechanisms important in the catalytic cycles affecting ozone. Our one-dimensional model yields an NO mixing ratio of 0.1 ppbv at 20 km, gradually increasing to 9.0 ppbv at 50 km. This theoretical profile is approximately in the middle of the available data. Without a simultaneous measurement of NO$_2$, individual NO data will be of steadily declining usefulness in the future.

Modeling of stratospheric NO$_2$ distributions suffers the same difficulty as that of NO due to their coupling through the NO$_x$ catalytic cycle. Although a one-dimensional model can approximate the low NO$_2$ column measurement above 50°N by using the proper seasonal solar flux, temperature, and ozone (Noxon et al., 1978a), a full explanation involves the coupling of three-dimensional transport and photochemistry (Noxon, 1978). Nevertheless, on the average, simple one-dimensional models do produce NO and NO$_2$ distributions that are consistent with stratospheric data.

Stratospheric NO$_3$ abundance as estimated by photochemical models falls far short of the observed amount (Noxon et al., 1978b). This could be due to errors in the accepted kinetics rate coefficients as suggested by Noxon et al. (1978a). But this involves extrapolation of preliminary data at higher temperatures than are in the stratosphere. Fortunately, this unsettled state of affairs is of minimal importance to this study.

The current estimates on stratospheric N$_2$O$_5$ concentrations are all consistent with the model. The upper limit of 0.1 ppbv at 18.3 km by Murcray et al. (1978) and the 3 ppbv at 30 km deduced by Evans et al. (1978) compare well with the results from diurnal calculations under comparable conditions of 0.06 ppbv and 2.1 ppbv, respectively.

O(^{3}P):

The local concentrations of O(^{1}P) are directly proportional to the local ozone concentrations and solar flux intensity. Any disagreement between theory and experimental data on O(^{1}P) can be directly traced to disagreement in O$_3$, which is more dependent upon atmospheric motions.

Cl, ClO and ClONO$_2$:

The only available data on Cl and ClO are from Anderson et al. (1977, 1978). As the discussions on ClO, indicated, the high values of ClO are not reconcilable with current theoretical understanding and must be considered the major weakness in current theory. The low ClO measurements are in good agreement with theoretical models. The only possible exception is the rate of decrease in ClO as one approaches the tropopause. One-dimensional models yield a much more gradual decrease. The two-dimensional calculation by Pyle (1978) shows that near 30° N (where Anderson et al. (1977) collected their data) there indeed is a much sharper vertical gradient from 25 to 35 km. This is apparently a direct result of the detailed transport processes in this region. It should be pointed out that these two-dimensional model results, although preliminary, are highly encouraging. Although ClONO$_2$ was shown to be a critical species in the assessment of CFM impact on stratospheric ozone, up to now only an upper limit on stratospheric abundance has been suggested. The limit of 0.3 ppbv at 20 km is at least a factor of 2 higher than the model indicates. Hence, it is an inconclusive result, although somewhat reassuring.

HO, HO$_2$ and H$_2$O$_2$:

The concentrations of HO, shown in Fig. 4 are all diurnally averaged values. Both HO and HO$_2$ undergo gradual changes throughout the daylight hours. For both HO and HO$_2$ the ratio of noon values to the diurnally averaged values could be as much as 5 in the winter hemisphere high latitudes. In the present case (30° N, fall equinox) the ratio is approximately 2.5 in the altitude range of 10-20 km, and then gradually decreases to around 2 at 45 km. Because of this large averaging factor and the gradual diurnal changes, only diurnal models should be used to compare with experimental data. Between 30-40 km, the model-estimated HO$_2$ profile at comparable times of the day and fall conditions falls on the low side of the data by Anderson et al. (1978), the computed average concentration being 4.6×10^7 cm^{-3} as compared to an

average measured value of 8×10^7 cm^{-3}. At 30 km the local value near sunset is about a factor of 2 less than the data by Mihelcic *et al.* (1977).

The HO diurnal profiles compare very well with the available data between 30-40 km. At the corresponding time the theoretical profiles both (solar zenith angles of 41° and 80°) fall in the middle of the data range (Fig. 6). This is probably fortuitous since there is no corroborating data on CH_4, H_2O, and ozone which are essential in determining the local concentrations of HO. Unfortunately, in the critical region of 10-30 km there are no data on HO and HO_2.

The only estimated upper limit value for H_2O_2 at 20 km is well above the model concentrations to be of real use. Due to the central role played by HO, in determining the effect of changes in NO_x concentrations on ozone, measurements of HO, HO_2, and H_2O_2 in the lower stratosphere have become more important than ever.

Overall, the data on HO_x seem to support the adequacy of the theory for the present application, but for other prognostic applications refinement on the HO_x budget and chemical cycles must be carried out.

2.2 Possible Variations in Stratospheric Ozone Related to the 11-Year Solar Cycle

The suggestion of a relationship between ozone and the solar cycle dates to at least 1910 (Humphreys, 1910), and various researchers have found correlations of sunspot number with total ozone (Willet, 1962; Paetzold *et al.*, 1972; Christie, 1973; Angell and Korshover, 1976). Researchers studying total ozone fluctuations for the period from 1958 to the present have in general found less evidence to support an ozone-solar correlation (Angell and Korshover, 1978a; London and Oltmans, 1977), but the period over which ozone was studied may not have been long enough to properly establish a long-term cycle. Several plausible mechanisms linking the hypothesized ozone variations with the solar cycle have been suggested. Ruderman and Chamberlain (1975) first proposed that solar modulation of the source of nitric oxide produced by galactic cosmic rays might explain the ozone record, since the cosmic ray source of NO is approximately 30% smaller at solar maximum than at solar minimum. A subsequent study by Crutzen (1975) failed to support this mechanism (see also Ruderman *et al.*, 1976). Zerefos and Crutzen (1975) suggested that solar

proton events may also provide a link between ozone variations and the solar cycle, but the study was not conclusive. Since solar proton events are localized and of short duration (Heath *et al.*, 1977), it is not clear how they may affect global ozone concentrations.

Long-term variations in the solar uv flux provide a third mechanism of potentially much greater significance for ozone variability in a global sense. We have only a few sets of measurements that suggest there may be a significant variation in the solar flux between 180 and 340 nm from solar maximum to solar minimum (Heath and Thekaekara, 1977). In view of the possible importance of solar uv variability on ozone, we shall attempt to estimate the effects such a variability would have had on the ozone record to date. We are particularly concerned with the ozone record near 40 km where both the proposed variability and chlorine increases due to past fluorocarbon release should have had their greatest effects. Callis and Nealy (1978) first studied this problem with a steady-state model without chlorine chemistry. Our time-dependent model (Luther *et al.*, 1977, NAS, 1976) includes a full set of chlorine chemistry reactions and calculates temperature self-consistently. As we shall see, our calculated ozone and temperature responses differ significantly from those calculated by Callis and Nealy.

The radiative transfer model for the temperature calculation used is described in Luther *et al.* (1977). The full set of chemical reactions is given in Appendix A (Table A-1). Photolysis rates are computed at each altitude and time step consistent with all minor species distributions and the specified solar conditions. These calculations were made using the version of the model in which the water vapor profile is held constant. Consequently, our total HO_x at solar maximum and minimum is somewhat over- and under-estimated, respectively. The effects should not seriously alter our main results, since the calculated local variation for HO_x in our model is at most 20%.

Variability in the Solar Flux and Its Effect on Ozone

Figure 7 shows the ratio of the ultraviolet (uv) flux at solar minimum to the uv flux at solar maximum as a function of wavelength (Heath and Thekaekara, 1977; NASA, 1977). The measurements shown by $\triangle$ and $\square$ represent broad-band photometric observations. Those shown by ● were obtained using identical double monochromators. The measured variability below 255 nm depends on only three photometric observations taken near 180 nm in 1966, 1969, and 1970. The flux variation
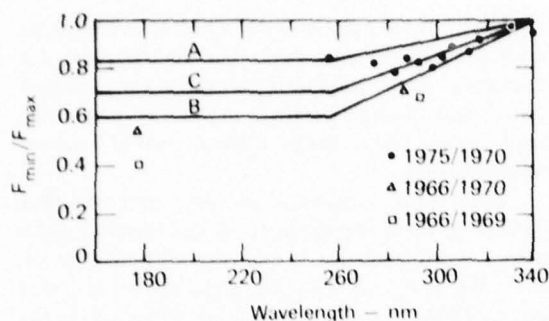
FIG. 7. Ratio of ultraviolet flux at solar minimum to the flux at solar maximum.

FIG. 8. Percent change in O_3 from solar minimum to solar maximum [(max-min)/min × 100]. The letters A and B refer to the flux change curves given in Fig. 1. For cases A1 and B1 the solar flux was only varied below 255 nm. For cases A2 and B2 the solar flux was only varied above 255 nm.

measured with these instruments at longer wavelengths overlaps the region measured by the double monochromators. the photometers show about a 15% larger variation than the double monochromators. We believe the double monochromator measurements at these wavelengths are more nearly correct, because they were made with identical instruments. Since there are no monochromator data below 255 nm, we applied a correction of about 15% to the average of the photometric measured flux variation near 180 nm. The curve in Fig. 7 marked "B" thus represents what we consider to be the largest probable variation. The curve marked "A" gives more weight to the measured variation near 255 nm and is also consistent with balloon measurements which indicate that the flux variation between 200 and 220 nm was not larger than 10% from 1972 to 1976 (Simon, 1978). The curve marked "C" represents an intermediate case and is used for most of the calculations shown in the following sections.

The calculated ozone response in our model depends fairly critically on the relative flux variation above and below 255 nm. Photons with wavelengths less than 255 nm can add to the total atmospheric reservoir of odd oxygen according to the reaction, O_2 + $h\nu \rightarrow O + O$. Photons in the entire range of wavelengths considered here are able to shift the balance between atomic oxygen and ozone according to O_3 + $h\nu \rightarrow O + O_2$, but by far the most efficient are those with wavelengths longer than 255 nm. The point is illustrated in Fig. 8. The curves marked A1 and B1 show the calculated ozone increase when the solar flux is only varied below 255 nm by the amounts indicated in curves A and B of Fig. 7, respectively. A larger flux at these wavelengths produces more ozone. The curves marked A2 and B2 show the ozone response to flux variations above 255 nm only. A large flux at these longer wavelengths shifts the balance of odd oxygen in favor of atomic oxygen so that ozone is decreased. The net result for flux variations over the entire wavelength range is to increase
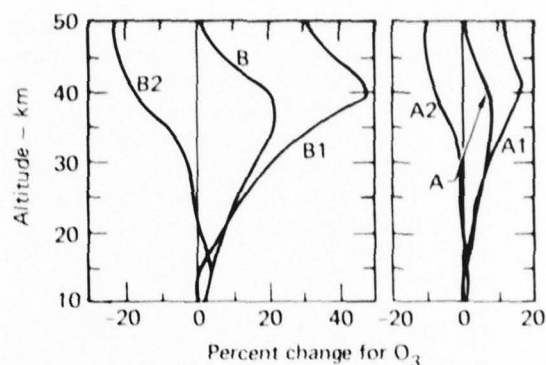
ozone over most altitudes, as shown by the curves marked B and A, and the total ozone response is approximately the sum of the variations calculated separately. This demonstrates the need for a precise determination of the relative flux variations in these wavelength bands. Since the net ozone response depends on the superposition of two effects of opposite sign, it is clear that the altitude of the maximum response depends on this relative flux variation.

Effects of Temperature Feedback

The primary source of heating for the upper stratosphere is the absorption of solar photons in the Hartley (200-300 nm) and Huggins (>300 nm) bands of ozone. We use the method of Lindzen and Will (1973) to calculate the heating rate from these bands. Figure 3 shows the calculated change in temperature and ozone when the solar flux is perturbed from minimum conditions by the amount shown by curve B in Fig. 7. Our calculations show a temperature increase of no more than about 13 degrees near 45 km. The Lindzen and Will parameterization ignores flux perturbations below 237.5 nm, but since these wavelengths contribute no more than about 10% of the ambient heating rate at 45 km our calculated temperature change should be correct to within 10%. The left panel of Fig. 3 shows the effects of including temperature feedback on calculated O_3 concentrations. With temperature feedback the peak response of ozone is reduced due to the temperature dependence of the reactions $O + O_3 \rightarrow O_2 + O_2$ and $O + O_2 + M \rightarrow O_3 + M$, and the altitude above which ozone decreases is lowered from 50 km to 41 km.

Our calculated temperature increase at solar maximum is significantly smaller than that calculated by Callis and Nealy (1978). This remains true

even for assumed flux perturbations as large as their case 1. We believe their primary thermal response is due to heating by wavelengths below 210 nm, since an examination of their calculated temperature response for case 3 (symbol $\triangle$ of their paper) shows a significant increase in temperature (20K near 45 km) even though the solar flux is not perturbed above 210 nm and their calculated ozone concentration at that altitude is decreased (compare Figs. 2 and 5 of their paper). A detailed calculation of the ambient heating rate from O_3 absorption at 45 km shows that the heating by wavelengths below 210 nm is only 0.07% of that for the entire interval from 175 to 350 nm, so that flux perturbations in this region should not greatly affect stratospheric temperature. Figure 9 shows that temperature feedback is important for calculating the change in ozone above about 25 km, but the calculated temperature change is not nearly so sensitive to flux variations as that calculated by Callis and Nealy.

Comparison With the Ozone and Temperature Records

The calculations described thus far were performed using a steady-state version of our model. Here we use our time-dependent model to examine the atmospheric response to a time-varying solar flux. We used the release rates for $CFCl_3$ and CF_2Cl_2 of McCarthy et al. (1977) and the solar flux variation C in Fig. 7 to calculate a time history for ozone over the past 47 years. The flux variation followed a sinusoidal 11-year cycle with maximum and minimum corresponding to the years 1936, 1947, 1958, 1969 and 1942, 1953, 1964, 1975, respectively. The calculation included all of the feedback mechanisms discussed above and simulates average conditions for 30° latitude. Seasonal variations in the solar flux were not included, since all one-dimensional models fail to accurately simulate the seasonal behavior of ozone due to their lack of horizontal transport. We compare our results to the analysis by Angell and Korshover (1978a,b,c) in which seasonal effects are partly removed by plotting seasonal deviations from seasonal means.

The calculated percentage deviation of total ozone from the mean is shown in Fig. 10 for the period 1957 to 1978 along with the total ozone record for 11 stations in North America and 14 stations in Europe (Angell and Korshover, 1978a). The record from North America and Europe was chosen for comparison because these areas have the largest number of stations (other than the Soviet Union) and are considered to be the most accurate and reliable. The error bars for the observations are two standard deviations of the mean. It should be pointed out that,

as shown in Fig. 9, the largest changes in O_3 concentration occur above 25 km where the chemical time constant for odd oxygen is only of the order of weeks to months. Consequently, the results in Fig. 10 show very little time delay.

Clearly, our calculated ozone variation for this period is at least not inconsistent with this record. The observed ozone increase during the late 1960's appears to be reasonably consistent with our assumed change in solar flux. We calculate an increase in total O_3 from the solar minimum in 1964 to the solar maximum in 1969 of 5.1%. For a similar variation in the solar flux before the introduction of CFM's we obtain an increase of 5.5%. This may be compared to the observed 5% increase in total O_3 for the Northern Hemisphere from the early 60's to 1970 and 2% increase for total O_3 for the Southern Hemisphere from 1960 to 1968. We calculate a decrease from 1970 to 1972 of 2.5% which agrees well with the observed 1-2% decrease in the Northern Hemisphere. The decrease in observed ozone appears to have leveled off after 1972, but we calculate a further
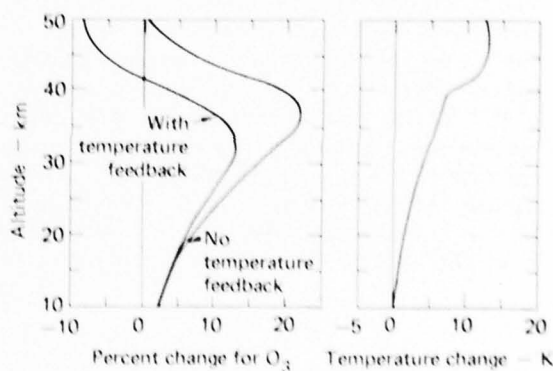

FIG. 9. Percent change in O_3 [(max-min)/min × 100] and temperature change from minimum to maximum.
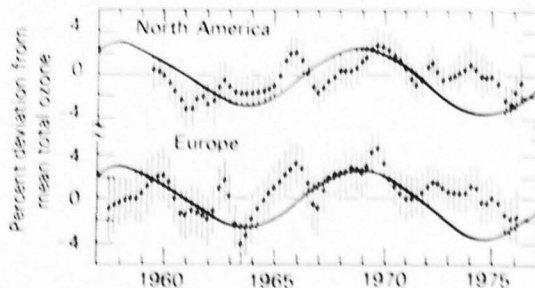

FIG. 10. Comparison of calculated total ozone deviations to the analysis of data by Angell and Korshover (1978a).

decrease through 1975. Our calculated decrease is primarily due to the solar flux variation, since the 1975 minimum is only 1.3% smaller than that calculated without the influence of increasing chlorofluoromethanes.

Clearly there are local disagreements between theory and observation throughout the period shown. Evidently some processes that control ozone on shorter time scales (3-4 years) are not accounted for by the model, and the solar uv connection and the effects of increasing chlorofluoromethanes will only be revealed by looking at the 'general' long-term picture. Thus, the apparent discrepancy between theory and observation after 1972 does not necessarily invalidate the background ozone cycle caused by solar uv flux variations and chlorine changes.

The calculated ozone deviation for the levels 32-46 km is compared to Umkehr measurements (Angell and Korshover, 1978a) in Fig. 11. Again, the two regions with the largest number of stations were chosen for comparison. Umkehr measurements are much more difficult to make than measurements for total ozone. The observations should accordingly be viewed with caution (see Dutsch and Ling, 1973). At these levels, Angell and Korshover estimate there was an 8% increase in north temperate latitudes between 1962 and 1973, and a slight decrease after 1974. (The observed decrease may be fictitious due to the presence of aerosols in the stratosphere after the eruption of Fuego in 1974.) We calculate a 5.8% increase for this layer from the solar minimum in 1964 to the maximum in 1969, and an 8.2% decrease from 1969 to 1975. This may be compared to an

increase of 6.8% from solar minimum to maximum and a decrease of 6.4% from maximum to minimum for the pre-CFM atmosphere. As shown in Fig. 11, our calculated decrease begins earlier and is larger than the observed decrease. This difference between the model and observation may be indicative of the presence of other physical processes controlling the local ozone concentrations that are not included in this model (see London et al., 1977).

As Fig. 12 shows, our calculated decrease after 1969 is consistent with the ozonesonde data for lower altitudes. The Umkehr data for 32-46 km is shown again along with our calculations and the ozonesonde record for the layers 24-32 km and 16-24 km (Angell and Korshover, 1978c). Our calculations agree fairly well with the record for Europe for these lower layers. Angell and Korshover estimate a 4% decrease in each of the two lower layers as an average for the north temperate latitudes as a whole. We calculate a decrease from the solar maximum in 1969 to the minimum in 1975 of 7.8% for the 24-32 km layer and 4.8% for the 16-24 km layer.

For the layers shown in Fig. 12, we calculate decreases of 6.4%, 6.9%, and 4.6%, respectively, for the same solar flux variations from the maximum in 1969 to the minimum in 1975 without the influence of increasing chlorofluoromethanes. For this period changes in ozone due to the release of CFM's are apparently small compared to changes resulting from our assumed solar flux variation. Therefore any effort to detect a trend in ozone due to the CFM releases must take into account the effects of solar uv variability.
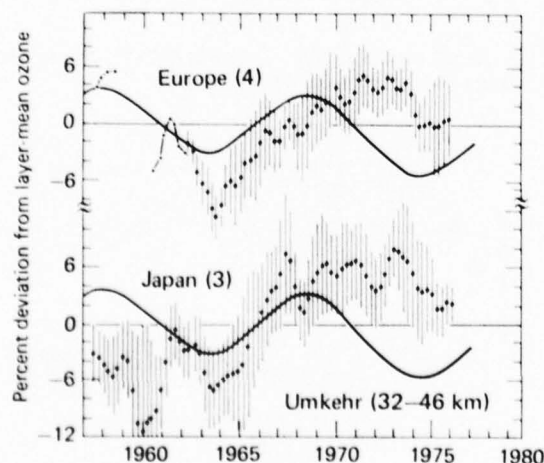

FIG. 11. Comparison of calculated layer-mean ozone variations to the analysis of Umkehr data by Angell and Korshover (1978a).
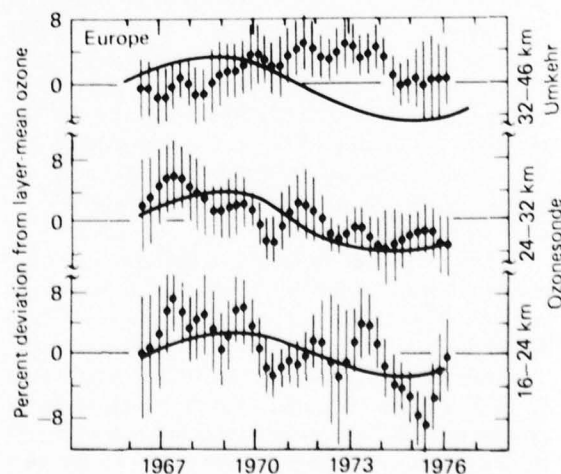
FIG. 12. Comparison of calculated layer-mean ozone variations to the analysis of ozone data by Angell and Korshover (1978c).

Figure 13 compares our calculated temperature variations for the layers 26-35 km, 36-45 km, and 46-55 km to rocketsonde temperature data (Angell and Korshover, 1978b). The temperature maxima and minima appear to be nearly in phase with the solar cycle variation except for the highest layer before 1968 (although the equatorial stations show a decrease through the entire time interval, see Angell and Korshover, 1978b). We calculate a decrease in temperature from 1969 to 1975 of 8.5 K, 6.5 K, and 3.1 K for layers 46-55 km, 36-45 km, and 26-35 km, respectively, in reasonable agreement with Angell and Korshover's estimate of about a 5 K decrease for the middle and upper stratosphere after 1970.
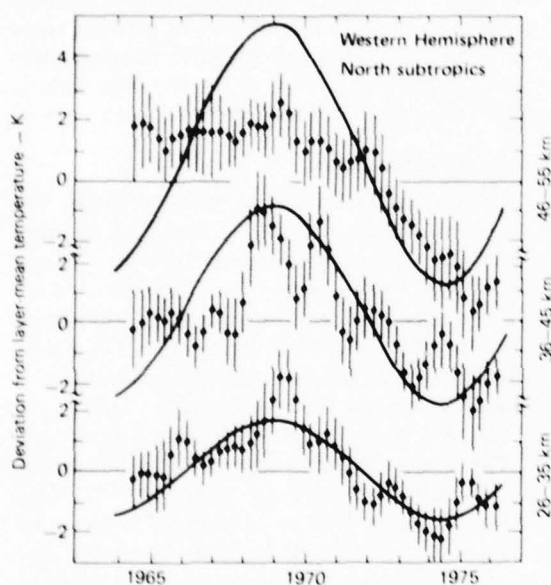

FIG. 13. Comparison of calculated layer-mean temperture changes to the analysis of rocketsonde data by Angell and Korshover (1978b).

Summary and Conclusions

The ozone response to a variety of solar conditions was examined and shown to depend on the relative ratio of uv variability above and below about 255 nm. The temperature increase due to increased heating by ozone absorption significantly affects the total ozone variation above 30 km. Ozone changes associated with solar flux variations are primarily due to changes in the photolysis rates for O_2 and O_3, and only secondarily due to changes in other minor species. We used what we consider to be the most reasonable variation in the solar uv flux consistent with available data to calculate a time history for ozone and temperature. We conclude that

the ozone record as published by Angell and Korshover (1978a,c) is apparently consistent with solar flux variations of the magnitude used, although more data are required to fully establish this relationship. Some of the less satisfactory results above 32 km require further analysis and more quantitatively reliable data. We calculate an ozone decrease of 3.6% for the 32-46 km layer from solar average conditions in 1966 to average conditions in 1977 due to the release of ClO_x from fluorocarbons. In our view this decrease would be difficult if not impossible to detect from the given ozone record if solar flux variations of the magnitude considered here were present during this period because the local ozone variations caused by solar flux variations could be as large as 13%. Insofar as the present calculations should be considered tentative, a long time series of measurements of the uv flux as a function of wavelength is needed to further establish the validity of these effects.

2.3 Effects of a Solar Eclipse on Stratospheric Chemistry

Solar eclipses are known to affect measurable quantities in the upper atmosphere. Various studies have discussed the response of ionospheric electron and positive ion densities to an eclipse (Landmark et al., 1970; Marriott et al., 1972; Anastassiades, 1970).

Other studies have discussed the possibility of changes in stratospheric and mesospheric ozone during an eclipse. Stranz (1961), using a Dobson ozonometer, measured approximately a 4% increase in total ozone shortly after the maximum phase of an eclipse in which only about 80% of totality was reached. Hunt (1965) attempted to explain this total ozone increase by using Chapman reactions in a theoretical study of the effect on ozone resulting from an eclipse. Hunt found that, at most, an increase of only 0.6% is to be expected, and that ozone should be affected only above 45 km.

In later observations, Randhawa (1968) and Ballard et al. (1969), both using rocket-borne ozonesondes, found measurable increases in ozone density above 50 km for the November 1966 eclipse near 22°S. Randhawa, for example, measured a factor of 2.6 increase in ozone at 57 km relative to the day before. However, Randhawa (1973) found no significant ozone change between 50 and 55 km for the July 1972 eclipse at 65°N. Grasnick et al. (1974) found no change in total ozone using a Dobson ozonometer for the March 1970 eclipse. They concluded that previous measurements had not corrected for solar limb darkening. However, Osherovich et al. (1974),

for the July 1972 eclipse, claim to have accounted for limb darkening and yet find approximately a 5% increase in the total ozone column.

Clearly, inconsistencies exist in the observations and in their utilization for validating ozone-related atmospheric chemistry as presently understood. In addition to ozone observations, measurements of other minor constituents during a solar eclipse could provide validation of the short lifetime chemistry used in atmospheric models. Consequently, experiments for upcoming solar eclipses, when properly supported by theoretical analysis, could contribute significantly to present understanding of atmospheric chemistry. In fact, proper measurements of trace species concentrations during an eclipse could provide a direct demonstration that currently proposed NO_x, HO_x, and ClO_x catalytic cycles are indeed concurrently functioning in the stratosphere in the manner suggested by laboratory chemistry. While detailed measurements of diurnal variations could provide similar knowledge, the difference in time scale between the diurnal cycle and a solar eclipse event suggests that the latter event may provide a clearer picture for understanding, as will be discussed.

The purpose of this study is to examine theoretically the expected effect of a solar eclipse on stratospheric minor constituents. Primary emphasis is given to calculations in advance of the total eclipse that will occur over North America on February 26, 1979 (Fiala and Lukac, 1977). Variations similar to those computed for this particular case should be expected for other total eclipses.

Methodology

The LLL one-dimensional model of tropospheric and stratospheric transport-kinetic processes from 0-55 km was used in these calculations. The full set of chemical reactions is given in Appendix A (Table A-1).

Fifty degrees north is the latitude at which totality will be the longest (3 minutes) for the February 1979 eclipse. In attempting to simulate typical expected atmospheric conditions for the February 26, 1979, solar eclipse, we modified the model by setting the temperature (Louis, 1974), tropospheric water vapor (Oort and Rasmussen, 1971), and the ozone distribution (Wilcox and Belmont, 1977) at 50° N winter conditions. Latitude and the solar declination angle in the model, necessary to calculate the solar zenith angle for photodissociation, were set to 50° and −8.8°, respectively.

While ozone in the model was held fixed for most calculations in order to simulate February 50° N conditions, the model was also run with calculated ozone to examine the expected response of

ozone to an eclipse. Our analysis has shown that fixing the ozone distribution does not significantly affect the temporal variations calculated for other species during the eclipse.

Assuming fixed total odd nitrogen and odd chlorine as calculated for midlatitudes, the model was run diurnally to equilibrium. The calculated daytime total column for NO_2 at 50° N of 1.9×10^{15} molecules/cm^2 is consistent with the observations of Noxon (1978).

Solar flux variations during the eclipse were based on Hunt (1965). The eclipse was assumed to start at 9:30 a.m. and end at 12:00 noon, corresponding to the February 1979 eclipse for 50° N in southern Canada. Totality was assumed to occur for 3 minutes beginning at 10:43:30 a.m. Based on measurements of sky brightness during an eclipse (Velasquez, 1971 and Dandekar and Turtle, 1971), the solar flux at totality, was reduced to 10^{-4} of the unobscured flux.

Results and Discussion

Those species having chemical lifetimes less than a few hours should be expected to vary significantly from normal diurnal behavior during a solar eclipse. In this study, we will emphasize the variations expected for those species most important to the chemistry of stratospheric ozone. Local concentrations of the species could be quite variable, and therefore we should focus on relative effects in the calculations rather than their absolute magnitudes.

The model calculated response of ozone during an eclipse essentially agrees with Hunt (1965). A significant increase in O_3 is to be expected in the upper stratosphere and in the mesosphere due to the conversion of $O(^3P)$ to ozone through the reaction $O(^3P) + O_2 + M \rightarrow O_3 + M$ accompanied by decreased photolysis of O_2 and O_3. The maximum increase in O_3, found at the end of totality, was computed to be 14 and 45% at 50 and 55 km, respectively. Larger percent changes should be expected in the mesosphere. Since most of the atmospheric ozone is at lower altitudes in the stratosphere, an insignificant change in the total ozone column is to be expected.

Figure 14 shows the variations expected during the eclipse in the concentration of nitric oxide, NO, and nitrogen dioxide, NO_2, at altitudes of 20, 30, and 40 km. The solid line indicates normal diurnal behavior from 8 a.m. to 2 p.m., while the dotted line shows the change in concentration expected during the eclipse. The decreased solar flux results in the NO_2 photolysis rate decreasing during the eclipse. Also, the rapid conversion of $O(^3P)$ to O_3 decreases the importance of $NO_2 + O(^3P) \rightarrow NO + O_2$. The NO is then rapidly converted to NO_2 during the eclipse primarily by the reactions $NO + O_3 \rightarrow NO_2 + O_2$ and $NO + ClO \rightarrow NO_2 + Cl$. By the end of totality, over a
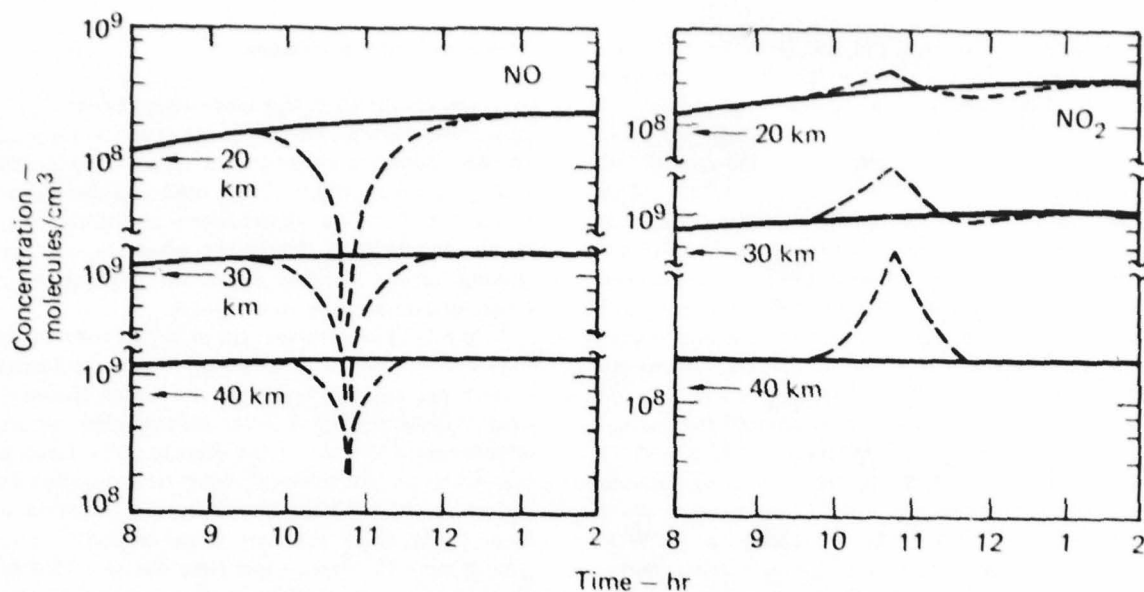
FIG. 14. Calculated responses of NO and NO₂ to a solar eclipse. The solid line indicates normal diurnal behavior; the dotted lines shows the expected solar eclipse effect.

factor of 10 decrease is calculated for NO at 20 and 30 km, with a factor of 6.5 decrease at 40 km. The maximum NO₂ concentration also occurs at the end of totality with values ranging from a factor of 1.4 higher than normal at 20 km to 6.4 at 40 km.

Except in the upper stratosphere (i.e., 40 km), the NO₂ increase is not directly proportional to the NO decrease. This is due to the relatively slow, yet significant, formation rates for ClONO₂ and N₂O₅ from NO₂. The peak increase in the ClONO₂ concentration occurs approximately 15 minutes after

totality due to the slow formation rate (ClO + NO₂). ClONO₂ is increased by 20% at 20 km and 42% at 30 km. N₂O₅ concentration increases by 11% at 20 km and 20% at 30 km. The slow reconversion of ClONO₂ and N₂O₅ to NO₂ causes the NO₂ to fall below the normal diurnal concentration at the end of the eclipse. The NO to NO₂ conversion is not affected in the upper stratosphere where neither ClONO₂ nor N₂O₅ is important as a temporary sink for NO₂.

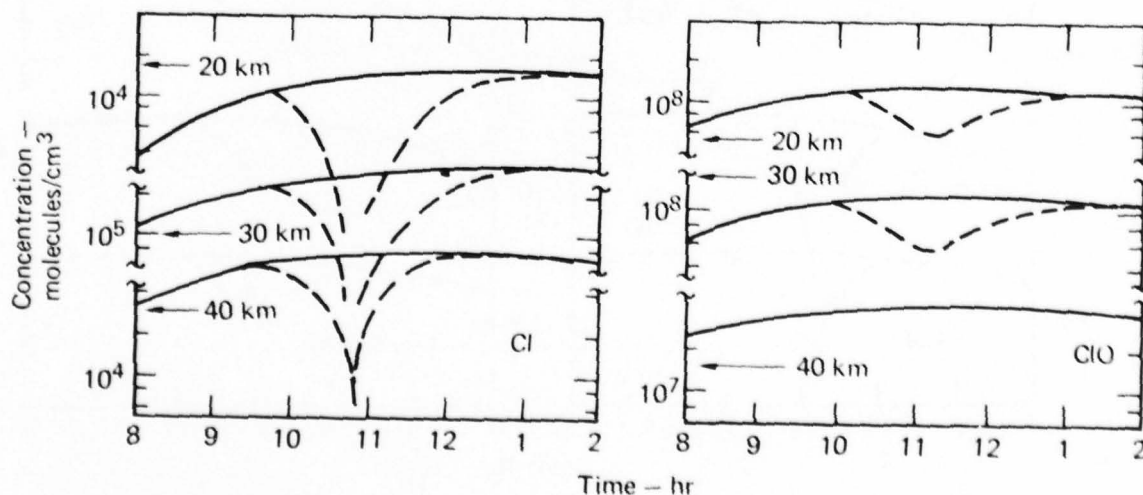The expected variations for Cl and ClO are shown in Fig. 15. Rapid conversion of Cl to ClO

FIG. 15. Calculated response of Cl and ClO to a solar eclipse.

17

during the eclipse occurs primarily through Cl + O₃ → ClO + O₂. The net effect on the ClO concentration is a decrease, however, due to more rapid formation of ClONO₂ resulting from increased NO₂ and reduced ClONO₂ photolysis. The minimum in ClO occurs approximately 25 minutes after totality. This time lag is caused by the slow formation rate of ClONO₂. As the solar flux increases after totality, the ClO concentration increases due to increased photolysis of ClONO₂. Little change in ClO is expected at 40 km where ClONO₂ formation is not important.

Both OH and HO₂ should decrease in concentration during an eclipse, as shown in Fig. 16. OH concentrations were reduced relative to the normal diurnal concentrations by a factor 2.7, 17.0, and 5.9 at 20, 30, and 40 km, respectively, with a minimum occurring at the end of totality. Smaller decreases are calculated for HO₂, with the minimum in HO₂ occurring approximately 15 minutes after totality. With the decreased importance of O(¹P) and NO during the eclipse, a balance between OH and HO₂ is maintained by the rapidly occurring reaction OH + O₃ → HO₂ + O₂ and the slightly slower reaction HO₂ + O₃ → OH + 2O₂. Odd hydrogen (OH and HO₂) loss occurs at a slower rate through conversion to water (OH + HO₂), H₂O₂ (HO₂ + HO₂) and HNO₃ (OH + NO₂ + M). Insignificant changes in the concentrations of H₂O₂ and HNO₃ were calculated. At 40 km, a slight increase in HO₂ is expected at totality due to the large rapid conversion of OH to HO₂ followed by the slower HO₂ loss mechanisms.

Summary and Conclusions

The results from this study suggest that significant and detectable variations are expected for some of the important stratospheric minor constituents during a solar eclipse. Such observations, particularly simultaneous observations of trace species, would demonstrate clearly the simultaneous functioning of the various important photochemical catalytic cycles in the stratosphere.

In principle, a similar type of information can be obtained by observations during a normal diurnal cycle, especially during sunrise and sunset. However, observations during a solar eclipse offer several advantages over that of the diurnal cycle. First, as was discussed, the relatively short time duration for the event followed a more clear identification of some of the major reactions in the important catalytic cycles. The same short time duration (2-3 hr) also minimizes the influence of atmospheric transport process in altering the local trace species concentrations. A longer observation period would subject the local chemistry to the influence of significant and usually unquantifiable mixing processes. Thus it is difficult to assess the relative role of chemistry and dynamics in determining the observation data. Also, because of the longer time scale, more interference through conversion to such temporary sinks as ClONO₂, N₂O₅ and HNO₃ should be expected. This increased interference makes it even more difficult to sort out the effects of the
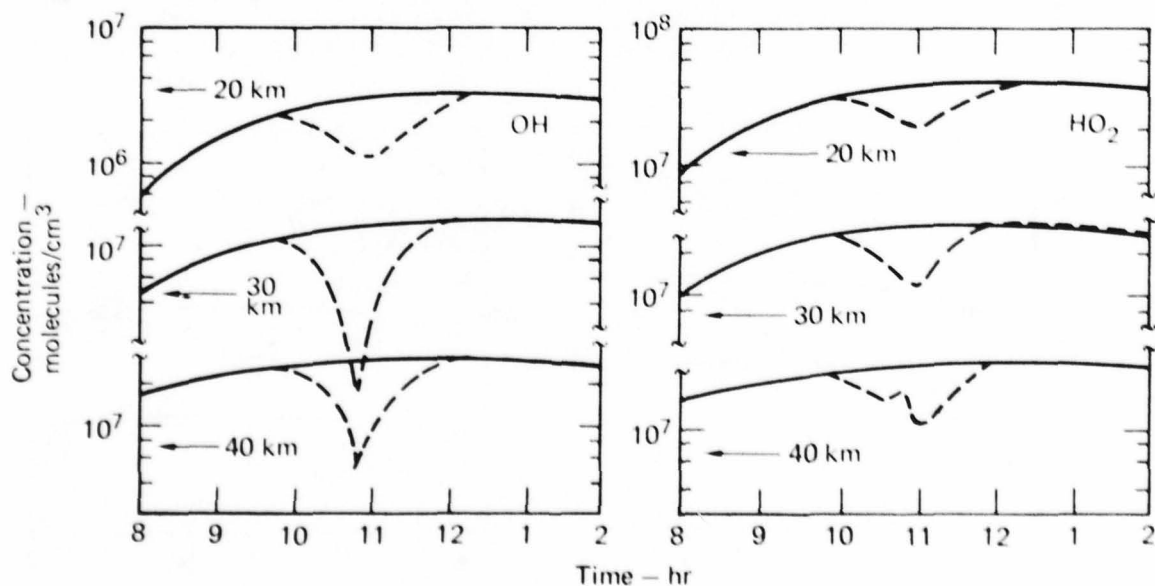

FIG. 16. Calculated response of OH and HO₂ to a solar eclipse.

18

catalytic cycle reactions. Finally, at sunrise and sunset there is considerable uncertainty on the proper treatment for the direct and scattered solar flux as a function of altitude when the sun is near the horizon. This then leads to uncertainty in the representation of photodissociation processes in the theoretical calculations. At least for the coming eclipse this will not be a limitation on the model, i.e., the eclipse takes place near local noontime. We would like to reemphasize the point that the theoretical predictions should be viewed mostly in a qualitative sense. The rates of decrease and increase in individual trace species concentrations and the relative changes in magnitudes at totality are the interesting parameters for comparison in the measurements. If an experimental program can be

established, and sufficient local conditions are known, new calculations can be carried out to truly test our understanding of stratospheric chemistry.

Although we have focused mainly on the local changes at individual altitudes, clearly total column changes are also observable. Since the variations for individual species at all altitudes all follow the same general individual trends, the total column for them also varies in the same manner. For example, the ClO column shows the same approximately 25-min delay in reaching minimum as is shown in Fig. 15, and the NO_2 column shows a factor 2 increase at totality. For those interested experimentalists, a more detailed report including various changes in total column and individual vertical profiles is available.

3. ASSESSMENT STUDIES

3.1 Change in Ozone because of SST Emissions, Chlorofluoromethanes, and Nitrous Oxide

The one-dimensional transport-kinetics model has been used to assess the potential chemical effects of several man-made perturbations to the stratosphere. Whenever significant changes occur to the model chemistry or the treatment of other physical processes, the assessment studies are repeated in order to assess the effect of the changes on the model sensitivity. The results presented here were obtained using the latest version of the model.

SST Emissions

The perturbation we use as a test case is an NO_x injection at a rate of 1000 molecules $cm^{-3}s^{-1}$ over a 1-km-thick layer centered at either 17 or 20 km altitude. This is equivalent to an annual injection rate of 6.2×10^8 kg/yr of NO_2 into the Northern Hemisphere. Using the NO_x emission indexes from the CIAP Report of Findings (Grobecker *et al.*, 1974), this injection rate is approximately equivalent to a fleet of 1200 Concorde-type SST's with a cruise altitude of 17 km or approximately 600 advanced SST's with a cruise altitude of 20 km.

With current technology the NO_x emission index is 18 g/kg of fuel. In the future it may be possible to reduce the NO_x emission index to 6 g/kg fuel. In addition to NO_x, water vapor is also emitted as a product of combustion but with an emission index of 1250 g/kg fuel. Future reductions in the NO_x emission index would not change the water vapor

emission index. Consequently, for an NO_x injection rate of 1,000 molecules $cm^{-3}s^{-1}$, the H_2O injection rate would be 177,000 molecules $cm^{-3}s^{-1}$, for current technology and 531,000 molecules for future technology. The latter case is equivalent to increasing the SST fleet size by a factor of three since the total NO_2 injection remains unchanged.

The computed change in total ozone is given in Table 2 for various NO_x and H_2O injections into an ambient atmosphere that includes current levels of chlorofluoromethanes. The ambient concentration of ClO_x is 1.19 ppbv.

Injecting only NO_x results in an increase in total ozone of slightly more than 2% for both 17- and 20-km injections. These increases in total ozone are larger than those computed a year ago (Luther *et al.*, 1977). Injecting only water vapor into the stratosphere results in a net reduction of total ozone. In the

Table 2. Change in total ozone due to emissions of NO_x and H_2O at injection altitudes of 17 and 20 km.

Species	Injection rate molecules $cm^{-3}s^{-1}$	Change in total ozone, %	
		17-km injection	20-km injection
NO_x	1,000	1.90	2.25
H_2O	0		
NO_x	1,000	1.72	1.82
H_2O	177,000		
NO_x	1,000	1.38	0.90
H_2O	531,000		

calculations in which both NO_x and H_2O are injected, the effect of the water vapor is small compared with that of NO_x. The change in the local ozone concentration is shown in Fig. 17 for the 17-km injection altitude.
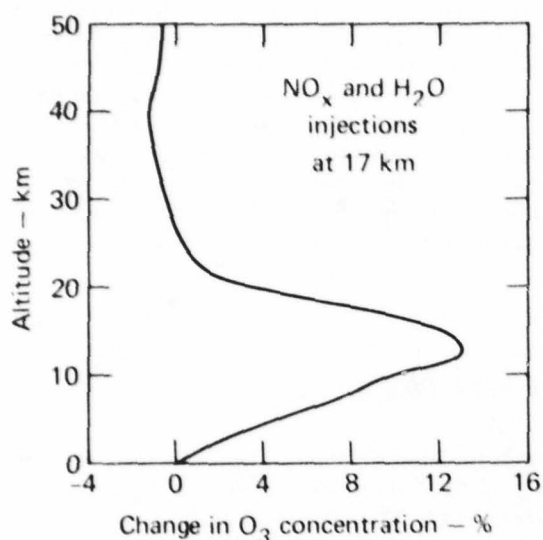

FIG. 17. The ΔO_3 vs NO_x injection with/without H_2O injection.

Chlorofluoromethanes

The perturbation we considered was the historical release of CFM's up to 1975 followed by a constant release rate at 1975 levels until steady state. The steady-state release rates are assumed to be 308 kt/yr for $CFCl_3$ and 380 kt/yr for CF_2Cl_2. The computed change in total ozone at steady state is -15.9%, which is slightly greater than the ozone reduction we computed a year ago (Luther et al., 1977, p. 20). The model calculations indicate a present-day reduction in total ozone of 2.2% relative to 1950. The change in local ozone concentration versus altitude at steady state is shown in Fig. 18.

Nitrous Oxide

Denitrification resulting from the use of nitrogen-base fertilizers has been proposed as a source of increased N_2O concentrations in the atmosphere (Crutzen, 1974). Increased world-wide use of nitrogen-base fertilizers may result in a doubling of N_2O concentration in the next 50-100 years, but the rate of increase of N_2O is highly uncertain. We have computed the change in total ozone for a range of increases of the N_2O concentration in the troposphere, and the results are shown in Fig. 19. A small
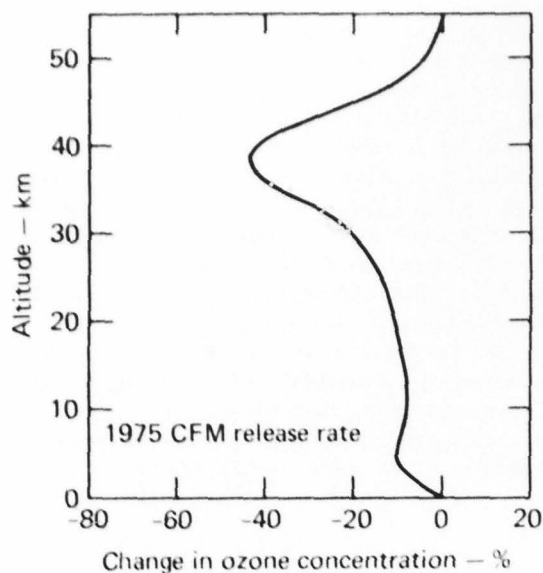
FIG. 18. The ΔO_3 vs z for CFM release at steady state.
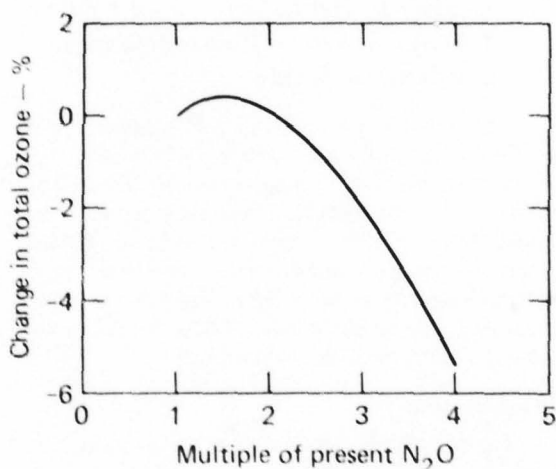
FIG. 19. Change in total ozone due to an increase in N_2O concentration at the earth's surface.

increase ($<0.5\%$) in total ozone is computed for increases in N_2O up to a doubling of the present tropospheric concentration (320 ppbv). Further increases in N_2O result in a decrease in total ozone ($\Delta O_3 = -2.0\%$ for $3 \times N_2O$ and $\Delta O_3 = -5.4\%$ for $4 \times N_2O$).

3.2 Potential Effects of Space-Shuttle Emissions

In 1976, we studied the potential effect of HCl in the exhaust of the space shuttle on the stratosphere.

Assuming 60 space-shuttle flights per year, we calculated a 0.25% reduction in total ozone at steady state using the LLL one-dimensional transport-kinetics model. Subsequent to these calculations, numerous changes occurred in the measured values of chemical reaction rates important to stratospheric chemistry. Probably the most important of these changes was the measurement of the rate of $HO_2 + NO \rightarrow OH + NO_2$ by Howard and Evenson (1977). This reaction was found to have a rate approximately 20 times faster than previously estimated, with a measured room temperature value of 8×10^{-12} cm^3/sec. In addition there were a number of smaller but nonetheless significant changes to other reaction rates (due to new measurements or estimates), particularly to reactions involving chlorine species. Details of these changes can be found in Chang *et al.* (1977). Because of these changes to model chemistry, it is useful to reexamine the potential stratospheric effects from future utilization of the space shuttle.

Besides emissions of approximately 60,000 kg of HCl per flight into the stratosphere (based on NASA estimates), there are also other exhaust products to be considered. There are expected to be approximately 260,000 kg of H_2O, 130,000 kg of CO, and 4,200 kg of NO emitted per flight in the exhaust. Aluminum oxides emitted in the exhaust may also be important to particulate formation, but the impact of this effect will not be assessed here. Water vapor and carbon monoxide are important minor constituents in the stratosphere with mixing ratios by volume of approximately 4-5 ppm for H_2O and 30 ppb for CO. This is to be compared with approximately 1.6 ppb of total odd chlorine, ClO_x (Cl, ClO, $ClONO_2$, and HCl), calculated for the present atmosphere in the model. Assuming 60 flights per year for the shuttle, emissions of HCl lead to approximately a 5% increase in ClO_x. Nitrogen oxide emissions are approximately 15 times smaller than the HCl emission, while the natural NO_x (NO, NO_2 and HNO_3) concentrations are approximately 8-10 times larger than the ClO_x concentration. Therefore, the NO emissions from space shuttles should be insignificant relative to the natural concentrations. The emissions of H_2O and CO from space shuttles are much larger than that of HCl, but their ambient concentrations are also much larger such that space shuttles should not be a significant perturbation to water vapor and carbon monoxide.

Model Results

The effect of chlorine emissions from space shuttles has been tested with the LLL one-dimensional transport-kinetics model. The chemistry in the model is essentially that recommended by the recent evaluation in the NASA report on Chloro-

fluoromethanes and the Stratosphere (Hudson, 1977). The hemispherically averaged HCl source function used in the calculation is shown in Fig. 20. This source function is based on data provided by NASA assuming 60 space shuttle flights per year. There are also emissions below 10 km, but these are in the troposphere where it is assumed that the HCl is rapidly removed from the atmosphere by heterogeneous or rainout processes.
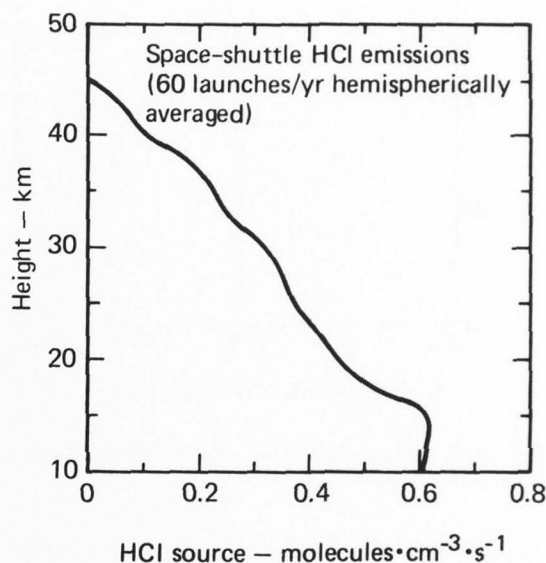

FIG. 20. Hemispherically averaged HCl emission rate in the stratosphere for an assumed 60 space-shuttle flights per year.

The calculated concentrations of atmospheric species derived for current levels of chlorofluoromethanes ($CFCl_3$ and CF_2Cl_2) were used as the initial conditions for this study. The model was then run to steady state (approximately 20 years of model time) using the assumed space shuttle HCl emission rate in Fig. 20. At steady state, total ozone was reduced 0.27% resulting from an increase in atmospheric ClO_x of 0.08 ppbv (a 5% increase in stratospheric odd chlorine). The calculated change in local ozone concentration is shown in Fig. 21. The maximum ozone reduction of approximately 1% occurs near 40 km. This is probably too small to have a significant impact on stratospheric circulation or climate.

The calculated change in total ozone is very similar to that computed previously in 1976. Based on calculations of the effect of chlorofluoromethanes on the stratosphere, a doubling in the computed effect of ozone would have been expected from the change in the rate for $HO_2 + NO$ (Hudson, 1977). However, other changes to model chemistry since the previous calculations have compensated for
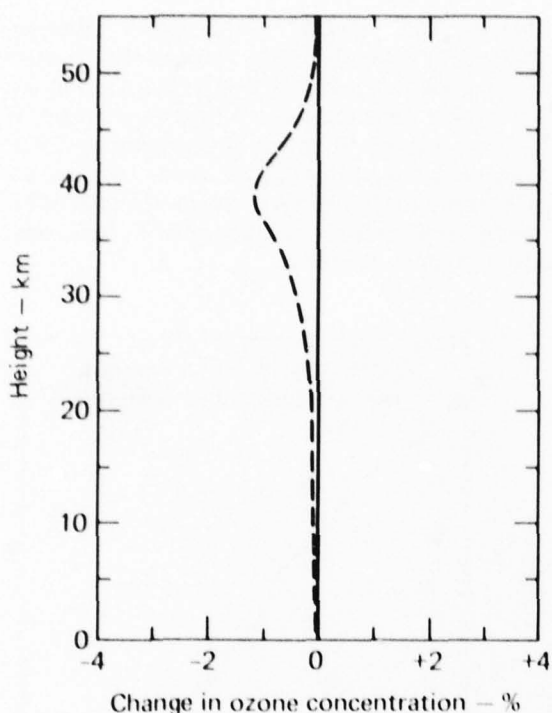
FIG. 21. Percent changes in local ozone at steady state resulting from space shuttle calculations.

this. In particular, reductions in the rates for the reactions $ClO + O \rightarrow Cl + O_2$ and $OH + HCl \rightarrow H_2O + Cl$ have occurred. The rate for $ClO + NO \rightarrow Cl + NO_2$ has increased slightly, and the N atom sink (Duewer *et al.*, 1977) for nitrogen oxides has been reduced in importance due to rate changes. In addition, the previous calculations had a smaller background ClO_x concentration because present levels of $CFCl_3$ and CF_2Cl_2 were not included. The additional ambient chlorine should reduce slightly the computed effects of an HCl injection.

3.3 Potential Effects of Solar Power Satellite Launch Vehicles

The feasibility of using giant solar power satellites to transmit energy to the earth is being studied by the Department of Energy. The system currently proposed would involve as many as 100 solar power satellites in geosynchronous orbit. Each satellite would provide 5 GW of electrical power which would be beamed to receiving stations at the ground by microwave transmission. Partial assembly of the satellites would be done at low-earth orbit before moving them to a geosynchronous orbit. A

Heavy Lift Launch Vehicle (HLLV) would be used to get raw materials into low-earth orbit. The two-staged (orbiter and booster) winged launch vehicle would carry a payload of about 400,000 kg. The booster would be capable of flying back to the launch site using air-breathing engines. The orbiter would glide back to the launch site upon returning from orbit. CH_4 and O_2 would be used as fuel for the booster and H_2 and O_2 would be used for the orbiter. The primary exhaust products of the HLLV are H_2O and CO_2. Some NO_x would be produced in the trailing shock wave.

Using preliminary estimates of the injection rates of NO_x and H_2O, we have examined the potential effect on the stratosphere of HLLV rocket-engine emissions. The one-dimensional transport-kinetics model was used for these calculations. Using data from Boeing for its proposed launch vehicle and assuming 391 flights per year, we used a source rate for H_2O in the model of 1.9×10^4 metric tons/km per year between the altitudes of 16 and 50 km and 6.8×10^3 metric tons/km per year above 50 km. All material is assumed to be deposited into the Northern Hemisphere in the calculation. The source rate for CO_2 should be comparable to that for water vapor, but this is expected to have a negligible effect on the amount of CO_2 in the stratosphere because of the high concentration of carbon dioxide relative to that for water vapor. The results indicate a maximum increase in water vapor of 1%, whereas there is a factor of 10^5 more ambient CO_2 than H_2O in the stratosphere.

The NO_x injection rates, shown in Fig. 22, are based upon data from NASA Langley. Estimates are for solid fuel motors of the type used with the space shuttle and have been scaled up by the number of rocket engines to be used in the HLLV (16) and by the projected number of flights per year (391). The NO_x injection rates were input into the model as nitric oxide. Again, the injections are assumed to be in the Northern Hemisphere.

The ambient atmosphere assumed in these calculations is that containing natural sources of odd chlorine but no chlorofluoromethanes. The added chlorine from chlorofluoromethanes should have little impact on these results. The unperturbed concentrations of H_2O and NO_x are given in Table 3. The model was run to equilibrium with the source rates described above.

A change in total ozone of -0.03% was calculated. Local percent changes in H_2O, HO_x, and O_3 are given in Table 4. The maximum calculated change in local ozone was -0.25% near the top of the stratosphere, corresponding to an increase in water vapor of 1.03%. The decrease in ozone is due to the added HO_x resulting from $O(^1D) + H_2O \rightarrow 2OH$.

22

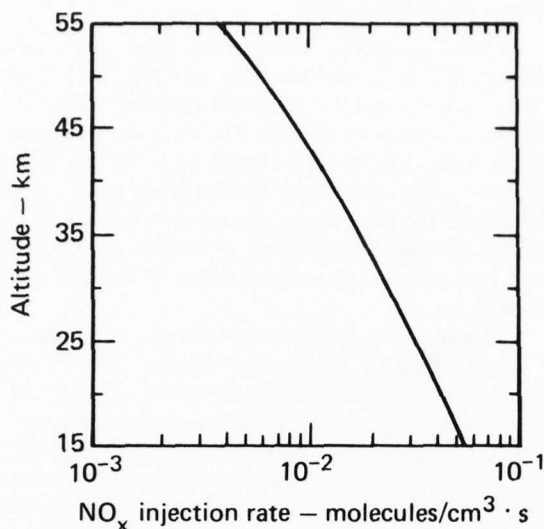FIG. 22. The NO$_x$ injection rate vs altitude, as caused by 391 HLLV flights per year.

Table 4. Changes in species concentrations.

| Altitude, km | Local percent changes[a] | | | |
	H_2O	HO_x[b]	NO_x[c]	O_3
20	0.20	0.06	0.04	0
25	0.50	0.46	0.09	−0.01
30	0.63	0.53	0.07	−0.01
35	0.74	0.49	0	−0.10
40	0.84	0.49	0	−0.17
45	0.95	0.48	0	−0.23
50	1.02	0.44	0	−0.25
55	1.03	0.41	0	−0.25

[a]Many of these percent changes are based on the last significant figure in computer printout from the model.

[b]$HO_x = OH + HO_2 + 2 \times H_2O_2$.

[c]$NO_x = NO + NO_2 + HNO_3$.

Perhaps a more important effect on the atmosphere may come from the launch vehicle injections of water vapor into the mesosphere, since this might affect ion recombination rates. Because our model has a maximum altitude of 55 km and does not treat ion chemistry in detail, we were unable to examine this effect.

Table 3. Unperturbed species profiles.

Altitude, km	Water vapor mixing ratio, ppmm	NO_x mixing ratio, ppmv
16	2.28	1.37×10^{-3}
18	2.35	2.59×10^{-3}
20	2.45	4.57×10^{-3}
22	2.58	7.40×10^{-3}
24	2.71	9.80×10^{-3}
26	2.80	1.13×10^{-2}
28	2.88	1.24×10^{-2}
30	2.95	1.34×10^{-2}
32	3.01	1.44×10^{-2}
35	3.10	1.57×10^{-2}
40	3.23	1.77×10^{-2}
45	3.31	1.82×10^{-2}
50	3.35	1.72×10^{-2}
55	3.36	1.64×10^{-2}

3.4 Effects of a Massive Pulse Injection of NO$_x$ into the Stratosphere

In the early nineteen-seventies, the important role of NO$_x$ in regulating stratospheric ozone was recognized (Crutzen, 1970; Johnston, 1971) and potential anthropogenic sources of NO$_x$ comparable to the natural sources were identified. These anthropogenic sources of NO$_x$ have included emissions from supersonic transports (Grobecker et al., 1974; Johnston, 1971; National Research Council, 1975a), N_2O produced as a result of denitrification from fertilized soils (Crutzen, 1974), and NO$_x$ from past nuclear tests (Foley and Ruderman, 1973) or from a future nuclear war (Hampson, 1974).

Largely as a result of the incorporation of recent measurements of chemical reaction rates that had previously been poorly known (Burrows et al., 1977; DeMore et al., 1977; Howard and Evenson, 1978; Molina et al., 1977), model-predicted ozone reductions from NO$_x$ sources designed to simulate a stratospheric aviation effluent (Broderick, 1977; Popoff et al., 1978; Wuebbles et al., 1977), N_2O increases (Logan et al., 1978) or nuclear tests (Chang et al., 1978) have been greatly reduced, and ozone increases are calculated for some scenarios. However, it has been estimated that the NO$_x$ input to the stratosphere after a nuclear exchange might be nearly two orders of magnitude greater than that produced by the other hypothesized NO$_x$ sources (MacCracken and Chang, 1975; National Research Council 1975a, b). Because the processes that have led to major

changes in model sensitivity to other types of NO$_x$ injection might be overwhelmed by such perturbations, we have reinvestigated model response to very large NO$_x$ pulse injections comparable to those that might be produced in a nuclear exchange.

We have used our one-dimensional transport-kinetics model to examine its response to large pulse NO$_x$ injections. The reaction rates are the same as those given in Table A-1 (Appendix A) with the exception of the reactions listed in Table 5.

The perturbations we considered consisted of pulse injections of NO$_x$ into the layers 9.5-16.5 km (approximately the stabilization altitude range expected for a 0.25-Mt device), 12.5-21.5 km (the approximate stabilization altitude range expected for a 1-Mt device), and 17.5-28.5 km (the approximate stabilization altitude range expected for a 4-Mt device). It was assumed that 6.7×10^{31} molecules of NO were produced per megaton of yield (COMESA, 1975) and that the NO produced is distributed uniformly over the Northern Hemisphere. NO$_x$ injections corresponding to total nuclear yields of 100, 1000, 5000, and 10000 megatons were considered for each of the three injection altitudes. These injection scenarios were designed to explore the effects of a range of device yields and total nuclear yield over a range that might be plausible and were not intended as realistic scenarios.

Results and Discussion

Two computed changes in total ozone are shown in Fig. 23 as functions of time. Very large ozone reductions are computed for a total yield of 10^4 Mt for 1- and 4-Mt devices. These ozone reductions differ little from those we obtained in 1975 for these device yields and total yield (MacCracken and Chang, 1975). In contrast, the ozone reductions computed for smaller total yield or smaller device yield are currently much smaller than computed previously.

Figure 24 shows the computed ozone profiles at 0.05, 0.5, and 1 year after the injection for a 10^4 Mt total yield and different device yields. The corresponding changes in local ozone concentration are shown in Fig. 25. For 4-Mt devices, ozone is greatly depleted at early times in the region of the initial injection, and substantial changes occur in the troposphere as a result of the increase in tropospheric photodissociation rates even before much injected NO$_x$ is transported into the troposphere. At later times the injected NO$_x$ mixes to higher and lower altitudes, reducing ozone at high altitudes while increasing ozone in the lower stratosphere and troposphere. Similar effects are shown for the results using 1-Mt devices, although tropospheric ozone is affected by NO$_x$ even at 0.05 years. For 0.25-Mt devices much of the perturbation appears in the

Table 5. Reaction rates that differ from 1977 Chemistry.

Reaction	k	
$O + HO_2 \rightarrow OH + O_2$	3.5×10^{-11}	a
$OH + HO_2 \rightarrow H_2O + O_2$	3.0×10^{-11}	a
$NO + HO_2 \rightarrow NO_2 + OH$	8×10^{-12}	a
$N + O_3 \rightarrow NO + O_2$	$2 \times 10^{-11} e^{-1070/T}$	a
$CO + OH \rightarrow CO_2 + H$	$1.4 \times 10^{-13} + 7.3 \times 10^{-33} M$	b
$NO + ClO \rightarrow NO_2 + Cl$	$1 \times 10^{-11} e^{+200/T}$	a
$NO_2 + ClO + M \rightarrow ClNO_3 + M$	$\dfrac{3.3 \times 10^{-23} T^{-3.34}}{1 + 8.7 \times 10^{-9} T^{-0.6} M^{0.5}}$	a
$ClNO_3 + O \rightarrow ClO + NO_3$	$3 \times 10^{-12} e^{-808/T}$	a
$H_2O_2 + h\nu \rightarrow 2OH$	Molina et al. (1977)	b
$O_3 + h\nu \rightarrow O_2 + O(^1D)$	We now use quantum yields from Demore et al. (1977)	

[a] These changes were made to bring us into consistency with the recommendations of Demore et al. (1977).

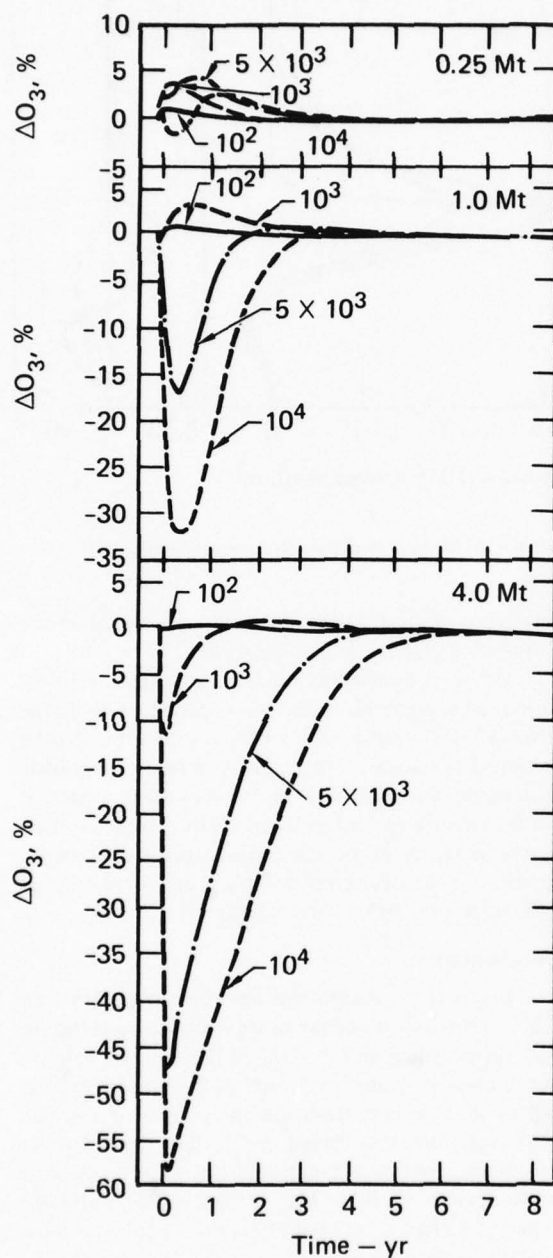[b] Based on our evaluation of recent measurements.

FIG. 23. Calculated change in total ozone vs time for various total nuclear yields in megatons. Calculations apply to individual device yields of 0.25, 1.0, and 4.0 megatons.

FIG. 24. Calculated ozone concentration vs altitude after a 10^4 Mt total yield pulse for various device yields.

troposphere immediately after the injection, and relatively small changes in ozone occur above the height of injection.

To understand the small change since 1975 in model sensitivity to very large NO_x injections in the middle stratosphere, it is necessary to understand the sources of altered model sensitivity to smaller injections. Two factors have been materially affected by changes in chemical reaction rates involving HO_2 used in the model.

Use of 3×10^{-11} cm^3/sec (DeMore et al., 1977) rather than 2×10^{-10} cm^3/sec for the reaction

$$HO_2 + OH \rightarrow H_2O + O_2$$
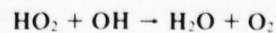
has substantially increased the computed concentrations of HO_x radicals in the model stratosphere. As a result, reactions of HO_x radicals with O and O_3 are more important sinks for ozone in current models than they used to be.

Use of 8×10^{-12} cm^3/sec (Howard and Evenson, 1978) rather than 2×10^{-13} cm^3/sec for the reaction

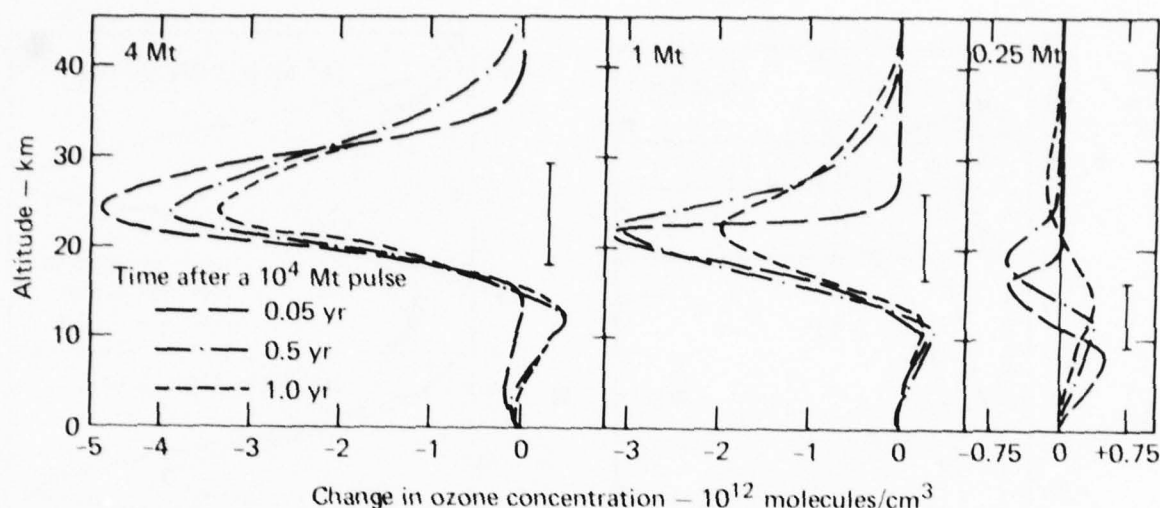$$HO_2 + NO \rightarrow NO_2 + OH$$

25

FIG. 25. Calculated change in ozone concentration versus altitude after a 10^4 Mt total yield pulse for various device yields.

has caused HO_x and NO_x catalyzed-ozone destruction cycles to interfere with each other to a greater extent, and has increased the efficiency of the NO_x enhanced methane "smog" mechanism for producing ozone. Both HO_x catalyzed-ozone destruction and methane "smog" ozone production are important in the lower stratosphere, and the use of newer data for HO_x reactions has led to a situation in which calculated ozone increases below about 20 km can be comparable to ozone decreases computed in the 20-45 km region. (NO_x induced ozone changes above ~45 km are small for NO_x injections below 30 km.) There is also an interference between NO_x and ClO_x ozone destruction cycles as a result of the reactions

$$NO + ClO \rightarrow NO_2 + Cl$$

and

$$NO_2 + ClO + M \rightarrow ClNO_3 + M .$$
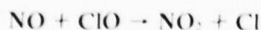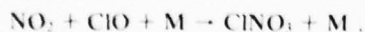
It should be noted that ozone production via the "smog" mechanism is ultimately limited by the methane flux, and if ozone destruction via HO_x or ClO_x is suppressed to the point it becomes negligible, further suppression of these processes will not cause further O_3 increases. Thus, the NO_x induced increases in lower stratospheric ozone cannot be increased without limit. Our largest injection scenarios result in 100-fold increases in the stratospheric burden of NO, and more than 10-fold increases in the burden of NO_y ($NO + NO_2 + HNO_3 + NO_3 + 2N_2O_5$). If a large NO_x pulse reaches the middle stratosphere, it will cause a very substantial computed ozone reduction which can overwhelm the

relatively modest ozone increases computed in the lower stratosphere and troposphere.

If NO_x is injected at a low enough altitude, most of it is transported into the troposphere partly in the form of HNO_3 and NO_2 where it is assumed to be removed by rainout processes. As a result, very little is transported into the midstratosphere where it would effectively reduce ozone. Thus the computed ozone increases in the lower stratosphere and troposphere are the dominant effects even for very large NO_x injections below approximately 15 km.

Conclusions

From these results we see that in contrast to other perturbation scenarios we continue to compute very large reductions in stratospheric ozone following a massive pulse injection of NO_x akin to that expected if several thousand megatons of nuclear explosives in the megaton range were to be detonated. However, smaller injections or injections from devices of 0.25 Mt or less yield would be expected to have a smaller effect on the total column of stratospheric ozone.

The ozone column recovers more rapidly in these calculations than it did in our earlier calculations (MacCracken and Chang, 1975). To a very large extent this is a reflection of our use of substantially faster transport above 22 km than in the earlier calculations. The growth of lower stratospheric ozone increases is a lesser contributor to the faster recovery.

A major limitation of these calculations is that no attention is paid to interactions of changes in stratospheric chemistry with the atmospheric structure. For perturbations as large as some of those

26

calculated here, such interactions might be important. Because of this as well as the other limitations of one-dimensional models (Chang *et al.*, 1978), the computed recovery rates should be interpreted cautiously. The computed peak ozone depletions are only weakly dependent on the transport parameters, K_z, for the very large injection scenarios at the higher altitudes. However, both the recovery time and the computed sensitivity to intermediate injections are sensitive to K_z since K_z influences the residence time of injected NO_x and the ambient distributions of NO_x and other species.

3.5 Effects of Stratospheric Perturbations on the Earth's Radiation Budget, and the Climatic Implications

Since the end of the CIAP program in 1975, there have been many changes to the numerical models used to compute the effects of stratospheric perturbations on O_3. New species (mostly chlorine containing) and new reactions have been added. Poorly known reaction rates have been remeasured using more accurate methods, and the O_3 photodissociation rate calculation has been improved. Temperature coupling and feedback on reaction rates have been added, and diurnal averaging has been accounted for more accurately. These changes have significantly modified the O_3 impact assessments. It is important, therefore, to re-analyze the impact of the potential changes in stratospheric composition on the global radiation budget.

In a previous assessment of the effects of changes in O_3 and NO_2 concentrations on solar absorption and stratospheric heating rates, Luther (1976) used species concentration profiles derived from our then-current transport-kinetics model. In updating the assessment, it is desirable to present the results in a more general way so that the radiative effects can be inferred for any transport-kinetics model results. This would also enable the radiative effects to be upgraded simply whenever there is a significant change in the stratospheric model assessments. We have attempted to do this for calculations of total solar absorption by O_3 and NO_2.

Comparison of Changes in Solar Absorption by O_3 and NO_2

In the case of a stratosphere perturbed by an NO_x injection, Luther (1976) showed that the increase in solar absorption by NO_2 at steady state was a significant fraction (35 to 50%) of the decrease in solar absorption by O_3. Since that time, the sen-

sitivity of O_3 to an NO_x injection has decreased in the transport-kinetics models. Consequently, the change in solar absorption by NO_2 is now expected to be a much larger fraction of the change in solar absorption by O_3.

Solar absorption by O_3 is shown in Fig. 26 as a function of O_3 column density. The absorption rate given is the instantaneous value for a solar zenith
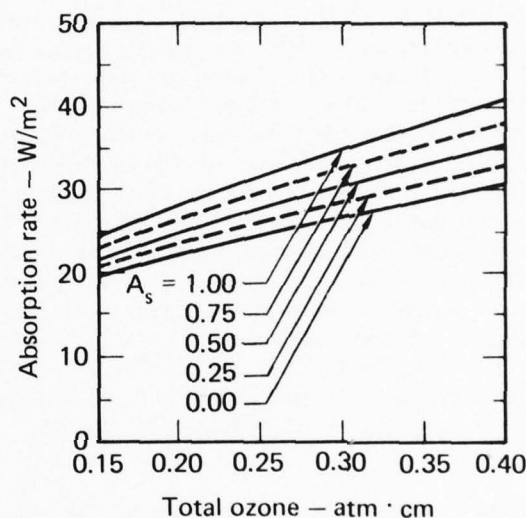

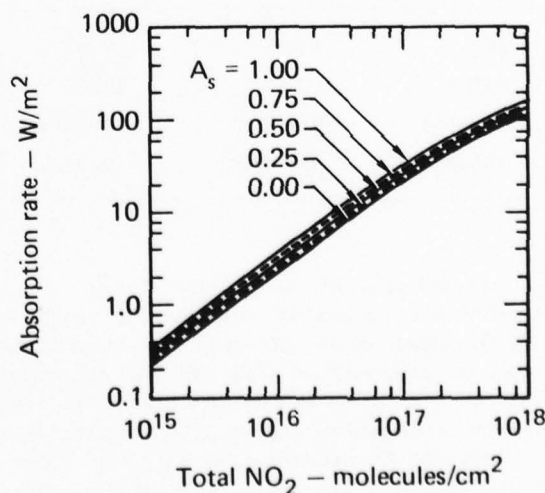FIG. 26. Solar absorption by ozone for a solar zenith angle of 60°. A_s is the surface albedo.

FIG. 27. Solar absorption by NO_2 for a solar zenith angle of 60°.

27

angle of 60°. The radiative transfer model used to compute the solar absorption rate includes Rayleigh scattering and assumes a cloudless, plane-parallel atmosphere above an isotropically scattering ground (Luther, 1976). The solar absorption by NO_2 is shown in Fig. 27 also for a solar zenith angle of 60°.

Ambient and perturbed species concentration profiles were computed using the LLL one-dimensional transport-kinetics model. The model chemistry is listed in Table A-1, except for a few reactions. The rates used for the reactions $O_3 + HO_2$, $O_3 + H$, $HO_2 + HO_2$, and $Cl + HO_2$ are given in Table A-2. The rate of 9.0×10^{-12} was used for the reaction $NO + HO_2$, and a rate of $5.0 \times 10^{-13} \exp(-1238/T)$ was used for $ClO + ClO$. The reactions $O(^1D) + O_3$ and $HO_2 + HO_2 + H_2O$ were not included. Two perturbation cases were considered: NO_x injections at 17 or 20 km at the rate of 1000 molecules $cm^{-3} s^{-1}$ uniformly distributed over a 1-km-thick layer. This corresponds to a hemispheric injection rate of 6.2×10^8 kg/yr of NO_2. Changes in the O_3 and NO_2 column densities and solar absorption rates for a solar zenith angle of 60° and a surface albedo of 0.25 are summarized in Table 6. The unperturbed column densities are 9.730×10^{18} molecules/cm^2 (0.382 atm.cm) for O_3 and 3.506×10^{15} molecules/cm^2 for NO_2.

Table 6. Increases in total atmospheric solar absorption by O_3 and NO_2 due to NO_x injections at the rate of 6.2×10^8 kg/yr. Calculations are for a solar zenith angle of 60° and a surface albedo of 0.25.

Quantity	NO_x injection altitude	
	17 km	20 km
ΔO_3	1.06%	0.39%
ΔNO_2	6.87%	15.60%
$\Delta Abs(O_3)$	0.16 W/m^2	0.06 W/m^2
$\Delta Abs(NO_2)$	0.06 W/m^2	0.13 W/m^2

In both cases the injection of NO_x resulted in a small increase in total O_3. Although the changes in the O_3 column density are small, the change in the local O_3 concentration (Fig. 28) may be several percent. The change in column density reflects the net difference between regions of O_3 increase (below 22 km) and O_3 decrease (above 22 km). Consequently, although the change in the net heating may be small, the redistribution in altitude of where this heating occurs may be significant. The change in the local concentration of NO_2 is shown in Fig. 29.
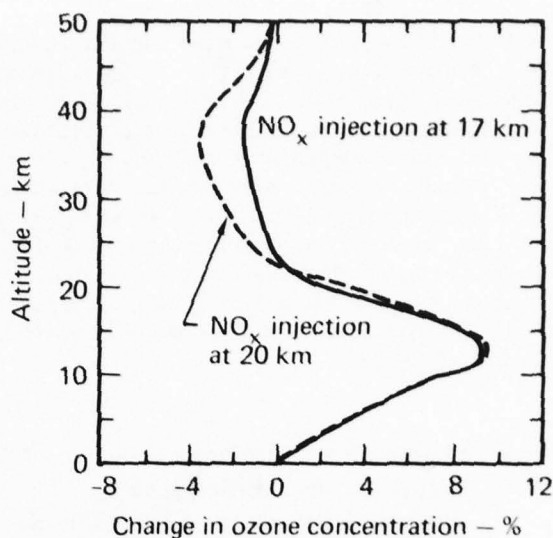
FIG. 28. Change in local ozone concentration due to NO_x injections (as NO_2) of 6.2×10^8 kg/yr.
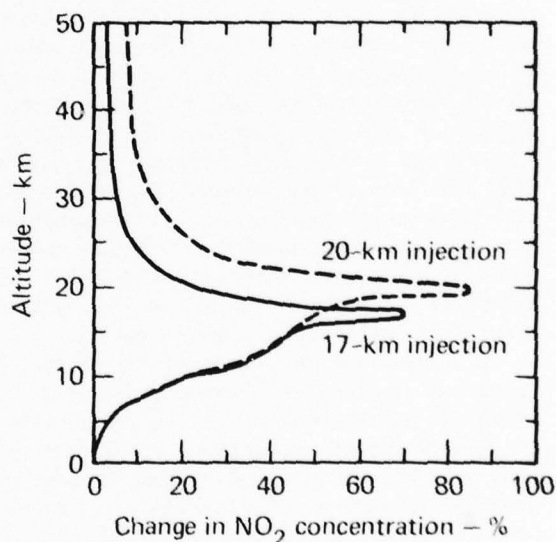
FIG. 29. Change in local NO_2 concentration due to NO_x injections (as NO_2) of 6.2×10^8 kg/yr.

Changes to the Solar Radiation Budget and Heating Rates

In addition to the two NO_x injection cases already described, we also considered the steady-state O_3 reduction due to CFM's at the 1975 release rate. The change in O_3 column density computed at steady state was −14.4%. For a solar zenith angle of 60° and a surface albedo of 0.25, there is a reduction

in solar absorption by O_3 of 2.45 W/m². The change in the local O_3 concentration is shown in Fig. 30. There is a reduction in O_3 concentration at all altitudes with the largest percent reduction occurring at 40 km.

In addition to affecting the gaseous absorption of solar radiation in the stratosphere, changes in stratospheric composition also affect solar absorption in the troposphere by changing the atmospheric transmissivity. A decrease in O_3 column density, for example, allows more solar radiation to reach the troposphere, thereby increasing both the amount of solar absorption and the amount of radiation scattered back to space. Changes to the solar radiation budget are presented in Table 7 for the three perturbation cases. The net solar flux at the top of the atmosphere is defined as the incoming flux minus the outgoing flux. The values for the change in solar absorption in the troposphere include the change in gaseous absorption and the change in absorption by the earth's surface. The changes in the instantaneous

solar absorption rates for the NO_x injection cases are small compared with the unperturbed values. The CFM perturbation case, on the other hand, represents a significant perturbation to the solar radiation budget. There is a significant reduction in the solar absorption in the stratosphere and an increase in the troposphere.

The changes in the O_3 and NO_2 solar heating rates are presented in Fig. 31 for the 17-km NO_x injection and in Fig. 32 for the 20-km NO_x injection. The O_3 and NO_2 both contribute to an increase in the heating rate in the lower stratosphere. Consequently, the change in solar heating tends to increase the temperature in the upper stratosphere.

The change in the solar heating rate due to a CFM perturbation is shown in Fig. 33. The reduction in the solar heating rate in the lower stratosphere is approximately the same magnitude as the increase in heating rate computed for the NO_x injection cases. The change in the solar heating rate is −0.07 K/day at 24 km, −0.02 K/day at 20 km, and −0.01 K/day at 18
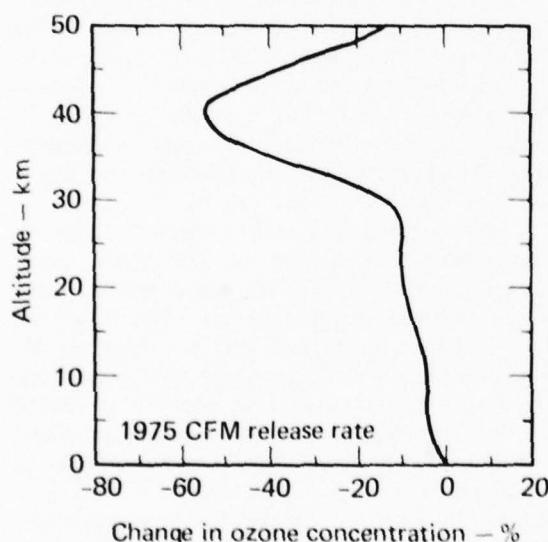
FIG. 30. Change in ozone concentration at steady state due to CFM's at the 1975 release rate
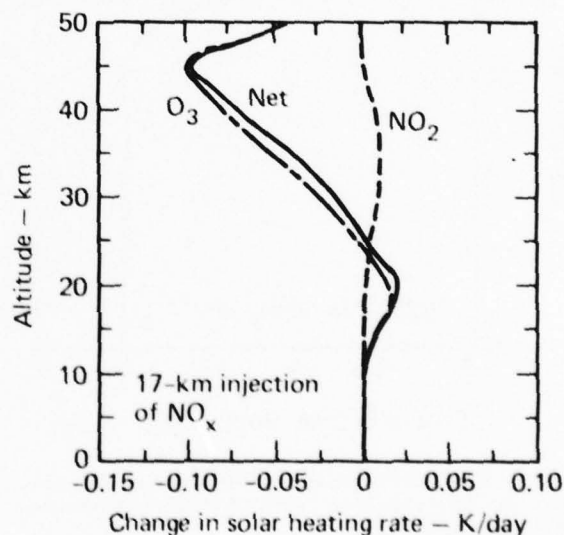
FIG. 31. Change in the instantaneous solar heating rates for a solar zenith angle of 60° at. A = 0.25 due to an NO_x injection at 17 km.

Table 7. The perturbed solar radiation budget (solar zenith angle = 60°, surface albedo = 0.25).

Quantity	Perturbation case			Unperturbed value
	NO_x, 17 km	NO_x, 20 km	CFM	
ΔNet solar flux at top of atmosphere	0.1 W/m²	0.0 W/m²	−1.0 W/m²	470 W/m²
ΔStratospheric solar absorption	0.13	0.08	−2.35	34.1
ΔTroposphere/surface solar absorption	−0.1	−0.1	1.3	436

29
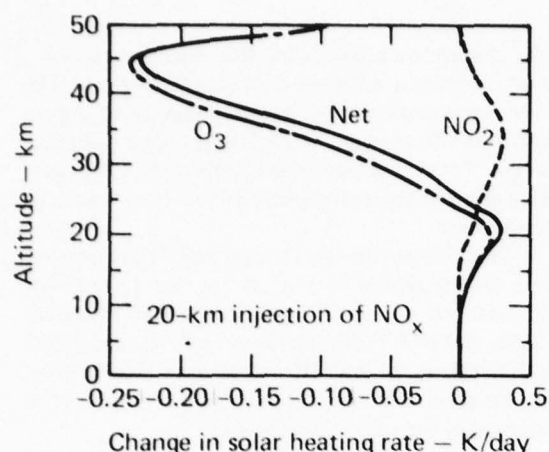
FIG. 32. Change in the instantaneous solar heating rates for a solar zenith angle of 60° and A. = 0.25 due to an NO₃ injection.
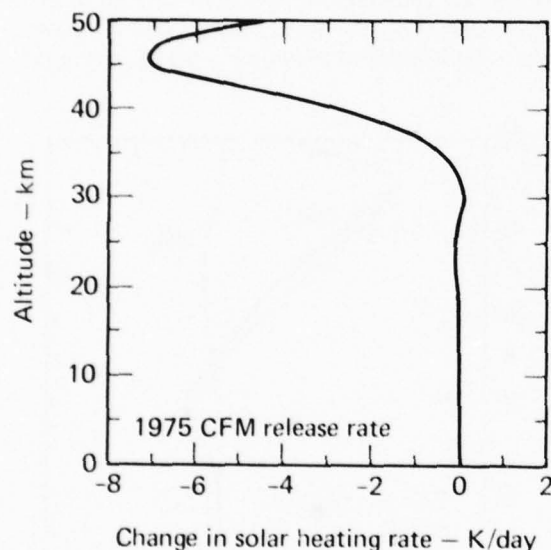
FIG. 33. Change in the solar heating rate of ozone at steady state for a solar zenith angle of 60° and A. = 0.25 due to CFM's at the 1975 release rate.

km. In this case there is cooling at all altitudes with the largest effect in the upper stratosphere.

Potential Climatic Impact

The climatic impact of changes in stratospheric composition depends upon both the solar and long-wave effects of the perturbation. Changes in temperature, in addition to affecting the transfer of longwave radiation, also affect atmospheric stability and transport. Here we will consider only the global impact of the solar and longwave effects and neglect any potential feedback on transport.

A previous assessment of the effect of changes in O_3 and NO_2 on surface temperature by Ramanathan et al. (1976) showed a cooling at the surface associated with a reduction in O_3 due to an NO_x injection. Only reductions in O_3 were considered (not increases), and it was assumed that the changes in O_3 and NO_2 were uniform (percentagewise) between 12 and 40 km. Our present results differ from these modeling assumptions in that the changes in O_3 and NO_2 concentrations are not uniform with altitude, and there is a net increase in O_3 column density rather than a decrease. Nevertheless, the work of Ramanathan et al. (1976) is useful because it demonstrates the importance of the longwave effect of the perturbation. The reduction in total O_3 tended to warm the troposphere by increasing the transmissivity of the stratosphere for solar radiation. The reduction in stratospheric temperature due to reduced O_3, however, had a greater effect on the longwave radiation emitted downward from the stratosphere. The net result was a slight reduction in surface temperature.

A similar calculation using our current modeling results would predict an increase in temperature in the lower stratosphere (Luther and Duewer, 1978). It is possible that the longwave effect would also dominate in this case. Although the net change in temperature is uncertain, it is clear that the longwave effect would tend to warm the troposphere, whereas the solar effect would tend to cool.

In attempting to assess the effect of changes in stratospheric composition on the global mean surface temperature, it is desirable that the same model be used throughout the study. Since we do not have a climate model that may be applied to this study, we will rely on the results of other researchers. The two methods used here are the published results of Ramanathan's radiative equilibrium model and Budyko's (1969) empirical formulation relating the change in outgoing longwave flux at the top of the atmosphere to the change in surface temperature.

According to Ramanathan's model (Ramanathan et al., 1976), the change in surface temperature is related to the change in ozone by

$$\Delta T_s = (0.009 \text{ to } 0.014 \text{ K}) \Delta O_3 ,$$

where ΔO_3 is the percent change in ozone concentration applied uniformly over the altitude region 12-40 km. The first coefficient applies to the assumption of constant cloud top altitude whereas the second coefficient applies to the assumption of constant cloud top temperature. A similar expression relates the change in surface temperature to the percent change in NO_3 concentration between 12 and 40 km:

$$\Delta T_s = (3 \times 10^{-4} \text{ to } 6 \times 10^{-4} \text{ K}) \, \Delta NO_2 \, .$$

The expressions are not applicable directly to our results, but they may be used to estimate an approximate upper limit on ΔT_s.

The present changes in O_3 and NO_2 averaged over various altitude ranges between 12 and 40 km are given in Table 8. Since the change in species concentrations in the lower stratosphere will have a greater effect on the downward longwave flux into the troposphere than changes at higher altitudes, we can get a rough estimate of ΔT_s by using the values of ΔO_3 and ΔNO_2 for the 12-22 km region. Using these values tends to overestimate ΔT_s because it assumes that the ozone concentration has increased by the same percentage at higher altitudes when the calculation indicates that smaller changes occur at higher altitudes.

Table 8. Percent change in O_3 and NO_2 concentrations averaged over various altitude ranges.

Perturbation	Quantity	Average over altitude range, km		
		12-22	22-40	12-40
NO_x injection at 17 km at rate of 6.2×10^8 kg/yr	ΔO_3, %	4.3	−0.7	0.7
	ΔNO_2, %	30	6.0	8.7
NO_x injection at 20 km at rate of 6.2×10^8 kg/yr	ΔO_3, %	4.9	−2.0	0.0
	ΔNO_2, %	56	15.6	20.1

Values of ΔT_s computed using the relations above and values of ΔO_3 and ΔNO_2 for the 12-22 km region are given in Table 9. The change in surface temperature is estimated to be less than 0.1 K for both the 17- and 20-km injection altitudes. For comparison, values are also given in Table 4 for ΔT_s using Budyko's empirical formulation

$$\Delta T_s = 0.701 \text{ K } \Delta F \, .$$

where ΔF is the change in the outgoing longwave flux in W/m^2 at the top of the atmosphere. The value for ΔF is obtained by dividing in half the change in net solar flux at the top of the atmosphere given in Table 7 to account for day-night averaging. At equilibrium the change in the outgoing longwave flux equals the change in the net incoming solar flux. Again the computed values of ΔT_s are significantly less than 0.1 K.

The same methods were applied to the CFM perturbation results. In this case, however, the value

Table 9. Estimated change in surface temperature using different assessment methods.

Perturbation	Change in surface temperature, K	
	Ramanathan	Budyko[a]
NO_x injection at 17 km		
ΔO_3	0.04 to 0.06[b]	
ΔNO_2	0.01 to 0.02[b]	
$\Delta O_3 + \Delta NO_2$		0.04
NO_x injection at 20 km		
ΔO_3	0.04 to 0.07[b]	
ΔNO_2	0.02 to 0.03[b]	
$\Delta O_3 + \Delta NO_2$		0.02
CFM's at 1975 release rate		
ΔO_3	−0.13 to −0.21	−0.35
$\Delta CFCl_3, \Delta CF_2Cl_2$[c]	0.44	0.44

[a] $\Delta T_s = 0.701 \text{ K } \Delta F(W/m^2)$.

[b] The method used to determine these values tends to overestimate the change in surface temperature.

[c] From Wang *et al.* (1976), $\Delta T_s = 0.38$ to 0.57 K.

of ΔO_3 averaged over 12-40 km (Table 8) was used to estimate ΔT_s. The resulting values of ΔT_s are presented in Table 9. In this case the change in the global mean temperature is on the order of several tenths of a degree, which may be a significant climatic perturbation since regional changes in temperature might be several times greater than the global mean. Pollack *et al.* (1976) suggest that 0.1 K is a threshold value for considering the change in global mean surface temperature to be significant. Computing values of ΔT_s associated with past major changes in climate, they infer that values below 0.1 K would not have major consequences.

In the case of a CFM perturbation, there is the additional effect of the longwave properties of CF_2Cl_2 and $CFCl_3$. At steady state we compute the tropospheric concentrations of the CFM's to be larger than present day levels by 0.6 ppbv for $CFCl_3$ and 1.52 ppbv for CF_2Cl_2. The greenhouse effect of CFM's has been studied by Ramanathan (1975), and he finds the following relationships between the change in surface temperature and the change in tropospheric CFM concentration:

$$\Delta T_s = 0.215 \text{ K } \Delta CF_2Cl_2 \text{ (ppmv)}$$

$$\Delta T_s = 0.180 \text{ K } \Delta CFCl_3 \text{ (ppmv)} \, .$$

Ramanathan's model results therefore imply an increase in surface temperature of 0.44 K due to

CFM's, which is the same magnitude as predicted using Budyko's empirical formulation. A similar calculation has been performed by Wang *et al.* (1976) in which an increase in surface temperature of 0.38 to 0.57 K due to these CFM concentrations is predicted. This result brackets the value of 0.44 K obtained by the other methods.

We now consider the potential climatic effect of the water vapor injected into the stratosphere along with the NO_x from SST engine emissions. Assuming an emission index of 1250 g/kg fuel for water vapor and 18 g/kg fuel for NO_x, the associated water vapor injection rate would be 4.3×10^{10} kg/yr. According to our model calculations in which the stratospheric water vapor profile is computed, this would lead to an increase in the stratospheric water vapor mixing ratio of 0.1 ppmm for a 17-km injection and an increase of 0.31 ppmm for a 20-km injection. Ramanathan's model was also used in the CIAP study to estimate the change in surface temperature resulting from a change in stratospheric water vapor mixing ratio (Grobecker *et al.*, 1974):

$$\Delta T_s = (0.2 \text{ to } 0.3 \text{ K}) \Delta H_2O \text{ (ppmm)} .$$

The estimated change in surface temperature due to these changes in stratospheric water vapor are given in Table 10. These values of ΔT_s are larger than those due to ΔO_3 and ΔNO_2 resulting from SST engine emissions, but they are still less than 0.1 K.

In addition to NO_x and water vapor, SST engines also emit SO_2, which is converted to sulfate aerosols. Assuming an emission index of 1.0 g/kg fuel, the SO_2 injection rate would be 3.4×10^7 kg/yr when the NO_x injection rate is 6.2×10^8 kg/yr. The change in surface temperature due to increased stratospheric aerosols (75% H_2SO_4) has been computed by Pollack *et al.* (1976). Using a radiative-convective model, they find

$$\Delta T_s = (-6.3 \text{ to } -10 \text{ K}) \Delta \tau .$$

where $\Delta \tau$ is the increase in the stratospheric optical depth. Pollack *et al.* find that $\Delta \tau$ is related to the mass density (m) of surfate aerosols in $\mu g/m^3$ averaged over a 10-km thick layer by the expression $\Delta \tau = 0.031$ m. the expression $\Delta \tau = 0.038$ m was used in the CIAP Report of Findings (Grobecker *et al.*, 1974). The aerosol mass density is obtained from the expression

$$m = HFtc \, M_a/M_c .$$

where H is the fraction of the aerosols deposited in a given hemisphere, F is the SO_2 emission rate, t is the residence time, c is the conversion efficiency, M_a is the molecular weight of the aerosol, and M_c is the molecular weight of SO_2. For a sulfuric acid solution that is 75% H_2SO_4 by weight, $M_a/M_c = 1.6$. Values for the various quantities used by Pollack *et al.* (1976) and used in the CIAP Report of Findings are shown in Table 11. The resulting values for $\Delta \tau$ are considerably smaller (by nearly a factor of 3) using Pollack *et al.*'s values. In both cases the values for ΔT_s are estimated to be less than -0.01 K for a 17-km injection altitude and less than -0.02 for a 20-km injection altitude.

Conclusions

Changes in O_3 and NO_2 concentrations due to an NO_x injection lead to increases in the total solar absorption of both species. These increases are small, however, when compared to the total energy absorbed by the stratosphere, and the climatic effect is estimated to be negligible. Using the criterion that changes in surface temperature less than 0.1 K would not have major consequences, none of the SST engine emissions (NO_x, H_2O, and SO_2) are estimated to have a major climatic effect. The largest individual effect on surface temperature is that of water vapor, which is estimated to cause a temperature increase of 0.06-0.09 K for a 20-km injection at 4.3×10^{10} kg/yr. The combined effect of all engine emissions on climate is likely to be an increase in global mean temperature of less than 0.1 K.

In the case of a CFM perturbation, there is a significant impact on the solar radiation budget leading to a decrease in the solar heating of the stratosphere and an increase in solar heating of the troposphere and earth's surface. There is also an increase in the solar flux scattered back to space. There is considerable uncertainty about the change in surface temperature at steady state caused by the reduction of O_3 due to CFM's released at the 1975 rate. Our estimates range from -0.13 K to -0.35 K. The greenhouse effect of $CFCl_3$ and CF_2Cl_2, on the other hand, tends to warm the surface by an estimated 0.44 K. The net effect on surface temperature is

Table 10. Change in surface temperature due to an increase in stratospheric water vapor.

Altitude of injection, km	H_2O in stratosphere, ppmm	ΔT_s, K
17	0.11	0.02–0.03
20	0.31	0.06–0.09

Table 11. Factors used in calculating the change in surface temperature due to an SO$_2$ emission rate of 3.44×10^7 kg/yr in the Northern Hemisphere.

Source	Altitude of injection, km	Residence time, years	Conversion efficiency	Fraction in hemisphere	$\Delta\tau$	ΔT_s,[a] K
Pollack et al., 1976	17	0.978	0.869	0.7	3.9×10^{-4}	−0.002 to −0.004
$\Delta\tau = 0.031$ m[b]	20	1.715	0.945	0.7	7.6×10^4	−0.005 to −0.008
CIAP Report of Findings, 1976	17	1.70	0.83	1.0	1.1×10^{-3}	−0.07 to −0.011
$\Delta\tau = 0.038$ m	20	3.00	0.93	1.0	2.3×10^{-3}	−0.014 to −0.023

[a] $\Delta T_s = (\text{-}6.3 \text{ to } \text{-}10 \text{ K}) \, \Delta\tau$.

[b] m is the mass density of sulfate aerosols in g/m^3 averaged over a 10-km thick shell.

uncertain, but it may be in excess of ±0.1 K, which would be considered significant. The potential climatic effect of a CFM perturbation needs further study to reduce the large uncertainty associated with these results.

3.6 Effect of Ozone Reductions on Erythema Dose

Because reductions in total ozone would permit greater amounts of uv radiation to reach the surface of the earth (Cutchis, 1974; Halpern et al., 1974), a number of studies have been performed with the goal of assessing biological sensitivity to ozone-induced changes in uv radiation (National Research Council, 1973). One approach has been to correlate skin cancer incidence data directly with ozone layer thickness. The possible influence of such factors as duration of sunlight, clothing and exposure habits, and optical path length have been considered (McDonald, 1971; van der Leun and Daniels, 1975). Another approach has been to explicitly consider the dose of uv radiation received as a function of ozone amount and other climatic variables (Green and Mo, 1975). The radiation dose is then related to cancer incidence after weighting by a wavelength-dependent function accounting for variation in radiation efficacy. This second approach, though less direct, is appealing because the mechanism of cancer production is more fully represented, and it allows for experimentation with combinations of independent variables outside the rather narrow range of reliable observation.

As the first step in this approach, Green and co-workers developed a semi-empirical model for calculating uv radiation at the surface of the earth in the spectral region 280-340 nm (Green et al., 1974a,b; Mo and Green, 1974). They have calculated erythema (sunburn) dose as a function of total ozone, solar zenith angle, latitude, season, and cloud amount. Their model was also used in the Climatic Impact Assessment Program's analysis of ozone depletion (Green et al., 1975).

One feature of this model, and uv dosimetry in general (Berger et al., 1975), is that the receiver is assumed to be horizontal. The geometry of humans, however, is such that the majority of exposed skin would normally be in a nonhorizontal position. In fact, the horizontal projection of an upright person amounts to only a few percent of total surface area (Fanger, 1970).

The report of the National Research Council (1976a) summarizes the specific sites of origin of primary melanoma skin cancer. The data show the predominant localization of sites of origin to areas of the skin that are constantly exposed, such as the trunk and legs of males. These are, in general non-horizontal surfaces, which suggests that receiver orientation should be considered in the study of uv dose.

In last year's annual report (Luther et al., 1977), we reported the results of a study of the effect of receiver orientation on erythema dose. The work reported here expands upon that earlier effort. Although the same numerical model is used for the current study, we will repeat the description of the model.

33

Model Description

The procedure employed here involves using the Green model (Green et al., 1974a) to obtain total local uv radiation ($Q_h + q_h$) as a function of wavelength (λ) and solar zenith angle (θ). Valid for clear sky conditions, it is essentially a Beer-Bouguer formulation for both direct beam (Q_h) and diffuse (q_h) radiation. It is assumed that the latter is isotropically distributed. These fluxes are determined using the relationships

$$Q_h(\theta,\lambda) = H(\lambda)\ V^2 \exp[-A_t(\theta,\lambda)]\ \cos\theta \qquad (1)$$

and

$$q_h(\theta,\lambda) = H(\lambda)\ V^2 \exp[-D_t(\theta,\lambda)]\ . \qquad (2)$$

where $H(\lambda)$ is the extraterrestrial solar irradiance at the mean earth-sun distance (taken from Howard et al., 1960). The symbol V, which does not appear in the Green model, is the ratio of mean earth-sun distance to that distance on a particular day. It thus allows for eccentricity in the earth's orbit, which causes variations in the extraterrestrial flux of ±3.5%.

The terms A_t and D_t are optical thickness functions accounting for the presence of ozone, air, and particulate matter, and they are given by Green et al. (1974a). For the spectral region considered here, the total ozone optical depth is of special interest.

To calculate the direct beam radiation incident on an inclined surface (Q_p), it is necessary to replace θ in Eq. (1) with the angle between the position of the sun and a line normal to the surface (i).

$$Q_p(\theta,\lambda)$$
$$= H(\lambda)\ V^2 \exp[-A_t(\theta,\lambda)]\ \cos i\ . \qquad (3)$$

where

$$\cos i = \cos\alpha\ \cos\theta$$
$$+ \sin\alpha\ \sin\theta\ \cos(a - a')\ . \qquad (4)$$

Here a' is the solar azimuth (relative to north), a is the azimuth of the receiver, and α is the angle of the receiver's inclination (relative to horizontal). For a horizontal receiver, $\alpha = 0$. Equations required to find θ and a' as a function of latitude, season, and time of day may be found in Dave et al. (1975), Sellers (1965) or the Smithsonian Meteorological Tables (List, 1958). The last reference also contains tabled values of V.

Diffuse radiation incident on an inclined surface has two components: that arriving from the sky as scattered radiation (q_s) and that reflected from the earth's surface (q_g). Under the assumption of isotropic reflection and the earlier assumption of isotropic atmospheric scattering, these quantities are given by (Dave et al., 1975):

$$q_s(\theta,\lambda) = \frac{1}{2}\ q_h(\theta,\lambda)\ (1 + \cos\alpha) \qquad (5)$$

and

$$g_g(\theta,\lambda) = \frac{r}{2}\ [Q_h(\theta,\lambda) + q_h(\theta,\lambda)]\ (1 - \cos\alpha)\ . \qquad (6)$$

The ground reflectivity r is small for surfaces other than snow and ice at uv wavelengths (Kondratyev, 1973). A value of 0.1 was chosen here for r.

The sum $Q_p + q_s + q_g$ represents the total radiation incident per unit area on a plane inclined at an angle α and with azimuth a. Because radiation is not equally efficient at all wavelengths in producing a biologic response, it is not possible to integrate incident radiation directly over wavelength and obtain a meaningful measure of skin tissue insult. It is necessary to know the relative response of skin to uv radiation as a function of wavelength. In the case of sunburn the so-called action spectrum (or erythema efficiency) has been studied using uv lamps (e.g., Coblentz and Stair, 1934; Mangus, 1964; Cripps and Ramsey, 1970) and can be represented by (Green et al., 1974b):

$$\epsilon(\lambda) = \left[4 \exp\left(\frac{\lambda - 297}{3.21}\right) \right]$$
$$\times \left[1 + \exp\left(\frac{\lambda - 297}{3.21}\right) \right]^{-2} \qquad (7)$$

The action spectrum for skin cancer in humans is not known; it is usually assumed to be the same as for erythema or similar to the DNA action spectrum (Setlow, 1974).

Procedure and Results

Equations (4) through (7) may be used to calculate the instantaneous erythema dose for any time of day, date, latitude, ozone amount and receiver position. In analyzing the effects of receiver orientation, we have numerically integrated over wavelength and time to produce daily erythema doses for Northern Hemisphere latitudes assuming the receiver is stationary. Integrations were performed for the 15th day of each month using a time step of

approximately 20 minutes. The total ozone was specified as a function of latitude based on data from the Nimbus III satellite reported by Lovill (1972). The values of total ozone used in the calculation are shown in Table 12. Ozone reductions of 10 and 20% were also considered in the calculations.

The azimuth of the receiver was specified in two ways. First, to obtain a measure of the upper bound on erythema dose at middle latitudes in the Northern Hemisphere, the receiver was held fixed in a south-facing position. Second, to estimate the average dose for a population where there is random orientation (i.e., no preferred orientation), calculations were made while averaging over azimuth angle (a rotated receiver). Doses were computed at 20° intervals in the azimuth angle, and the average of these was used for integration. The inclination angle α was held fixed at values of 0, 45, and 90 degrees. Introducing time dependence for this term would require modeling specific body sites and activities; we have chosen to present more general calculations.

Figure 34 shows the daily total erythema dose for a south-facing surface as a function of latitude in the Northern Hemisphere for different ozone amounts and receiver inclinations for the 15th day of June, September, and December. The relationship between dose magnitude and inclination is such that inclined surfaces generally receive less daily integrated dose than a horizontal surface at the same latitude. Exceptions to this occur in some low sun situations (large θ) where the dose on the inclined, south-facing surface slightly exceeds that of the horizontal surface (e.g., $\alpha = 45°$, 50-60° N in September and $\alpha = 45°$, 20-30° N in December). This result is in contrast to the study of Dave *et al.* (1975) using the full solar spectrum where the total radiation on south-facing surfaces was shown to grow larger than that received by a horizontal surface at high latitudes. At the wavelengths contributing to erythema, the radiation is predominantly diffuse. Consequently, the angle of incidence does not exert as strong an influence as it would when the radiation is predominantly in the direct beam, as was the case in the study by Dave *et al.* (1975).

Figure 34 also indicates that the daily erythema does not change uniformly with inclination angle. For example, changing α from 0 to 45° results in less change in the daily erythema dose than results from changing α from 45 to 90°.

Variations in α affect the latitudinal gradient of erythema dose. Increasing α decreases the latitudinal gradient in erythema dose poleward of the peak dose. There is a small reduction in the gradient for $\alpha = 45°$ as compared to $\alpha = 0°$, but the gradient is reduced by approximately half for $\alpha = 90°$.

For a horizontal surface, the latitude of the peak daily erythema dose corresponds closely to the solar declination angle. As α increases there is a poleward shift in the latitude of the peak dose. In June, for example, as α is changed from 0 to 90°, the latitude of peak dose moves from 20° N to approximately 40° N. A shift of similar magnitude occurs in September. This shift is the result of several factors.

The inclination angle affects the amount of direct solar flux received by the inclined surface. At latitudes toward the equator from the latitude of solar declination, increasing α results in a decrease in the direct solar flux. At higher latitudes there may be either an increase or a decrease depending on the value of α.

As already mentioned, the contribution to erythema dose due to diffuse radiation has two components: that arriving from the sky (Eq. 5) and that reflected from the earth's surface (Eq. 6). An inclined surface receives less diffuse radiation from the sky with increasing angle of inclination because less sky is visible. For example, a vertical surface receives half the flux of that received by a horizontal surface, assuming isotropic diffuse radiation. On the other hand, as α increases there is an increase in the diffuse flux component from the earth's surface. This flux component is generally small, however, because of the low surface albedo assumed.

The net result of the various factors just discussed is that there is a change in the partitioning of the direct and diffuse flux contributions to erythema dose as α is varied. This is illustrated for a south-facing surface in Fig. 35 which shows the

Table 12. Values of total ozone in atm·cm.

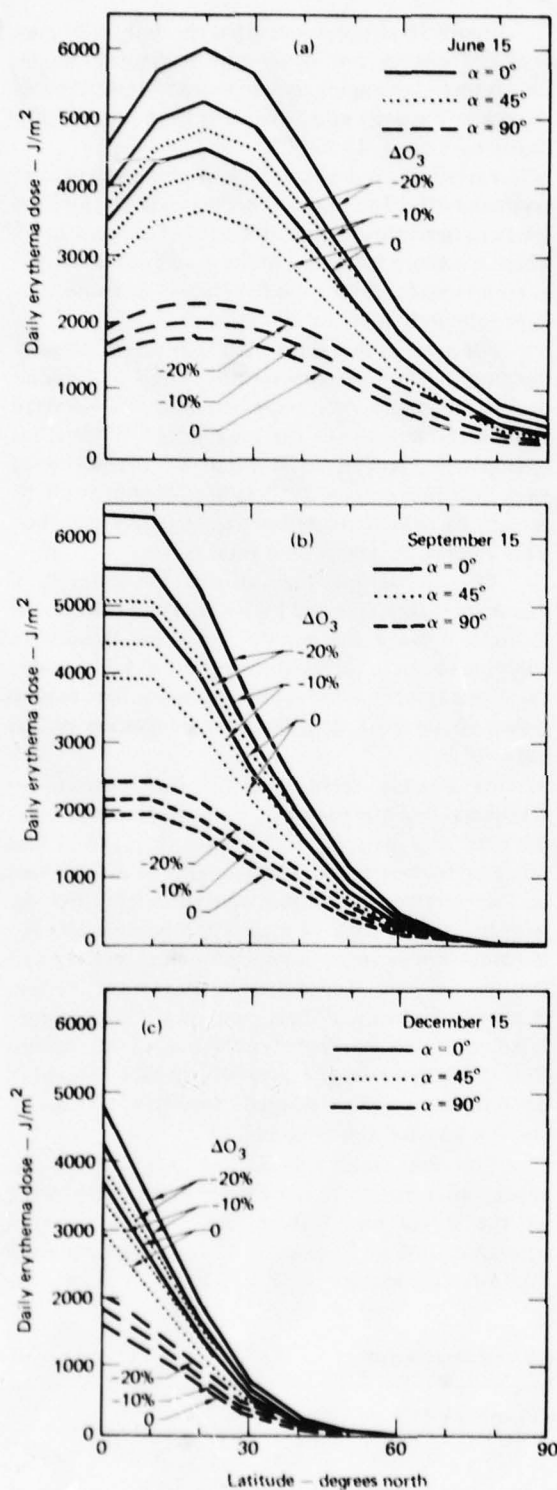| Months	Latitude (degrees north)								
	EQ	10	20	30	40	50	60	70	80
June	0.256	0.259	0.274	0.295	0.326	0.362	0.391	0.400	0.410
September	0.249	0.246	0.262	0.295	0.316	0.344	0.364	0.372	0.378
December	0.256	0.256	0.273	0.303	0.334	0.366	0.393	0.399	0.402

FIG. 34. Daily total erythema dose for a south-facing surface as a function of latitude, inclination angle α, and ozone amount: (a) June 15, (b) September 15, and (c) December 15.
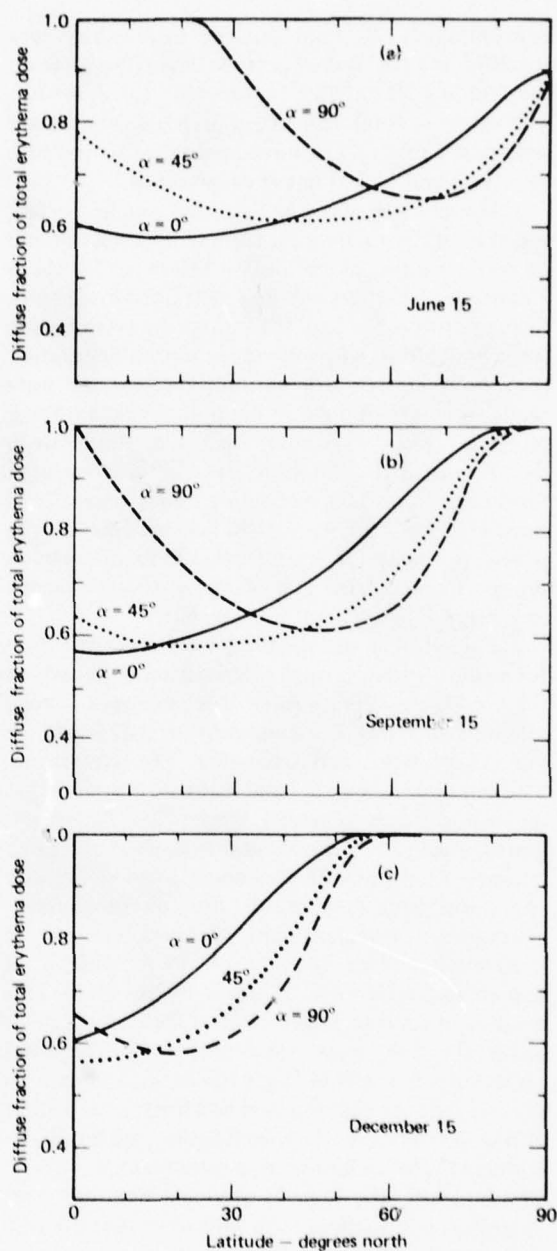

FIG. 35. The fraction of the total daily erythema dose for a south-facing surface due to diffuse radiation (sky plus ground reflection): (a) June 15, (b) September 15, and (c) December 15.

fraction of the total erythema dose due to the diffuse flux (sky plus ground reflection). In low sun situations (e.g., at high latitude), increasing α causes a decrease in the diffuse fraction of the total erythema dose, whereas the opposite is true in the case of a high sun (small θ).

Figure 36 shows the daily erythema dose for a rotated, inclined surface as a function of latitude for
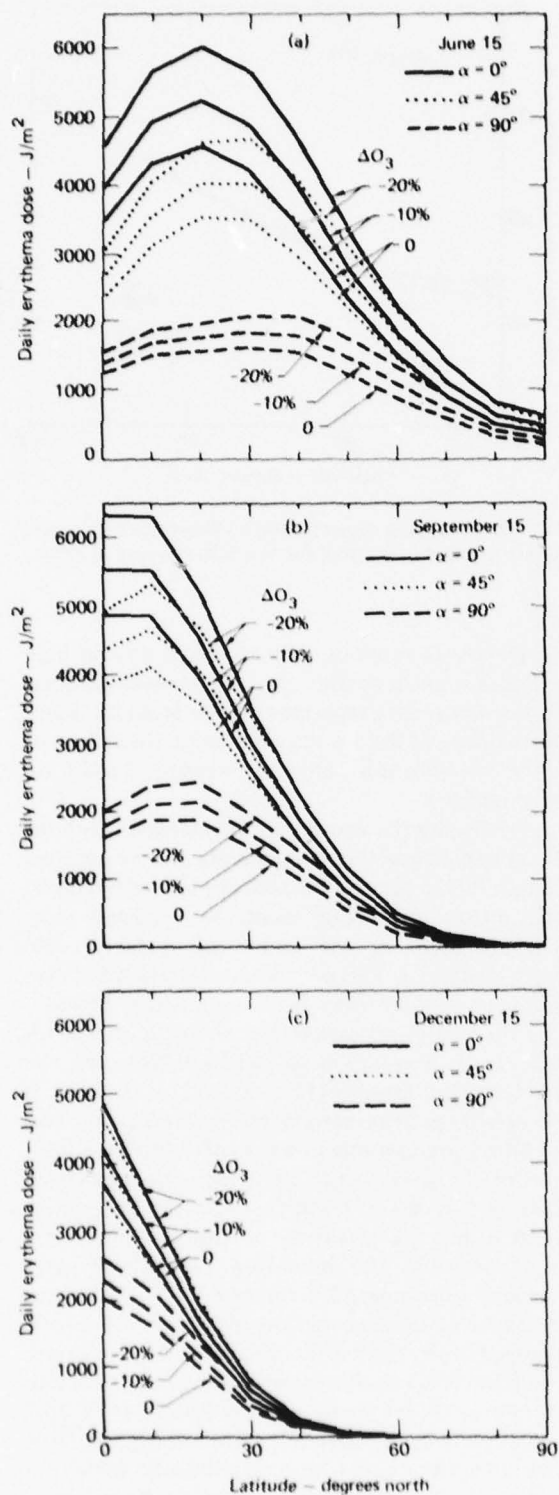
FIG. 36. Daily total erythema dose, same as Fig. 34 except for a rotated surface.

the same values of total ozone as used in Fig. 34. The dose received by the rotated surface never exceeds that for a horizontal surface, whereas it is possible at times for a south-facing, inclined surface to receive a slightly greater dose than the horizontal surface.

There is not a poleward shift in the latitude of the peak erythema dose with increasing α as was the case for the south-facing surface. Under the assumption of isotropic diffuse radiation, the contribution to erythema dose due to the total diffuse flux is the same for both the south-facing and rotated surfaces for a given α and latitude. Consequently, differences between Figs. 34 and 36 are due to differences in the direct flux component. The direct flux component is generally larger for the rotated surface than for the south-facing surface at latitudes near the equator, and the converse is true at high latitudes. In middle latitudes (30-50° N) the daily erythema dose is smaller for the rotated surface than for the south-facing surface.

Figure 37 shows the daily erythema dose averaged over a year for a south-facing surface assuming cloudless conditions. In middle latitudes the daily average erythema dose on a surface with $\alpha = 45°$ ranges from 90 to 96% of the dose on a horizontal surface. The dose is significantly less for inclination angles greater than 45°.

Figure 38 shows the daily erythema dose averaged over a year for a rotated surface. In this case the daily average erythema dose in middle latitudes on a surface with $\alpha = 45°$ is approximately 83% of the dose on a horizontal surface. At higher latitudes the dose on the rotated surface is significantly less than that on the south-facing surface.
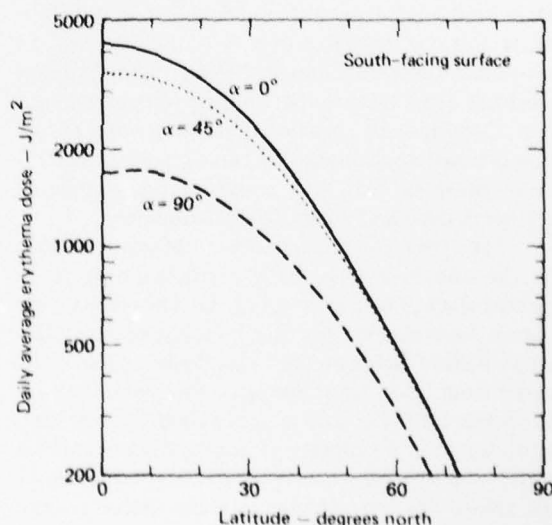

FIG. 37. Daily erythema dose averaged over a year for a south-facing surface.
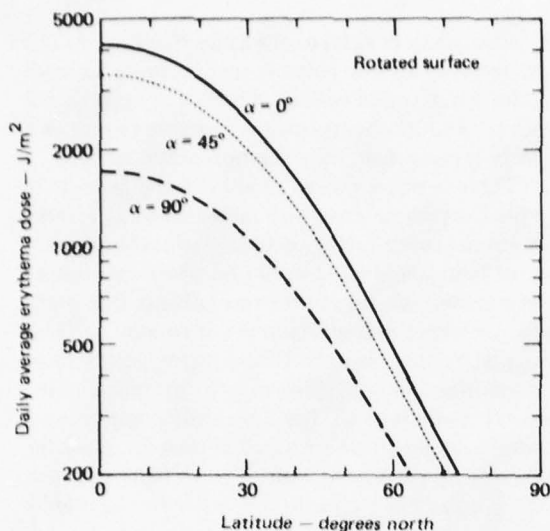
37

FIG. 38. Daily erythema dose averaged over a year for a rotated surface.

FIG. 39. The percent change in daily erythema dose for a rotated surface averaged over a year due to a 10% reduction in ozone.

A semilog scale is used in Figs. 37 and 38 to demonstrate the effect of inclination angle on the doubling distance for erythema dose. In middle latitudes the computed erythema dose on a horizontal surface doubles over 16° of latitude moving toward the equator. The angle of inclination has very little effect on the doubling distance as evidenced by the similar slopes of the curves in Figs. 37 and 38.

The computed doubling distance is consistent with measurements of annual-average erythema dose (Urbach and Davies, 1975), but it differs from the doubling distance for the incidence of skin cancer. Data on the incidences of skin cancer in middle latitudes show a doubling over 8 to 12° of latitude (National Research Council, 1976b), indicating that there are other factors contributing to the incidence rate. Consequently, predicting the effect of a reduction in total ozone on the skin cancer incidence rate is more complex than just assessing the change in erythema dose and scaling proportionately.

The effect of a reduction in total ozone of 10% on the annual-average daily erythema dose for a rotated surface is shown in Fig. 39. The results were almost identical for the south-facing surface. The amplification factor on erythema dose (Δdose/ΔO_3) varies from 1.3 to 1.4 at low latitudes, from 1.6 to 2.0 at middle latitudes, and is approximately 3 at high latitudes. It is a property of atmospheric transmission that a 10% reduction in the ozone column causes the greatest percent change in transmission for the largest optical depth. Because the ozone column and solar zenith angle both increase with latitude, the am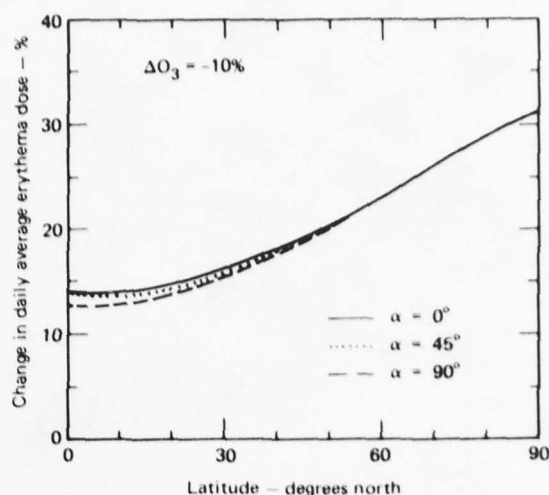plification factor is largest at high latitudes. While the percent increase in daily erythema dose at high latitudes is much greater, the total amount of radiation is very small compared to lower latitudes. Since the majority of the world's population lives south of 55° N, amplification factors in the range 1.3 to 2.0 are most realistic.

Reducing the ozone column increases both the direct and diffuse flux components, but by different factors. Since the relative contribution of the direct and diffuse flux components to erythema dose depends upon α, the amplification factor also depends upon α. This dependence is lessened at high latitudes where the flux is almost entirely diffuse.

As mentioned earlier, the action spectrum for skin cancer is an unknown function. However, van der Leun and Daniels (1975) argue that the peak in the action spectrum should occur near 270 nm. This is shifted considerably in wavelength from the location of the peak in the erythema action spectrum described by Eq. (7), which occurs at 297 nm. In order to test the sensitivity of dose to action spectrum position, the preceding calculations were repeated substituting 270 nm in Eq. (7). Aside from the expected decrease in dose magnitude, very little changed from the results obtained. An important exception concerns the percent change in the annual-average daily erythema dose produced by a 10% reduction in ozone, which is shown in Fig. 40. Dose amplification factors are significantly higher at middle and low latitudes compared to the results in Fig. 39. The amplification factor ranges from 1.8 to 2.0 at low latitudes and from 1.9 to 2.3 at middle latitudes. The reason for the larger amplification factors is related to the ozone absorption cross
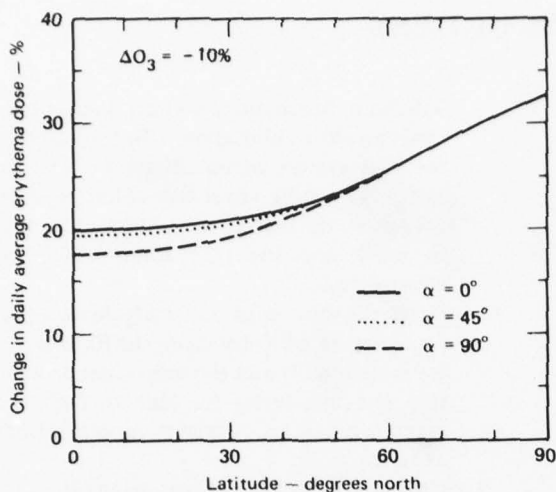
38

FIG. 40. The percent change in daily erythema dose for a rotated surface averaged over a year with the peak in the action spectrum shifted to 270 nm.
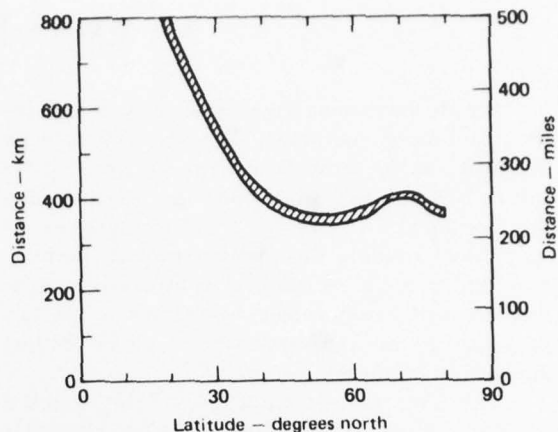

FIG. 41. The distance moved south equivalent to a 10% ozone reduction computed for a rotated surface. The shaded area indicates the range of values as the inclination angle is varied from 0 to 90°.

section, which in the region near 300 nm is a rapidly decreasing function of wavelength. Shifting the action spectrum to shorter wavelengths, where the uv fluxes are more sensitive to variations in ozone amount, leads to larger amplification factors.

Figure 41 shows the distance moved south, which is equivalent to a 10% reduction in ozone based on the annual average data for a rotated surface shown in Fig. 38. The shaded area indicates the range of values as α is varied from 0 to 90°, the largest values corresponding to $\alpha = 90°$. In middle latitudes the increase in daily average erythema dose due to a 10% ozone reduction is roughly equivalent to moving south a distance of 350 to 450 km with no ozone perturbation. The equivalent distance is much greater at latitudes toward the equator from 30°N. There is no equivalent distance for latitudes less than 15°N, because the erythema dose at these latitudes with a 10% ozone reduction is greater than the unperturbed erythema dose at the equator.

Summary

According to the simplified model used here, erythema doses have a significant dependence upon receiver orientation. Although it is possible at times for an inclined surface to receive a larger erythema dose than a horizontal surface, in general the highest doses are received by horizontal surfaces. In middle and high latitudes, inclined surfaces (south-facing or rotated) with inclination angles up to 45° receive at least 80% of the daily erythema dose received by a horizontal surface. Much larger reductions in daily erythema dose occur for $\alpha > 45°$, which can result in a significant reduction in the latitudinal gradient of erythema dose. In the case of a south-facing surface, the inclination angle affects the latitude of the peak erythema dose. Varying the inclination angle, however, does not have a significant effect on the doubling distance for average daily erythema dose. Finally, if the skin cancer action spectrum peaks near 270 nm as argued by van der Leun and Daniels (1975), skin cancer rates may be more sensitive than erythema to variations in total ozone.

4. WORK IN PROGRESS

We are developing a new solution technique for the one-dimensional model. The new code is being designed so that certain species or species families can be held constant while other short-lived species are calculated. We may then use the program to study how latitudinal variations in species concentrations and temperature feedback control OH concentrations in the troposphere. We expect to use this program to test the sensitivity of global budget analyses to latitudinal variations.

The new solution method is also being designed to allow either steady-state or time-dependent calculations. It may be possible to extend the method to the two-dimensional model. The basic solution scheme is as follows (this is subject to change, since the method has not been tested):

1. Predict values of individual species concentrations at next time step, $t + \Delta t$.
2. Predict values of species family concentrations (e.g., NO_x, ClO_x, etc.).
3. Use the concentrations from (1) to estimate the time derivative and flux terms of the species conservation equation. Scale each specie's time derivative by the predicted time derivative for its family from (2). This

will damp fluctuations in short-lived species concentrations and allow a full solution of the stiff system of equations we wish to solve. As a fully consistent solution is approached, the scaling factor becomes equal to unity and the true solution will be approached.

4. Solve the system of linear algebraic equations that result from using the fixed terms estimated in (3) and the individual production and loss terms for each species. The result is a new set of species concentrations at time $t + \Delta t$.
5. Check to see if the concentrations from (4) are the same as those from (1). If not, use the new values from (4) and repeat the procedure starting with step (2).

A special code is being written that will enable the model's vertical grid structure to be easily changed. The first utilization of this code will be to develop a more detailed model of atmospheric chemical and dynamical processes in the troposphere. This model will be used to derive a global distribution of OH to be compared with recent measurements by Doug Davis.

5. REFERENCES

Anastassiades, M., Ed., *Solar Eclipses and the Ionosphere* (Plenum Press, New York, N.Y., 1970).

Anderson, J. G. (1978), "Free Radicals in the Stratosphere: HO_2, OH, ClO, Cl, O, NO," presented at the WMO Symposium on the Geophysical Aspects and Consequences of Changes in the Composition of the Stratosphere, Toronto, June 26-30, 1978.

Anderson, J. G., J. J. Margitan and D. H. Stedman (1977), "Cl and ClO in the Stratosphere, Three *In Situ* Observations," *Science* **198**, 501-503.

Anderson, J. G., H. J. Grassl, R. E. Shetter, J. J. Margitan (1978), "Stratospheric Free Chlorine Measured by Balloon Borne *In Situ* Resonance Fluorescence," *J. Geophys. Res.*, in press.

Angell, J. K. and J. Korshover (1976), "Global Analysis of Recent Total Ozone Fluctuations," *Mon. Wea. Rev.* **104**, 63.

Angell, J. K. and J. Korshover (1978a), "Global Ozone Variations: An Update into 1976," *Mon. Wea. Rev.* **106**, 725.

Angell, J. K. and J. Korshover (1978b), "Recent Rocketsonde-Derived Temperature Variations in the Western Hemisphere," *J. Atmos. Sci.*, in press.

Angell, J. K. and J. Korshover (1978c), "Comparison of Ozone Variations Derived from Ozonesondes, and Umkehr and Total Ozone Measurements, for the Period 1967-1976," submitted to *Mon. Wea. Rev.*

Ballard, H. N., R. Valenzuela, M. Izquierda, J. S. Randhawa, P. Morla, and J. F. Bettle (1969), "Solar Eclipse: Temperature, Wind, and Ozone in the Stratosphere," *J. Geophys. Res.* **74**, 711-712.

Berger, D., D. F. Robertson and R. E. Davis (1975), "Field Measurements of Biologically Effective UV Radiation," Appendix D of Chapter 2 in *Impacts of Climatic Change on the Biosphere*, CIAP Monograph 5, U.S. Department of Transportation, Washington, D.C., 1975.

Budyko, M. I. (1969), "Climatic Change," *Tellus* **21**, 611.

Callis, L. B., Jr. and J. E. Nealy (1978), "Solar UV Variability and Its Effect on Stratospheric Thermal Structure and Trace Constituents," *Geophys. Res. Letters* **5**, 249.

Chang, J. S. (1976), Eddy diffusion profile described in *First Annual Report of Lawrence Livermore Laboratory to the High Altitude Pollution Program*, F. M. Luther, Ed., Lawrence Livermore Laboratory, Rept. UCRL-50042-76 (1976).

Chang, J. S., W. H. Duewer, and D. J. Wuebbles (1978), "The Atmospheric Nuclear Tests of the 50's and 60's: A Significant Test of Ozone Depletion Theories," Lawrence Livermore Laboratory, Rept. UCRL-80246, Rev. 1, submitted to *J. Geophys. Res.*

Chang, J. S., A. C. Hindmarsh, and N. K. Madsen (1974), "Simulation of Chemical Kinetics Transport in the Stratosphere," in *Stiff Differential Systems*, R. A. Willoughby, Ed. (Plenum Publishing Corp., New York, N.Y., 1974), p. 51.

Chang, J. S. and J. E. Penner (1978), "Analysis of Global Budgets of Halocarbons," *Atmos. Environ.* **12**, 1867-1873.

Chang, J. S. and D. J. Wuebbles, "Fully Diurnal Averaged Model of the Stratosphere," presented at the IAGA/IAMAP Joint Assembly, Seattle, WA, August 22-September 3, 1977.

Christie, A. D. (1973), "Secular or Cyclic Change in Ozone," *PAGEOPH* **106-108**, 1000.

Coblentz, W. W., and R. Stair (1934), "Data on Spectral Erythemic Reaction of the Untanned Human Skin to Ultraviolet Radiation," *U.S. Bureau of Standards J. Res.* **12**, 13-14.

Cripps, D. J. and C. A. Ramsay (1970), "Ultraviolet Action Spectrum with a Prism-Grating Monochromator," *Brit. J. Dermatol.* **82**, 584-592.

Cox, R. A. (1978), "Kinetics of HO₂ Radical Reactions of Atmospheric Interest," paper presented at the WMO Symposium on the Geophysical Aspects and Consequences of Changes in the Composition of the Stratosphere, WMO No. 511, 1978.

Crom, D. R., R. A. Rasmussen, E. Robinson and D. E. Harsch (1977), "Halogenated Compound Identification and Measurements in the Troposphere and Lower Stratosphere," *J. Geophys. Res.* **82**, 5935-5947.

Crutzen, P. J. (1975), "A Two-Dimensional Photochemical Model of the Atmosphere Below 55 km: Estimates of Natural and Man-Caused Ozone Perturbations Due to NOₓ," in *Proceedings of the Fourth Conference on the Climatic Impact Assessment Program*, T. M. Hard and A. J. Broderick, Eds., p. 264, 1975.

Cutchis, P. (1974), "Stratospheric Ozone Depletion and Solar Ultraviolet Radiation on Earth," *Science* **184**, 12-19.

Dandekar, B. S. and J. P. Turtle (1971), "Day Sky Brightness and Polarization During the Total Solar Eclipse of 7 March 1970," *Applied Optics* **10**, 1220-1224.

Dave, J. V., P. Halpern, and H. J. Myers (1975), "Solar Energy Incident Upon a South-Facing, Tilted, Flat Surface Under Cloudless Conditions," IBM Palo Alto Scientific Center, Palo Alto, CA, 3320-3331, 1975.

Duewer, W. H., D. J. Wuebbles, and J. S. Chang (1977), "Effect of NO Photolysis on NOₓ Mixing Ratios, *Nature* **265**, 523.

Duewer, W. H., D. J. Wuebbles, H. W. Ellsaesser, and J. S. Chang (1977), "NOₓ Catalytic Ozone Destruction: Sensitivity to Rate Coefficients," *J. Geophys. Res.* **82**, 935-942.

Dutsch, H. U. and Ch. Ch. Ling (1973), "Fourteen-Year Series of Vertical Ozone Distribution Over Arosa, Switzerland, from Umkehr Measurements," *PAGEOPH* **106-108**, 1139.

Evans, W. F. J., H. Fast, J. B. Kern, C. T. McElroy, R. S. O'Brien, D. I. Wardle, J. C. McConnel and B. A. Ridley (1978), "Stratospheric Constituent Measurements from Project Stratoprobe," WMO Symposium on the Geophysical Aspects and Consequences of Changes in the Composition of the Stratosphere, WMO-511, pp. 55-59, 1978.

Fanger, P. O. (1976), *Thermal Comfort* (Danish Technical Press, Copenhagen, 1976).

Fiala, A. D. and M. R. Lukac (1977), "Total Solar Eclipse of 26 February 1979," U.S. Naval Observatory Circular No. 157, 1977.

Giese, A. C., Ed. (1968), *Responses of the Human Skin to Ultraviolet Light* (Academic Press, New York, 1968).

Grasnick, K. H., H. Worner and P. Plessing (1974), "Ozon Variationen über Havanna während der Sonnenfinsternis vom 7 März 1970 unter Berücksichtigung der Randverdunkelung," *Geodatische und Geophysikalische Veroffentlichungen* **2**, 87-101.

Green, A. E. S., J. Mo and J. H. Miller (1974a), "A Study of Solar Erythema Radiation Doses," *Photochem. Photobiol.* **20**, 473-482.

Green, A. E. S., T. Swada, and E. P. Shettle (1974b), "The Middle Ultraviolet Reaching the Ground," *Photochem. Photobiol.* **19**, 251-262.

Green, A. E. S., T. Swada, and E. P. Shettle (1975), Chapter 2, *Impact of Climatic Change on the Biosphere*, CIAP Monograph 5, U.S. Department of Transportation, Washington, D.C., 1975.

Grobecker, A. J., S. C. Coroniti, and R. H. Cannon, Jr. (1974), "CIAP Report of Findings, The Effects of Stratospheric Pollution by Aircraft," Rept. DOT-TST-75-50, U.S. Department of Transportation, Washington, D.C., 1974.

Halpern, P., J. V. Dave, and N. Braslau (1974), "Sea-Level Solar Radiation in the Biologically Active Spectrum," *Science* **186**, 1204-1208.

Hampson, R. F. and D. Garvin, Ed. (1978), "Reaction Rate and Photochemistry Data for Atmospheric Chemistry — 1977," NBS Special Publication 513, 1978.

Heath, D. F. and M. P. Thekaekara (1977), "The Solar Spectrum Between 1200 and 3000 A," in *The Solar Output and Its Variation*, O. R. White, Ed., Colorado Assoc. Univ. Press, Boulder, CO., 1977), p. 193.

Hill, W. J. and P. N. Sheldon (1975), "Statistical Modeling of Total Ozone Measurements with an Example Using Data from Arosa, Switzerland," *Geophys. Res. Letters* **2**, 541.

Howard, C. J. (1978), "Recent Developments in Atmospheric HO_2 Chemistry," paper presented at the WMO Symposium on the Geophysical Aspects and Consequences of Changes in the Composition of the Stratosphere, WMO No. 511, 1978.

Howard, C. J. and D. M. Evenson (1977), "Kinetics of the Reaction HO_2 with NO," *Geophys. Res. Letters* **4**, 437.

Howard, J. N., J. I. F. King, and P. R. Gast (1960), "Thermal Radiation," Chapter 16 in *Handbook of Geophysics* (Macmillan, New York, 1960).

Hudson, R. D., Ed. (1977), "Chlorofluoromethanes and The Stratosphere," NASA Reference Publication No. 1010, 1977.

Humphreys, W. J. (1910), "Solar Disturbances and Terrestrial Temperatures," *Astrophys. J.* **32**(2), 97.

Hunt, G. G. (1965), "A Theoretical Study of the Changes Occurring in the Ozonosphere During a Total Eclipse of the Sun," *Tellus* **18**, 516-523.

Kondratyev, K. Ya (1973), *Radiation Characteristics of the Atmosphere and the Earth's Surface* (Amerind Publishing Co., New Delhi, 1973).

Krueger, A. J. and R. A. Minzner (1976), "A Mid-latitude Ozone Model for the 1976 U.S. Standard Atmosphere," *J. Geophys. Res.* **81**, pp. 4477-4481.

Landmark, B., A. Haug, E. V. Thrane, J. E. Hall, A. P. Willmore, M. Jespersen, B. Moller Penderson, M. Anastassiades, E. Tsagakis, and J. A. Kane (1970), "Ionospheric Observations During the Annular Solar Eclipse of 20 May 1966 — V. Interpretation of Observed Results," *JATP* **32**, 1873-1883.

Lazrus, A. L., B. W. Gandrud, J. Greenberg, J. Bonelli, E. Mroz and W. A. Sedlacek (1977), "Mid-latitude Seasonal Measurements of Stratospheric Acidic Chlorine Vapor," *Geophys. Res. Letters* **4**, pp. 587-589.

Leach, J. F., A. R Pingstone, K. A. Hall, F. J. Ensell, and J. L. Burton (1976), "Interrelation of Atmospheric Ozone and Cholecalciferol (Vitamin D_3) Production of Man," *Aviation Space Environ. Med.*, 630-633, June 1976.

Lindzen, R. S. and D. I. Will (1973), "An Analytic Formula for Heating Due to Ozone Absorption," *J. Atmos. Sci.* **30**, 513.

List, R. J. (1958), *Smithsonian Meteorological Table* (Smithsonian Institute Press, Washington, D.C., 1958).

London, J., J. E. Frederick and G. P. Anderson (1977), "Satellite Observations of the Global Distribution of Stratospheric Ozone," *J. Geophys. Res.* **82**, 2243.

London, J. and S.J. Oltmans (1977), "The Global Distribution of Total Ozone Variations During the Fifteen Year Period 1957-72," paper presented at IAGA/IAMAP Joint Assembly, Seattle, Washington, August 22-September 3, 1977.

Louis, J. F. (1974), *A Two Dimensional Transport Model of the Atmosphere*, Ph.D. thesis, University of Colorado, Boulder, CO (1974).

Lovill, J. E. (1972), "Characteristics of the General Circulation of the Atmosphere and the Global Distribution of Total Ozone as Determined by the Nimbus III Satellite Infrared Interferometer Spectrometer,"Colorado State University, Atmospheric Science Department Paper No. 180, 1972.

Luther, F. M. (1976), "Solar Absorption in a Stratosphere Perturbed by NO, Injection," *Science* **192**, 49-51.

Luther, F. M. *et al.* (1976), *High Altitude Pollution Program First Annual Report (1976)*, Lawrence Livermore Laboratory, Livermore, CA, Rept. UCRL-50042-76.

Luther, F. M., *et al.* (1977), *Annual Report of Lawrence Livermore Laboratory to the High Altitude Pollution Program — 1977*, Lawrence Livermore Laboratory, Livermore, CA, Rept. UCRL-50042-77 (1977).

Luther, F. M. and W. H. Duewer (1978), "Effect of Changes in Stratospheric Water Vapor on Ozone Reduction Estimates," *J. Geophys. Res.* (in press).

Luther, F. M., D. J. Wuebbles, and J. S. Chang (1978), "Temperature Feedback in a Stratospheric Model," *J. Geophys. Res.* **82**, 4935.

Luther, F. M., D. J. Wuebbles, W. H. Duewer, and J. S. Chang (1978), "Effect of Multiple Scattering on Species Concentrations and Model Sensitivity," *J. Geophys. Res.* **83**, 3563-3570.

Magnus, I. A. (1964), "Studies with a Monochromator in the Common Idiopathic Photodumatoses," *Brit. J. Dumatol.* **76**, 245-264.

Marriott, R. T., D. E. St. John, R. M. Thorne, and S. V. Venkatesworan (1972), "Ionospheric Effects of Two Recent Solar Eclipses," *JATP* **34**, 695-712.

McCarthy, R. L., F. A. Bower, and J. P. Jesson (1977), "The Fluorocarbon Ozone Theory — I. Production and Release — World Production and Release of CCl_3F and CCl_2F_2 (Fluorocarbons 11 and 12) through 1975," *Atmos. Env.* **11**, 491.

McDonald J. E. (1971), "Relationship of Skin Cancer Incidence to Thickness of Ozone Layer," *Congressional Record* **117**, 3493, March 19, 1971.

Mihelcic, D., D. H. Ehhalt, G. F. Kulessa, J. Klomfab, M. Trainer, U. Schmidt and H. Rohrs (1978), "Measurements of Free Radicals in the Atmosphere by Matrix Isolation and Electron Paramagnetic Resonance," *Pageoph* **116**, 530-536.

Mo, J., and A. E. S. Green (1974), "A Climatology of Solar Erythema Dose," *Photochem. Photobiol.* **20**, 483-496.

Molina, L., S. D. Shinke, and M. Molina (1977), "Ultraviolet Absorption Spectrum of Hydrogen Peroxide Vapor," *Geophys. Res. Letters* **4**, 580.

Murcray, D. G., J. W. Williams, D. B. Barker, A. Goldman, C. Bradford, and G. Cook (1978), "Measurements of Constituents of Interest in the Photochemistry of the Ozone Layer Using Infrared Techniques," WMO Symposium in the Geophysical Aspects and Consequences of Changes in the Composition of the Stratosphere, WMO-511, p. 61-68, 1978.

National Research Council (1973), *Biological Impacts of Increased Intensities of Solar Ultraviolet Radiation*, NRC Environmental Studies Board, National Academy of Sciences, Washington, D.C., 1973.

National Research Council (1975), *Long-Term Worldwide Effects of Multiple Nuclear Weapons Detonations*, National Academy of Sciences, Washington, D.C., 1975.

National Research Council (1976a), *Halocarbons: Effects on Stratospheric Ozone*, National Academy of Sciences, Washington, D.C., 1976.

National Research Council (1976b), *Halocarbons: Environmental Effects of Chlorofluoromethane Release*, National Academy of Sciences, Washington, DC., 1976.

Neely, W. B. and J. H. Plonka (1978), "An Estimation of the Time-Averaged Hydroxyl Radical Concentration in the Troposphere," preprint, 1978.

Noxon, J. F. (1978), "Stratospheric NO_2. I. Global Behavior," preprint, 1978.

Noxon, J. F. (1978), "Stratospheric NO_2. II. Global Behavior," preprint, 1978.

Noxon, J. F., R. B. Norton, and W. R. Henderson (1978), "Observation of Atmospheric NO_3," *Geophys. Res. Letters* **5**, pp. 675-678.

Noxon, J. F., E. C. Whipple, Jr., and R. S. Hyde (1978), "Stratospheric NO_2: I. Observational Method and Behavior at Mid-Latitude," preprint, 1978.

Oort, A. H. and E. M. Rasmussen (1971), "Atmospheric Circulation Statistics," NOAA Professional Paper 5, 1971.

Osherovich, A. L., N. S. Shpakov, and V. T. Zarubaylo (1974), "Measurement of Total Ozone Content During the Total Solar Eclipse of 10 July 1972," *Atmos. and Oceanic Phys.* **10**, 1221-1224.

Paetzold, H. K., F. Piscalar, and H. Zschorner (1972), "Secular Variation of the Stratospheric Ozone Layer Over Middle Europe During the Solar Cycles from 1951 to 1972," *Nature Phys. Sci.* **240**, 106.

Pollack, J. B., O. B. Toon, A. Summers, W. Van Camp and B. Baldwin (1976), "Estimates of the Climatic Impact of Aerosols Produced by Space Shuttles, SST's, and Other High Flying Aircraft," *J. Atmos. Sci.* **15**, 247-258.

Pyle, J. A. (1978), "A Zonal Mean Model of the Stratosphere Including Feedback Between Chemistry, Radiation and Dynamics," WMO Symposium on the Geophysical Aspects and Consequences of Changes in the Composition of the Stratosphere," WMO-511, p. 239-245.

Ramanathan, V. (1975), "Greenhouse Effect due to Chlorofluorocarbons: Climatic Implications," *Science* **190,** 50-51.

Ramanathan, V., L. B. Callis, and R. E. Boughner (1976), "Sensitivity of Surface Temperature and Atmospheric Temperature to Perturbations in the Stratospheric Concentration of Ozone and Nitrogen Dioxide," *J. Atmos. Sci.* **33,** 1092-1112.

Randhawa, J. S. (1968)., "Mesospheric Ozone Measurements During a Solar Eclipse," *J. Geophys. Res.* **73,** 493-495.

Randhawa, J. S. (1973), "An Investigation of Solar Eclipse Effect on the Subpolar Stratosphere," *J. Geophys. Res.* **78,** 7139-7144.

Ruderman, M. A. and J. W. Chamberlain (1975), "Origin of the Sunspot Modulation of Ozone: Its Implications for Stratospheric NO Injection," *Planet. Space Sci.* **23,** 247.

Ruderman, M. A., H. M. Foley, and J. W. Chamberlain (1976), "Eleven Year Variation in Polar Ozone and Stratospheric-ion Chemistry," *Science* **192,** 555.

Sellers, W. D. (1965), *Physical Climatology*, (University of Chicago Press, Chicago, IL, 1965).

Setlow, R. B. (1974), "The Wavelengths in Sunlight Effective in Producing Skin Cancer: A Theoretical Analysis," *Proc. National Academy of Sciences* **71,** 3363-3366.

Simon, P., private communication, 1978.

Stranz, D., (1961), "Ozone Measurements During Solar Eclipse," *Tellus* **13,** 276-279.

Urbach, F., Ed. (1969), *The Biological Effects of Ultraviolet Radiation with Emphasis on the Skin*, Pergamon Press, Oxford, 1969.

Urbach, F. and R. E. Davies, "Estimate of the Effect of Ozone Reduction in the Stratosphere on the Incidence of Skin Cancer in Man," in *Proc. Conf. on the Climatic Impact Assessment Program, 4th* T. M. Hard and A. J. Broderick, Eds., DOT-TSC-OST-75-38, U.S. Department of Transportation, Washington, D.C., February 4-7, 1975.

van der Leun, C. J. and F. Daniels, Jr. (1975), "Biological Effects of Stratospheric Ozone Decrease: A Critical Review of Assessments," Appendix B, Chapter 7 of *Impacts of Climatic Change in the Biosphere*, U.S. Department of Transportation, Washington, D.C., CIAP Monograph 5, 1975.

Velasquez, D. A. (1971), "Zenith Sky Brightness and Color Change During the Total Solar Eclipse of 12 November 1966 at Stana Ines, Peru," *Appl. Optics* **10,** 1211-1214.

Watanabe, T. and T. Tohmatsu (1976), "An Observational Evidence for the Seasonal Variation of Ozone Concentration in the Upper Stratosphere and the Mesosphere," *Report of Ionosphere and Space Research in Japan, 30,* 47-50.

Waters, J. W., J. J. Gustincie, R. K. Kakar, H. K. Koscoe, P. N. Swanson, T. deGraauw, A. R. Kerr, T. G. Phillips, and W. J. Wilson (1978), "Microwave Measurement of Upper Atmospheric Gases: H_2O, O_3, CO, ClO, N_2O," WMO Symposium in the Geophysical Aspects and Consequences of Changes in the Composition of the Stratosphere, WMO-511, p. 79, 1978.

Wilcox, R. W. and A. D. Belmont (1977), "Ozone Concentration by Latitude, Altitude, and Month, Near 80° W," Department of Transportation Report No. FAA-AEQ-77-13, 1977.

Willett, H. C. (1962), "The Relationship of Total Atmospheric Ozone to the Sunspot Cycle," *J. Geophys. Res.* **67,** 661.

Williams, W. J., J. J. Coster, H. Goldman, and D. G. Murcray (1976), "Measurement of the Stratospheric Mixing Ratio of HCl Using Infrared Absorption Technique," *Geophys. Res. Letters* **3,** 383-385.

Zerefos, C. S. and P. J. Crutzen (1975), "Stratospheric Thickness Variations Over the Northern Hemisphere and Their Possible Relation to Solar Activity," *J. Geophys. Res.* **80,** 5041.

RMD

APPENDIX A.   CHANGES TO THE ONE-DIMENSIONAL TRANSPORT-KINETICS MODEL DURING THE PAST YEAR

The chemical reactions incorporated in our current model are given in Table A-1 along with the rate expressions. Nearly all of the rate expressions come from Hampson and Garvin (1978). Most of the exceptions reflect recently reported measurements, although a few minor reactions not treated by Hampson and Garvin (1978) come from other compendia.

We have adopted the measurements of Howard *et al.* (1978) for the reactions

$$O_3 + HO_2 \rightarrow OH + 2O_2$$

and

$$NO + HO_2 \rightarrow NO_2 + OH .$$

Table A-1. Chemical reactions and rate coefficients currently used in the one-dimensional transport-kinetics model.

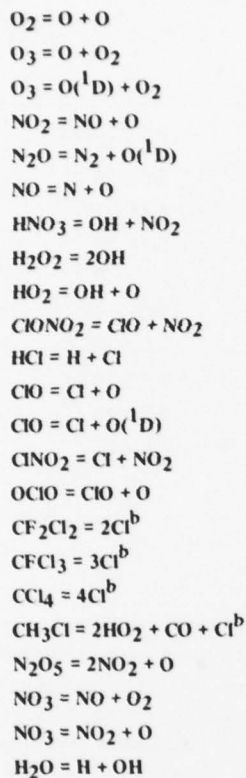| Reaction	Rate coefficient ($k = Ae^{B/T}$)		
	A	B	Ref.
$O + O_2 + M = O_3 + M$	1.1×10^{-34}	510	1
$O + O_3 = 2O_2$	1.9×10^{-11}	-2300	1
$O_3 + NO = NO_2 + O_2$	2.1×10^{-12}	-1450	1
$O + NO_2 = NO + O_2$	9.1×10^{-12}	0	1
$N_2O + O(^1D) = N_2 + O_2$	5.5×10^{-11}	0	1
$N_2O + O(^1D) = 2NO$	5.5×10^{-11}	0	1
$N + O_2 = NO + O$	5.5×10^{-12}	-3220	1
$N + NO = N_2 + O$	8.2×10^{-11}	-410	1
$O(^1D) + H_2O = 2OH$	2.3×10^{-10}	0	1
$O(^1D) + CH_4 = OH + 2HO_2 + CO^a$	1.3×10^{-10}	0	1
$O_3 + OH = HO_2 + O_2$	1.5×10^{-12}	-1000	1
$O + OH = O_2 + H$	4.2×10^{-11}	0	1
$O_3 + HO_2 = OH + 2O_2$	1.4×10^{-14}	-590	2
$O + HO_2 = OH + O_2$	3.5×10^{-11}	0	1
$H + O_2 + M = HO_2 + M$	2.08×10^{-32}	290	1
$O_3 + H = OH + O_2$	1.42×10^{-10}	-478	3
$HO_2 + HO_2 = H_2O_2 + O_2$	Note 1		4
$HO_2 + OH = H_2O + O_2$	3.0×10^{-11}	0	1
$OH + NO_2 + M = HNO_3 + M$	Note 2		1
$OH + HNO_3 = H_2O + NO_3$	8.9×10^{-14}	0	5
$H_2O_2 + OH = H_2 + HO_2$	1.0×10^{-11}	-750	1
$N_2 + O(^1D) + M = N_2O + M$	3.5×10^{-37}	0	1
$N + NO_2 = N_2O + O$	2.0×10^{-11}	-800	1
$NO + O + M = NO_2 + M$	1.6×10^{-32}	584	1
$NO + HO_2 = NO_2 + OH$	3.3×10^{-12}	254	2
$H_2 + O(^1D) = OH + H$	9.9×10^{-11}	0	1
$OH + OH = H_2O + O$	1.0×10^{-11}	-550	1
$N + O_3 = NO + O_2$	2.0×10^{-11}	-1070	1
$NO_2 + O_3 = NO_3 + O_2$	1.2×10^{-13}	-2450	1
$OH + CH_4 = H_2O + 2HO_2 + CO^a$	2.36×10^{-12}	-1710	1
$OH + OH + M = H_2O_2 + M$	1.2×10^{-32}	900	1

Reaction	Rate coefficient ($k = Ae^{B/T}$)		Ref.
	A	B	
$H_2O_2 + O = OH + HO_2$	2.75×10^{-12}	-2125	1
$O + CH_4 = OH + 2HO_2 + CO^a$	3.5×10^{-11}	-4550	1
$CO + OH = H + CO_2$	Note 3		6
$O(^1D) + M = O + M$	2.2×10^{-11}	99	1
$Cl + O_3 = ClO + O_2$	2.7×10^{-11}	-257	1
$Cl + OClO + 2ClO$	5.9×10^{-11}	0	1
$Cl + CH_4 = HCl + 2HO_2 + CO^a$	7.3×10^{-12}	-1260	1
$Cl + NO_2 + M = ClNO_2 + M$	6.9×10^{-34}	2115	7
$Cl + ClNO_2 = 2Cl + NO_2$	3.0×10^{-12}	0	1
$ClO + O = Cl + O_2$	7.7×10^{-11}	-130	1
$NO + ClO = NO_2 + Cl$	1.0×10^{-11}	200	1
$ClO + O_3 = Cl + O_2 + O_2$	1.0×10^{-12}	-4000	1
$ClO + O_3 = OClO + O_2$	1.0×10^{-12}	-4000	1
$ClO + NO_2 + M = ClONO_2 + M$	Note 4		1
$ClO + ClO = Cl + OClO$	2.1×10^{-12}	-2200	1
$ClO + ClO = 2Cl + O_2$	1.5×10^{-12}	-1238	1
$HCl + O(^1D) = Cl + OH$	1.4×10^{-10}	0	1
$OH + HCl = H_2 + Cl$	3.0×10^{-12}	-425	1
$O + HCl = OH + Cl$	1.14×10^{-11}	-3370	1
$O + OClO = ClO + O_2$	2.0×10^{-11}	-1100	1
$NO + OClO = NO_2 + ClO$	3.4×10^{-13}	0	8
$N + OClO = NO + ClO$	6.0×10^{-13}	0	8
$H + OClO = OH + ClO$	5.7×10^{-11}	0	1
$Cl + OH = HCl + O$	1.0×10^{-11}	-2970	1
$Cl + HO_2 = HCl + O_2$	4.1×10^{-11}	0	9
$Cl + HNO_3 = HCl + NO_3$	1.0×10^{-11}	-2170	1
$CFCl_3 + O(^1D) = 2Cl^b$	2.3×10^{-10}	0	1
$CF_2Cl_2 + O(^1D) = 2Cl^b$	2.0×10^{-10}	0	1
$Cl + H_2 = HCl + H$	4.7×10^{-11}	-2340	10
$Cl + H_2O_2 = HCl + HO_2$	1.6×10^{-12}	-384	1
$ClONO_2 + O = ClO + NO_3$	3.0×10^{-12}	-808	1
$CH_3Cl + OH = Cl + H_2O + HO_2^b$	2.2×10^{-12}	-1142	1
$NO + NO_3 = 2NO_2$	8.7×10^{-12}	0	11
$NO_2 + O + M = NO_3 + M$	1.0×10^{-31}	0	1
$NO_2 + NO_3 = NO + O_2 + NO_2$	2.0×10^{-13}	-2000	1
$NO_2 + NO_3 + M = N_2O_5 + M$	Note 5		6
$N_2O_5 + M = NO_2 + NO_3 + M$	Note 6		6
$N_2O_5 + O = 2NO_2 + O_2$	1.0×10^{-14}	0	12
$N_2O_5 + H_2O = 2HNO_3$	1.0×10^{-20}	0	1
$O(^1D) + O_3 = 2O_2$	1.2×10^{-10}	0	1
$HO_2 + HO_2 + H_2O = H_2O_2 + O_2 + H_2O$	Note 7		4

Photolysis reactions

$O_2 = O + O$

$O_3 = O + O_2$

$O_3 = O(^1D) + O_2$

$NO_2 = NO + O$

$N_2O = N_2 + O(^1D)$

$NO = N + O$

$HNO_3 = OH + NO_2$

$H_2O_2 = 2OH$

$HO_2 = OH + O$

$ClONO_2 = ClO + NO_2$

$HCl = H + Cl$

$ClO = Cl + O$

$ClO = Cl + O(^1D)$

$ClNO_2 = Cl + NO_2$

$OClO = ClO + O$

$CF_2Cl_2 = 2Cl^b$

$CFCl_3 = 3Cl^b$

$CCl_4 = 4Cl^b$

$CH_3Cl = 2HO_2 + CO + Cl^b$

$N_2O_5 = 2NO_2 + O$

$NO_3 = NO + O_2$

$NO_3 = NO_2 + O$

$H_2O = H + OH$

Note 1: $\dfrac{3.25 \times 10^8 + M \times 4 \times 10^{-10}}{(1 + 3.5 \times 10^{-16} \times M \times e^{-2060T})\,(8M + 4 \times 10^{+20})}$.

Note 2: Tsang (1977) as given by Hudson (1977).

Note 3: $1.4 \times 10^{-13} + M \times 7.3 \times 10^{-33}$.

Note 4: $\dfrac{3.3 \times 10^{-23}\,T^{-3.34}}{1. + 8.7 \times 10^{-9}\,T^{-0.6} \times (M)^{1/2}}$.

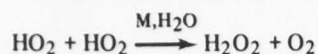Note 5: $\dfrac{2.9 \times 10^{-12}}{7.0 \times 10^{+21}\,e^{-2670/T} + M}$.

Note 6: $\dfrac{6 \times 10^{+14}\,e^{-10970/T}}{7.0 \times 10^{21}\,e^{-2670/T} + M}$.

Note 7: $\dfrac{1.1 \times 10^{-34}\,e^{+3730/T}}{1 + M \times 3.5 \times 10^{-16}\,e^{-2060/T}}$.

[a] Methyl radical production is assumed to yield $2HO_2 + CO$.

[b] Products such as F, H_2, CO, COF_2, etc. are not followed when produced from halocarbons.

We have adopted the pressure, temperature and water-vapor-dependent expression for
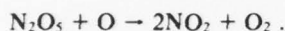
$$HO_2 + HO_2 \xrightarrow{M, H_2O} H_2O_2 + O_2$$

as given by Cox (1978) in his errata. We have adopted values given by Watson (1978) for

$$H + O_3 \rightarrow OH + O_2$$
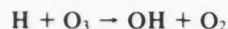
and Thrush (1978) for

$$Cl + HO_2 \rightarrow HCl + O_2 .$$

A privately communicated estimate by Johnston (1977) is used for

$$N_2O_5 + O \rightarrow 2NO_2 + O_2 .$$

Several minor reactions involving OClO were retained based on expressions cited by Watson (1975). None of these has any effect on model predictions. Simple pressure-dependent rate expressions for

$$NO_2 + NO_3 \xrightarrow{M} N_2O_5 ,$$

$$N_2O_5 \xrightarrow{M} NO_2 + NO_3$$

$$HO + CO \rightarrow CO_2 + H ,$$
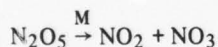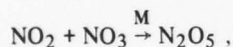
were developed from data cited by Hampson and Garvin (1978).

It should be noted that we do not use a detailed mechanism for the oxidation of methyl radicals. Instead we assume that a methyl radical is oxidized in such a way as to release two HO_2 radicals and CO.

Rate coefficients were changed for several reactions during the past year. These reactions are listed in Table A-2 along with the rate coefficients that were used previously. The most significant changes are the new rate for $HO_2 + O_3$, the new temperature dependence for $HO_2 + NO$, and a pressure- and water-vapor dependent rate for $HO_2 + HO_2$.

Water-vapor concentration is now computed at altitudes greater than 12 km in the model. The water-vapor distribution in the troposphere (0-12 km) is specified based on the global average distribution given by Oort and Rasmusson (1971). The derived ambient water-vapor distribution increases in concentration from 3.5 ppmv at the tropopause to 5.4

Table A-2. Chemical rate coefficients used in the 1977 model chemistry. Only those reactions that were changed during the past year are listed.

Reaction	Rate coefficient $(k = Ae^{B/T})$	
	A	B
$O_3 + HO_2 \rightarrow OH + 2O_2$	1.0×10^{-13}	-1250
$O + HO_2 \rightarrow OH + O_2$	3.0×10^{-11}	0
$O_3 + H \rightarrow OH + O_2$	1.23×10^{-10}	-562
$HO_2 + HO_2 \rightarrow H_2O_2 + O_2$	1.7×10^{-11}	-500
$HO_2 + OH \rightarrow H_2O + O_2$	2.0×10^{-11}	0
$NO + HO_2 \rightarrow NO_2 + OH$	4.28×10^{-11}	-500
$N + O_3 \rightarrow NO + O_2$	4.0×10^{-12}	-650
$CO + OH \rightarrow H + CO_2$	1.4×10^{-13}	0
$NO + ClO \rightarrow NO_2 + Cl$	2.2×10^{-11}	0
$ClO + NO_2 + M \rightarrow ClONO_2 + M$	5.1×10^{-33}	1030
$Cl + HO_2 \rightarrow HCl + O_2$	3.0×10^{-11}	0

ppmv in the upper stratosphere. Water vapor is produced in the upper stratosphere by the reactions $OH + HO_2 \rightarrow H_2O + O_2$ and $OH + CH_4 \rightarrow H_2O + CH_3$.

A new scheme was developed to calculate the multiple scattering factors used in the calculation of photodissociation rates. A computationally fast method for calculating the multiple scattering factor was needed for the diurnal model, and this method is also used in the diurnal-averaged model. Multiple scattering factors are no longer read in but are computed internally for the given solar zenith angle and species distributions. A detailed description of the method will be prepared in the near future.

An effort has been made to program the model to run as efficiently as possible, to use a minimum amount of storage, and to exist in a modular form for ease of future modifications. To minimize the use of storage, the model was divided into sections with the use of overlays so that at runtime all coding used to initialized the problem is released. There is now more space to add future chemistry. A significant reduction in running time was accomplished by using machine language versions of two subroutines. The user now has the option of running either diurnal or diurnal-averaged versions of the model with or without including the effect of temperature feedback.

References for Reaction Rate Coefficients Listed in Table A-1

1. Hampson, R. F. and D. Garvin (1978), "Reaction Rate and Photochemical Data for Atmospheric Chemistry — 1977," NBS Special Publication 513, 1978.
2. Howard, C. J. (1978), "Recent Developments in Atmospheric HO_2 Chemistry," Toronto WMO Conference, 1978.
3. Watson, R. W. (1978), "Atmospheric Kinetics," Toronto WMO Conference, 1978.
4. Cox, R. A. (1978), "Kinetics of HO_2 Radical Reactions of Atmospheric Interest," Toronto WMO Conference, 1978 (corrigendum values used, not those in the proceedings).
5. Margitan, J. J., F. Kaufman, and J. G. Anderson (1975), "Kinetics of the Reaction $OH + HNO_3 \rightarrow H_2O + NO_3$," *Int. J. Chem. Kinetics,* Symp. No. 1, 281-287, 1975.
6. Pressure-dependent fit to data cited in Ref. 1.
7. Clynne, M. A. A., Private communication, 1975.
8. Watson, R. T. "Rate Constants of ClO, of Atmospheric Interest," NBSIR-74-516.
9. Thrush, B. A. (1978), "Recent Results," Toronto WMO Conference, 1978.
10. Preliminary value communicated to the NAS Committee 1977 and accidentally retained.
11. Hampson, R. F. and D. Garvin (1975), "Chemical Kinetic and Photochemical Data for Modeling Atmospheric Chemistry," NBS Technical Note 866, 1975.
12. Johnston, H. S., Private communication, 1977.

APPENDIX B. BIBLIOGRAPHY OF LLL PAPERS AND TECHNICAL PRESENTATIONS DURING THE PAST YEAR

Burt, J. E. and F. M. Luther (1978), "Effect of Receiver Orientation on Erythema Dose," accepted for publication in *Photochemistry and Photobiology*, 1978.

Chang, J. S. (1978), "On the concept of Net Odd-Oxygen Destruction Rate," Manufacturing Chemist Association Technical Session on Stratospheric Chemistry, Boulder, CO, March 14-15, 1978.

Chang, J. S. (1978), "An Assessment of the Diagnostic Capabilities of Stratospheric Models," presented at the WMO Symposium on the Geophysical Aspects and Consequences of Changes in the Composition of the Stratosphere, Toronto, June 26-30, 1978.

Chang, J. S., W. H. Duewer, and D. J. Wuebbles (1978), "The Atmospheric Nuclear Tests of the 50's and 60's: A Possible Test of Ozone Depletion Theories," Lawrence Livermore Laboratory Report UCRL-80246, Rev. 2, submitted for publication to *J. Geophys. Res.*, 1978.

Chang, J. S. and J. E. Penner (1978), "Analysis of Global Budgets of Halocarbons," *Atmos. Environ.* **12**, 1867-1873.

Duewer, W. H., D. J. Wuebbles, and J. S. Chang (1978), "The Effects of a Massive Pulse Injection of NO_x into the Stratosphere," Lawrence Livermore Laboratory Report UCRL-80397, also in *Papers Presented at the WMO Symposium on the Geophysical Aspects and Consequences of Changes in the Composition of the Stratosphere*, WMO-No. 511, Toronto, June 26-30, 1978.

Luther, F. M. (1978), "The Ozone Layer: Assessing Man-Made Perturbations," *Energy and Technology Review*, 17-25, January 1978.

Luther, F. M. (1978), "Effects of Stratospheric Perturbations on the Solar Radiation Budget," Lawrence Livermore Laboratory Report UCRL-80429, also in *Papers Presented at the WMO Symposium on the Geophysical Aspects and Consequences of Changes in the Composition of the Stratosphere*, WMO-No. 511, Toronto, June 26-30, 1978.

Luther, F. M., and W. H. Duewer (1978), "Effect of Changes in Stratospheric Water Vapor on Ozone Reduction Estimates," *J. Geophys. Res.* **83**, 2395-2402.

Luther, F. M., D. J. Wuebbles and J. S. Chang (1977), "Temperature Feedback in a Stratospheric Model," *J. Geophys. Res.* **82**, 4935-4942.

Luther, F. M., D. J. Wuebbles, W. H. Duewer and J. S. Chang (1978), "Effect of Multiple Scattering on Species Concentrations and Model Sensitivity," *J. Geophys. Res.* **83**, 3563-3570.

Penner, J. E. and J. S. Chang (1978), "Possible Variations in Atmospheric Ozone Related to the 11 Year Solar Cycle," *Papers Presented at the WMO Symposium on the Geophysical Aspects and Consequences of Changes in the Composition of the Stratosphere*, WMO-No. 511, Toronto, June 26-30, 1978.

Wuebbles, D. J. (1977), *A Reexamination of Potential Space Shuttle Effects on the Stratosphere*, Lawrence Livermore Laboratory, Rept. UCID-17689 (1977).

Wuebbles, D. J. (1978), "A Theoretical Study of Solar Eclipse Effects on the Stratosphere," Lawrence Livermore Laboratory Report UCRL-80936, to be presented at the AMS Meeting on Meteorology of the Upper Atmosphere, Boston, MA, October 24-27, 1978.

Wuebbles, D. J. and F. M. Luther (1978), *Preliminary Study of Solar Power Satellites Program Potential Effect on Stratospheric Chemistry*, Lawrence Livermore Laboratory, Rept. UASG 78-41 (1978).